Dissertation zur Erlangung des Doktorgrades

der Fakultät für Chemie und Pharmazie

der Ludwig-Maximilians-Universität München

MicroRNA-200c as Chemosensitizer and Metastasis Suppressor: Novel Insights from *In Vitro* and *In Vivo* Investigations

Bianca Köhler

aus

Landsberg am Lech, Deutschland

2024

Erklärung

Diese Dissertation wurde im Sinne von § 7 der Promotionsordnung vom 28. November 2011 von Herrn Prof. Dr. Ernst Wagner betreut.

Eidesstattliche Versicherung

Diese Dissertation wurde eigenständig und ohne unerlaubte Hilfe erarbeitet.

München, den 13.09.2024

Bianca Köhler

Dissertation eingereicht am: 13.09.2024

1. Gutachter: Prof. Dr. Ernst Wagner

2. Gutachter: Prof. Dr. Stefan Zahler

Mündliche Prüfung am: 06.11.2024

„Man muss an seine Berufung glauben und alles daransetzen, sein Ziel zu erreichen.“ (Marie Curie)

gewidmet

meiner Familie

Table of Content

1. Introduction 7
1.1 Breast Cancer 7
1.1.1 Types of Breast Cancer 9
1.1.2 Treatment Options 11
1.2 Hallmarks of Cancer 13
1.2.1 Chemoresistance and Glutathione S-transferases 14
1.2.2 Migration and Metastasis Formation 16
1.3 MicroRNAs 17
1.3.1 Biogenesis 17
1.3.2 MicroRNA-200c 18
1.3.3 MicroRNA-200c in Chemoresistance and Migration 20
1.4 Aim of the Thesis 23
2. Material and Methods 25
2.1 Reagents 26
2.2 Cell Culture 27
2.3 Materials and Methods to Evaluate the Role of miR-200c in Chemoresistance and Migration *In Vitro* 29
2.3.1 Quantification of RFP Expression in the Inducible Cell Systems 29
2.3.2 Proteomics Sample Preparation 29
2.3.3 Proteomics LC-MS/MS Analysis 29
2.3.4 LC-MS/MS Data Analysis 30
2.3.5 Generation of 3′UTR GSTM3 Mutations in pISO 30
2.3.6 Co-Transfection and Luciferase Reporter Assay 31
2.3.7 RNA Lysis and Purification 31
2.3.8 cDNA Synthesis 31
2.3.9 Quantitative Real-Time Polymerase Chain Reaction (qRT-PCR) 32
2.3.10 Protein Lysis and Western Blot 33
2.3.11 Analysis of Total Glutathione Using the GSH/GSSG-Glo Assay 34
2.3.12 Evaluation of Cell Death Using Propidium Iodide Assay 34
2.3.13 Analysis of Long-Term Effects of hsa-miR-200c *In Vitro* Using the Cellwatcher System 35
2.3.14 Proliferation Analysis Using the PHIO Cellwatcher 35
2.3.15 Clinical Impact Using Kaplan–Meier Plotter 35
2.3.16 *In Vitro* Confined Cell Motility Analysis (1D Dumbbells) 36
2.3.17 Analysis of Single- and Collective-Cell Motility Using Transwell Assays 38

2.3.18 Analysis of Undirected (Random Walk) and Directed Migration (Scratch Assay) in Cell Clusters 39
2.3.19 Quantification of Cluster Cell Migration in Cell Aggregates in Collagen .. 40
2.3.20 Cell Survival Quantified with an Anoikis Assay 41
2.4 Materials and Methods to Evaluate the Role of miR-200c in Chemoresistance and Metastasis Formation *In Vivo* 42
2.4.1 *In Vivo* Xenograft Studies of hsa-miR-200c as Genetic Biomarker for Chemoresistance 42
2.4.2 H&E Staining of *In Vivo* Tumors 43
2.4.3 Analysis of Metastatic Formation in Distant Organs of Mice with or without miR-200c-Expressing Breast Cancer Tumors 43
2.5 Software 45
2.6 Statistical Analysis 45
3. Results Chapter I: MicroRNA-200c Prevents Drug Resistance by Downregulating Glutathione S-transferases 47
3.1 Proteomic Analysis of a hsa-miR-200c Knockout upon Doxorubicin Treatment Reveals a Higher Abundance of the Glutathione Pathway 47
3.2 Glutathione S-Transferase mu 3 Is a Novel Target of hsa-miR-200c-3p 50
3.3 Hsa-miR-200c Controls the Expression of Additional Glutathione S-Transferases 52
3.4 GSTM3 as Target of the hsa-miR-200c Is Differentially Expressed upon Chemotherapeutic Treatment 54
3.5 Hsa-miR-200c Influences the GSH Pool and Mediates Drug Resistance *In Vitro* 55
3.6 Xenograft Mouse Models Present Drug Resistance *In Vivo* upon Modulation of hsa-miR-200c Expression 58
4. Results Chapter II: Unraveling the Metastasis-Preventing Effect of miR-200c *In Vitro* and *In Vivo* 65
4.1 miR-200c Lowers the Metastatic Burden *In Vivo* 65
4.2 miR-200c Expression Modulates Undirected Collective Migration 72
4.3 The Migratory Behavior in Directed Collective Migration Assays Revealed Enhanced Predisposition of miR-200c Non-expressing Cells to Leave Cell Clusters 74
4.4 Migration is Reduced in miR-200c-Positive Cells in Transwell Assays 80
4.5 miR-200c Critically Determines Confined Cell Motility 81
5. Discussion 86
5.1 Discussion Chapter I: MicroRNA-200c Prevents Drug Resistance by Downregulating Glutathione S-Transferases 86

5.2 Discussion Chapter II: Unraveling the Metastasis-Preventing Effect of miR-200c *In Vitro* and *In Vivo* 91
6. Summary 97
7. Supplementary Materials 99
7.1 Supplementary Data Chapter I: MicroRNA-200c Prevents Drug Resistance by Downregulating Glutathione S-transferases 99
7.2 Supplementary Data Chapter II: Unraveling the Metastasis-Preventing Effect of miR-200c *In Vitro* and *In Vivo* 112
8. References 120
9. Indices 140
9.1 Index of Figures 140
9.2 Index of Supplementary Figures 141
9.3 Index of Videos 142
9.4 Index of Supplementary Videos 142
9.5 Index of Tables 143
9.6 Index of Supplementary Tables 143
9.7 Index of Abbreviations 143
9.8 Index of Genes and Proteins 145
10. Publications 149
10.1 Articles 149
10.1.1 First Author Publications 149
10.1.2 Co-author Publication 149
10.2 Poster 149
11. Copyright and licenses 150
12. Acknowledgements 151

1. Introduction

The following chapters are based on the content from the original publication which was published as Köhler *et al.*, Cancers (Basel) 2022 Nov; 14(22): 5554 as well as the original publication which was published as Köhler *et al.*, Mol Oncol. 2024 Oct 15 (see chapter 10.1 Articles). While there are partial overlaps text sections have been expanded with new and more detailed insights.

Cancer is a major cause of death before the age of 70 years in many countries worldwide (1, 2). In the year 2020, about 19.3 million new cancer cases and 10 million cancer deaths worldwide occurred (1). Although many therapeutic approaches for treating cancer, such as surgery and standard chemotherapy, exist, there is still a lack of curative and effective therapy options (3). To be able to kill tumor cells in a targeted manner with chemotherapy and to minimize relapses, new and specific forms of therapy are urgently needed. Despite the existing therapeutic approaches, an estimated increase of 47 %, the equivalent of 28.4 million new cancer cases, is expected by the year 2040 compared to 2020 (1). Reducing these numbers is the major goal in cancer research. Consequently, establishing improved and effective as well as personalized cancer treatment options is mandatory. Therefore, further development of biomarkers and prognostic markers is a valuable approach. In this thesis, novel insights on the application of chemotherapy together with non-coding RNAs in the treatment of breast cancer, especially triple negative breast cancer (TNBC), were revealed.

1.1 Breast Cancer

Breast Cancer is a heterogeneous disease in which various genetic and environmental as well as epigenetic factors play a major role in the development and progression of this disease (4, 5). Diversity in breast cancer is often explained by the cancer stem cell and the clonal evolution hypotheses (5). In general, mutations in oncogenes or tumor suppressors lead to cancer onset and progression (6-8). Based on this biological foundation the clonal evolution model explains the tumor initiation as an accumulation of several sporadic mutations within any normal cell. This stepwise progression subsequently results in the development of tumors. Whereas the cancer stem cell

model hypothesizes that only a certain subpopulation of cancer stem cells is tumorigenic and can initiate tumor formation. These cancer stem cells are highly self-renewing and can differentiate into non-tumorigenic progenitor cells with which they can form the tumor mass (9-11). The mentioned heterogeneity in breast cancer is a major obstacle for effective treatment (4). This aspect together with high incidence and mortality rates in breast cancer makes it a major health challenge (12).

A total number of about 2.3 million women worldwide are estimated to be newly diagnosed with breast cancer in 2020. The number of new breast cancer cases even exceeds the number of new lung cancer cases which was usually stated to be the number one in worldwide cancer incidence. Therefore, breast cancer has the highest incidence worldwide. Taking all cancer cases into account female breast cancer makes up 11.7 % of all newly diagnosed cancer diseases as shown in Figure 1 (1).

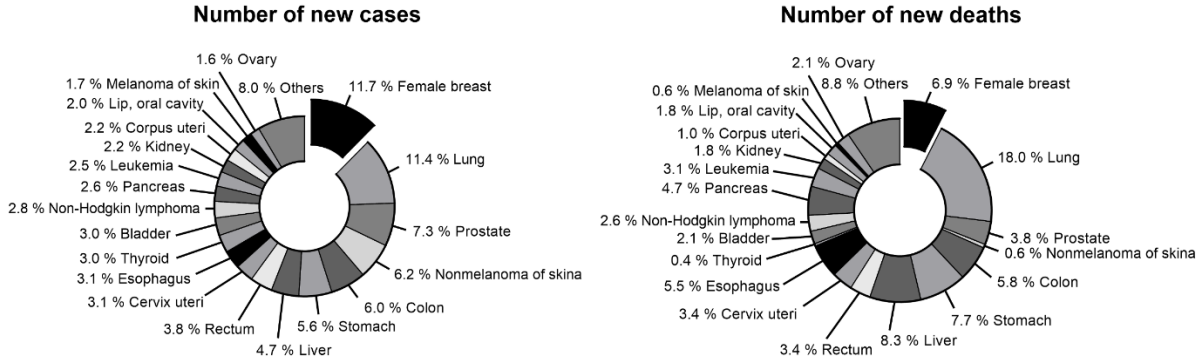

Figure 1: Worldwide cancer incidence and mortality distribution in both sexes according to cancer site. Others include the following cancer sites: Brain & nervous system, Larynx, Multiple myeloma, Nasopharynx, Gallbladder, Oropharynx, Hypopharynx, Hodgkin lymphoma, Testis, Salivary glands, Anus, Vulva, Penis, Kaposi sarcoma, Mesothelioma and Vagina. Numbers are transcribed from the publication of Sung *et al.* (1).

With an estimated value of 685,000 deaths female breast cancer is the fifth leading cause of cancer mortality in the world. Expressed in other numbers, one in four new cancer cases among women is breast cancer and one in six cancer deaths is caused by this disease (1).

1.1.1 Types of Breast Cancer

For appropriate treatment and accurate prognosis considerations a classification into different subtypes of breast cancer is necessary. In general, breast cancer can be categorized into four major molecular subtypes including: Luminal A, Luminal B, HER2 positive (HER2+) and basal-like also known as triple negative breast cancer (TNBC) (13-19). This classification is based on the immunohistochemical evidence of the presence of different (hormone) receptors: estrogen receptor (ER), progesterone receptor (PR), and human epidermal growth factor receptor 2 (HER2) (20). Also other strategies exist how to classify breast cancer, namely the classification upon histological subtypes including the most common invasive ductal carcinoma (75 % of invasive breast cancer), the second most common invasive lobular carcinoma (approximately 10 % of invasive breast cancer) and other rare subtypes (14). Throughout the following thesis the classification via the molecular subtypes will be used.

Luminal A breast cancer is the most common breast cancer type (68 %). It is characterized by the expression of ER and/or PR and less than 20 % positivity for Ki-67 (13). Ki-67 is a proliferation marker and can therefore give information on the proliferation rate of cancer in general (13, 21). Moreover, Luminal A is less aggressive, low grade and slowly growing and thus has the best prognosis amongst all four molecular breast cancer subtypes (13, 14, 21). This type of breast cancer shows a decent response to hormonal therapy (14).

Luminal B breast cancer is defined as ER positive (ER+) and/or PR positive (PR+) as well as HER2 positive (HER2+) and/or Ki-67 positive (Ki-67+) (higher than 20 %) and compared to the Luminal A subtype it is characterized with a poorer prognosis, higher invasiveness and higher proliferative rate and grade (14, 18, 22, 23). Patients diagnosed with Luminal B breast cancer usually benefit from the treatment with hormones and/or chemotherapeutics (13). If HER2 is expressed also targeted therapies are applied as a treatment option (19).

HER2+ breast cancer is the least common breast cancer subtype (13, 14). It is defined by the absence of ER and PR and presence of HER2 (13, 24). In comparison to the luminal subtypes of breast cancer this type shows a higher proliferative rate and is more aggressive (14, 17). This behavior is due to the fact that the HER2 receptor is known to play a role in many cancer related pathways i.e., cell proliferation, survival,

invasion and metastasis (17). The prognosis for HER2-positive breast cancer increased through the introduction of targeted therapy e.g., the trastuzumab (Herceptin®) launch in 1998 (14, 25). Besides the HER2 targeted therapy this subtype of breast cancer also highly responses to the treatment with chemotherapeutic agents (25).

Breast cancer with the worst prognosis is TNBC which is defined as the breast cancer subtype which does not express any of the aforementioned receptors (13, 14). Young women and women with a mutation in the breast cancer gene 1 (BRCA1) are more affected by this type of breast cancer (14, 26-28). TNBC harbors many characteristics which make the treatment of this breast cancer subtype difficult and the prognosis bad. To name just a few, TNBC is more aggressive than other subtypes and shows higher risk of metastasis and early relapse, it is highly proliferative and alteration in DNA repair genes are common (13, 14, 29, 30). The treatment of this breast cancer subtype is usually limited to chemotherapy only (30). The individual specifications of the breast cancer subtypes are summarized in Table 1.

Subtypes	Receptors	Prevalence	Prognosis	Treatment options
Luminal A	ER+, PR+, HER2-, Ki-67 < 20 %	68 %	Good	Hormonal therapy
Luminal B	ER+, PR+, HER2+ or Ki-67 > 20 %	10 %	Intermediate	Chemotherapy, Hormonal therapy, HER2
HER2 positive	ER-, PR-, HER2+	4 %	Intermediate	Chemotherapy, HER2
Triple negative	ER-, PR-, HER2-	10 %	Bad	Chemotherapy

Table 1: Breast cancer molecular subtypes with the corresponding receptor expression, prevalence, prognosis, and treatment opportunities, adapted from Orrantia-Borunda *et al.*, American Cancer Society, Yersal *et al.* and Dai *et al.* (13, 14, 17, 18).

1.1.2 Treatment Options

As pointed out treatments with high prospect of success are dependent on the type of breast cancer and therefore the presence or absence of specific receptors. In general, non-metastatic breast cancer is removed performing surgical procedures as breast-conserving surgery (BCS) or mastectomy often with subsequent breast reconstruction (14, 21). Surgery is often combined with further treatment as radiation therapy, chemotherapy, hormone and targeted therapy (14). However, breast cancer patients with metastasis formation at distant organs are treated with systemic therapies i.e., chemotherapy, hormonal and targeted therapy, as well as immunotherapy (14). Chemotherapy as one of the possible systemic treatments affects fast growing cells and can be applied intravenously or orally, before (neoadjuvant) or after (adjuvant) surgery (14, 21). The most common application is after surgery to destroy potentially remaining cancer cells but for patients with locally advanced breast cancer, inflammatory breast cancer or HER2+ and TNBC subtypes chemotherapy is applied as neoadjuvant therapy (14, 21). Usually, two to three of the following chemotherapeutic drugs are simultaneously applied: platinum agents (carboplatin/cisplatin), alkylating agents (cyclophosphamide), antimetabolites (5-fluorouracil/capecitabine), mitotic inhibitors taxanes (paclitaxel, docetaxel), and anthracyclines as anti-tumor antibiotics (doxorubicin, epirubicin) (21, 30, 31). Treatment with chemotherapeutic agents is known to result in severe side effects for the patients like hair loss, nausea/vomiting, and fatigue, to name just a few (21).

In contrast to the systemic chemotherapeutic treatment, radiotherapy is a local treatment which is usually applied after surgery and/or chemotherapy (21). This therapy is often applied for metastatic or unresectable breast cancer but most importantly also to prevent breast cancer recurrence (21, 32).

A specific treatment option for luminal breast cancer is the endocrinal therapy (21). The mechanism of action of this treatment is to either lower estrogen levels or prevent estrogen-stimulation of breast cancer cells by blocking ERs to hamper tumor growth (14, 21). Selective estrogen receptor modulators (SERMs) like tamoxifen and toremifene and selective estrogen receptor degraders (SERDs) like fulvestrant, block the hormone receptors. Meanwhile, aromatase inhibitors (AIs) including letrozole, anastrazole and exemestane can lower estrogen levels (33, 34). All these drugs for hormonal therapy can be applied as a neoadjuvant or adjuvant therapy (21).

Premenopausal patients typically receive tamoxifen whereas postmenopausal women are treated with AIs (14).

Targeted therapy is an additional treatment option for breast cancer. This treatment can be provided as neoadjuvant or adjuvant therapy at every stage of breast cancer (21). Drugs belonging to this treatment group affect specific proteins which usually support tumor growth (14). This treatment option is commonly used in HER2+ breast cancer and includes drugs like trastuzumab, a monoclonal antibody directed against HER2, trastuzumab combined with emtansine (T-DM1) and trastuzumab deruxtecan, which are both antibody-drug conjugates, pertuzumab, and tyrosine kinase inhibitors such as lapatinib, and neratinib (13, 14, 21, 25, 35-41). Additionally, angiogenesis inhibitors (a recombinant humanized monoclonal anti-VEGF antibody or bevacizumab) are further potential targeted therapy drugs for the treatment of breast cancer (21, 42, 43). Therapy options for luminal breast cancer without HER2 expression need to be distinguished into pre- and postmenopausal women. While premenopausal patients commonly benefit from everolimus which is a mammalian target of rapamycin (mTOR) inhibitor together with exemestane, postmenopausal patients receive hormonal therapy in combination with cyclin-dependent kinase 4–6 (CDK 4–6) inhibitor like palbociclib or ribociclib (14, 21, 44-46). Luminal B breast cancer in particular can also be treated with targeted therapies. These include targets or target pathways like the insulin-like growth factor 1 (IGF-1), fibroblast growth factor (FGF) and phosphoinositide 3-kinase (PI3K) signaling pathways (16). Besides the PI3K inhibitors also further targeted therapy drugs as Poly(ADP-Ribose) polymerase (PARP) inhibitors (i.e. Olaparib) are in medical use, especially in the treatment regimens of patients with BRCA mutations and in TBNC (14, 30). Antibody-drug conjugates including e.g., Sacituzumab govitecan (an antibody targeting the human trophoblast cell-surface antigen 2 (Trop-2) linked to SN-38 a topoisomerase I inhibitor) are used especially in TNBC (14, 47). Additionally, checkpoint inhibitors, as part of the immunotherapy, are of great interest in recent years. In general, checkpoint inhibitors are stimulating the immune system which in turn can affect cancer cells (14). Atezolizumab (anti-PD-L1 monoclonal antibody) and pembrolizumab (anti-PD-1 monoclonal antibody) are two examples of checkpoint inhibitors which are specifically applicable in the therapy of TNBC (14, 21, 30, 48).

1.2 Hallmarks of Cancer

As early as 2000, Douglas Hanahan and Robert Weinberg shaped the term “Hallmarks of Cancer” (49). With their “The Hallmarks of Cancer” review, they summarized biological capabilities and characteristics which transform normal cells to malignant tumor cells. In general, tumor development is based on oncogenes with gain of function mutations or tumor suppressors with loss of function mutations (49). Originating from the fundamental knowledge that tumorigenesis is driven by genetic instability and that this is a multistep process, Hanahan and Weinberg defined six major cancer hallmarks: self-sufficiency in growth signals, insensitivity to anti-growth signals, tissue invasion and metastasis, limitless replicative potential, sustained angiogenesis, and evading apoptosis (49). Over the past decades Hanahan and Weinberg extended these hallmarks, due to constant progress in the cancer research field, in their popular reviews: “Hallmarks of Cancer: The Next Generation” (50) and “Hallmarks of Cancer: New Dimensions” (51). In 2011, Hanahan and Weinberg added two emerging hallmarks to their list of biological capabilities: deregulating cellular energetics and avoiding immune destruction, and two enabling capabilities: tumor-promoting inflammation and genome instability and mutation (50). All these hallmarks are challenges for a successful treatment of breast cancer (Table 2), regardless of stage of cancer or metastatic spread. To be able to treat as many hallmarks as possible, extensive cancer research was carried out.

Hallmarks of Cancer	Treatment options
Evading growth suppressors	Cyclin-dependent kinase inhibitors
Avoiding immune destruction	Immune activating anti-CTLA4 mAb
Enabling replicative immortality	Telomerase inhibitors
Tumor-promoting inflammation	Selective anti-inflammatory drugs
Activating invasion & metastasis	Inhibitors of HGF/c-Met
Inducing angiogenesis	Inhibitors of VEGF signaling
Genome instability & mutation	PARP inhibitors
Resisting cell death	Proapoptotic BH3 mimetics
Deregulating cellular energetics	Aerobic glycolysis inhibitors

Sustaining proliferative signaling	EGFR inhibitors

Table 2: Targeting approaches of the hallmarks of cancer, adapted from Hanahan and Weinberg (50).

By the year 2022, the list of hallmarks was once more extended by two emerging hallmarks: unlocking phenotypic plasticity and senescent cells, and two enabling characteristics: nonmutational epigenetic reprogramming and polymorphic microbiomes (51). These hallmarks of cancer are important starting points for cancer research to further expand the understanding of tumor development and tumor progression and to develop personalized therapeutic approaches wherever possible. This doctoral thesis deals with the two most prominent hallmarks of cancer: chemoresistance and metastasis formation in breast cancer with novel insights from *in vitro* and *in vivo* strategies. Gaining further knowledge on these obstacles can lead to the improvement of breast cancer treatment, can broaden the clinical applicability of chemotherapeutic drugs, and can prevent metastasis formation.

1.2.1 Chemoresistance and Glutathione S-transferases

Regardless of important improvements and advances in the treatment of cancer over the last decades, resistance formation to anti-cancer drugs is still the main reason for failure of current therapy in advanced tumors (52-54). 90 % of the cancer related deaths are due to ineffectiveness of drug treatment (3). Drug resistance can evolve, even if tumors initially respond to chemotherapeutic treatment, finally causing cancer recurrence in patients. One of the main factors of the development of resistance to chemotherapeutics is the chromosomal instability of cancer cells, which results in genetic heterogeneity of the tumor supporting the subsequent clonal selection of tumor cells surviving the chemotherapeutic treatment (55, 56). Besides intrinsic resistance which exists before (preexistent) the initial cancer treatment, acquired resistance is formed after therapy (3) and comprises multi-causal systems (57, 58), which can be classified into three major mechanisms (59). The first process involves the decrease in the drug influx of water-soluble drugs like cisplatin and nucleoside analogues as these therapeutics require transporters for cell uptake, the second one includes various changes within the cell, e.g. modified regulation of DNA replication, i.e. altered cell cycle, or increased DNA repair mechanisms, modification of drug targets, metabolic

changes of drugs, the decrease of apoptosis via altered expression of apoptosis-associated protein Bcl-2 and tumor suppressor protein p53, and third the enhancement of drug-detoxifying mechanisms and drug efflux pumps leading to an enhanced efflux of hydrophobic drugs via ATP-binding cassette (ABC) transporters (59-62). Whether tumors respond to the treatment with chemotherapeutic drugs has certainly impacts on the effectiveness of cancer therapy. One of the major mechanisms to foster drug resistance is the reduction in the intracellular concentration of chemotherapeutic drugs. In this context, besides the before mentioned mechanisms, the inherently occurring phase II detoxification, which is exploited by cancer cells (63), utilizes, besides others, glutathione S-transferases (GSTs) to catalyze the conjugation of the reduced form of the tripeptide glutathione (GSH) to electrophilic xenobiotics (3, 63-65). These conjugates are more water-soluble and can finally be eliminated, resulting in less drug accumulation within the cells (3, 63-65). In general, phase II biotransformation includes the processes of methylation, glucuronidation, acetylation, sulfation, conjugation with glutathione, and the conjugation with amino acids to increase the polarity of the transformed molecule and to make it more soluble (66). Human GSTs are divided into three major families: cytosolic, mitochondrial (also known as kappa (κ) family) and membrane-bound microsomal GSTs (also known as membrane-associated proteins in eicosanoid and glutathione (MAPEG)) (63-65, 67-69). The biggest group of GSTs is formed by the cytosolic glutathione S-transferases, which are even predominantly involved in phase II detoxification (63, 67, 70, 71). These soluble enzymes can be subdivided further into seven distinct classes: alpha (A), mu (M), pi (P), sigma (S), omega (O), theta (T), and zeta (Z) and show catalytical activity when present as a dimer (64, 68, 70, 71). Enhanced expression of these GSTs are reported to commonly contribute to drug resistance (63, 67, 72). As a consequence, GSH-xenobiotic drug conjugates are formed faster and are actively eliminated, notably via efflux pumps such as MRP1 and p-glycoproteins (67, 71), and this leads to a reduced damage rate within tumor cells. Besides that, GSTs can also alter the mitogen-activated protein kinase (MAPK) signaling pathway via interactions with c-Jun N-terminal kinase 1 (JNK1) and apoptosis signal-regulating kinase (ASK1) to modulate cell proliferation and apoptosis (69). GSMT3 is located on chromosome 1p13.3 and its expression levels differ amongst breast cancer subtype, especially in HER2-positive or ER-positive tumors GSTM3 levels are high (73). The mechanism of action for ER-positive carcinoma involves the stimulation of the estrogen receptor via estrogen to recruit the transcription

factors SP1, AP-1, and EP 300 which subsequently can bind to the promoter region of GSTM3 and lead to its upregulation (73-75).

To prevent resistance formation altering these detoxifying mechanisms is essential. Whether miRNAs, especially miR-200c, play a role in the phase II detoxification is the first subject of the present thesis.

1.2.2 Migration and Metastasis Formation

During the process of metastasis formation cells dissociate from a primary tumor and spread to distant tissues (76, 77). This significantly impedes effective breast cancer treatment and moreover, if metastatic breast cancer developed, the treatment focus is mostly limited to prolonging the patient's life and palliating symptoms (78, 79). Metastases are related to a high rate (about 90 %) of cancer deaths (80, 81) and in most cases (60 to 70 % of cancer patients) the development of metastases has often already been initiated at the time of diagnosis (82). Genetic heterogeneity, i.e. genetic but also epigenetic alterations often result in a favored selection of cells that exhibit increased migratory, invasive and metastatic capacity leading to cancer progression (83-87). But until now, the fundamental biological functions of metastasis are insufficiently understood (86, 88, 89). The formation of metastasis is a multi-step process, known as the invasion-metastasis cascade which includes the following coherent steps: invasion, intravasation, circulation, extravasation, and metastatic colonization of malignant cells (82, 85, 86, 90, 91). One prerequisite of metastasis formation is the migration of cancer cells (92, 93). Their way from the primary tumor to reach and disseminate into the pre-metastatic niches in distant organs requires the cells' ability to move through the basement membrane, prior to migration through different microenvironments i.e., tissue, stroma, blood vessels and lymphatics (85, 94, 95). Cancer cells can either migrate individually (single) or collectively. The later one being known to be the most common type of migration (85, 89, 92, 94, 96, 97). Whereas cells performing collective migration communicate with each other within the clusters and cell-cell adhesion is maintained (85, 89), a solitary cell detaches from the malignant tissue to reach distant parts of the body when completing single-cell migration (85, 91). To obtain the superior goal, the prevention or even reversal of metastasis in a targeted manner, it is mandatory to better resolve the process of metastasis including *in vitro* analysis of cell motility (90).

Whether sole expression of the miR-200c can reduce the metastatic burden and how this miRNA influences cell migration is the second subject of this thesis.

1.3 MicroRNAs

Amongst non-coding RNAs microRNAs (miRNAs) are endogenously expressed RNAs of approximately 22 nucleotides which are processed from longer RNA transcripts (pri- and pre-miRs). A single miRNA is capable to interfere with several oncogenes and thus, a miRNA can regulate several cancer hallmarks at a time. This fact makes them predestined molecules to target the complex biology of cancer (76, 98-100). MiRNAs change the expression of target genes through complementary binding to the three prime untranslated region (3'-UTR) of the messenger RNAs (mRNAs). This binding causes either the degradation or the translational inhibition of the target mRNA (98-100). MiRNAs have the ability to simultaneously regulate numerous target mRNAs (101, 102), causing complex miRNA-mRNA-interactions. They can either function as oncogenes or tumor suppressors (98). By now, an estimated number of over 60 % of the human genome is regulated by miRNAs (103, 104). Deregulation of miRNAs may trigger diseases such as cancer (105). Biological features of miRNAs like the high stability of circulating miRNAs in the blood stream and the unique expression profile of miRNAs in different diseases, including cancer, make these miRNAs an interesting prognostic and diagnostic biological marker (18). These innovative biomarkers may contribute to effective personalized treatment of breast cancer subtypes. For example, Dai *et al.* investigated miRNA profiles in ER, PR and HER2 subgroups and found a potential link between some miRNAs e.g., miR-135a, miR-135b, miR-365 and miR-7 and the possibility to distinguish breast cancer by ER status (18, 106). Improving clinical outcomes of breast cancer patients is of utmost importance. Therefore, comprehensive research in the field of miRNAs might unravel new paths for treatment options and finally cure cancer or at least prolong the patient's survival.

1.3.1 Biogenesis

Single-stranded miRNAs need to bind to mRNA to cleave the target mRNA, degrade the target or inhibit the translation of the target, all of these mechanisms resulting in gene silencing (107). To obtain a mature miRNA strand a multistep process needs to be executed. Figure 2 describes schematically the canonical pathway of the miRNA

biogenesis (108, 109). In brief, miRNAs are usually transcribed from miRNA genes or introns with the help of RNA polymerase II into so called primary miRNAs (pri-miRNAs). These are further cleaved into precursor miRNAs (pre-miRNAs). This first cleavage event is dominated by nuclear microprocessor complex enzymes, consisting of the Drosha and DiGeorge syndrome critical region gene 8 (DGCR8) proteins as well as RNA polymerase III. Afterwards these pre-miRNAs are exported from the nucleus into the cytoplasm via a complex of Exportin-5 and Ran-GTP. This double strand miRNA is still harboring a hairpin-loop structure which is subsequently cleaved in a second cleavage event by Dicer, TAR RNA binding protein (TRBP) and PKR-activating protein (PACT). This leads to the formation of the miRNA duplex. Together with Argonaute RISC Catalytic Component 2 (Ago2) one of the miRNA duplex strands (3p or 5p strand) is loaded into the RNA-induced silencing complex (RISC) finally resulting in the binding of the single-stranded mature miRNA strand to its target mRNA, while the second strand is degraded. Perfect pairing of the seed sequence of the miRNA with its complementary sequence on the 3' UTR of the mRNA is an essential process and leads finally to gene silencing (107, 109-112).

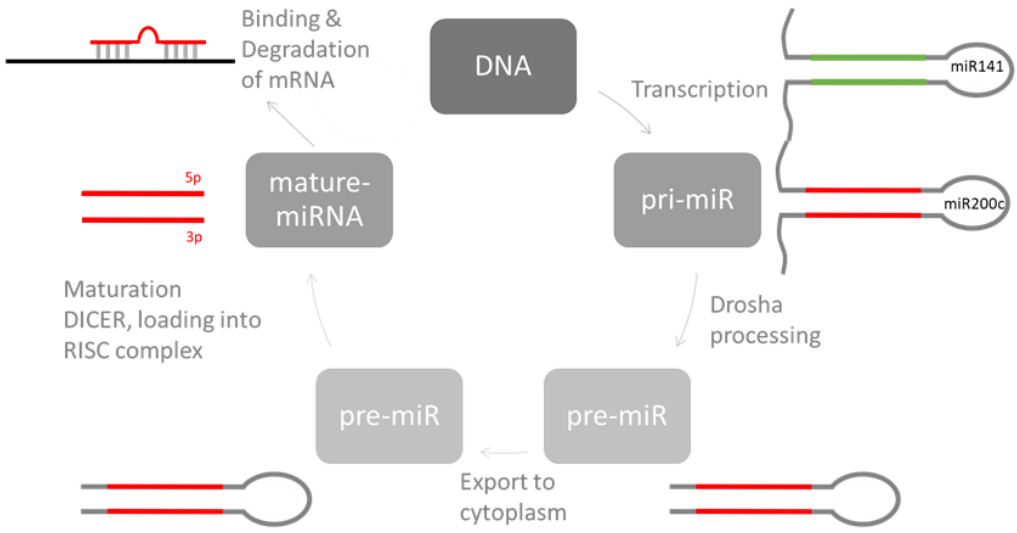

Figure 2: MicroRNA biogenesis. Schematic account of the major steps in the processing of miRs, adapted from Macfarlane *et al.*, O'Brien *et al.*, Winter *et al.*, Perron *et al.*, Nallamshetty *et al.* and Inui *et al.* (107-112).

1.3.2 MicroRNA-200c

miR-200c as part of the microRNA-200 family is the focus of this thesis. It is a tumor suppressor miRNA, which is involved in many processes of tumorigenesis, including

chemotherapy resistance, motility, epithelial-mesenchymal transition (EMT), metastasis and many more (113-118). The microRNA-200 family includes five members: miR-200a, -200b, -200c, -141 and -429. Together with miR-141, miR-200c is located on chromosome 12p13.31 while the rest of the family is located on chromosome 1p36.33. miR-200c, -200b and -429 form a functional family as they possess the same seed region: AAUACUG, the second family is formed by miR-200a and -141 (seed region: AACACUG) (76, 115, 119).

The binding of transcription factors like specificity protein 1 (Sp1) and p53 can activate the transcription of miRNA-200c (76). Loss of miRNA-200c is known to be the consequence of a hypermethylation of the promoter region of the miR-200c/-141 cluster or the binding of the transcription factors zinc finger e-box bind homeobox 1 (ZEB1) and 2 (ZEB2) to the promoter region of miRNA-200c (76, 120-124). Further principals on how miR-200c expression can be altered are described in chapter 5.1. Kumar *et al.* summarizes the role and the expression levels of miRNA-200c in cell lines and in tissues/circulation in various types of cancer namely breast, ovarian, endometrial, prostate, lung, colorectal, pancreatic, and gastric cancer (125). In respect to breast cancer cell lines, most mesenchymal cell lines e.g., MDA-MB 231, which are used in the present thesis, express low levels of miRNA-200c. However, epithelial breast cancer cell lines as MCF7, which are additionally utilized in this thesis, show enhanced expression of miRNA-200c, as additionally reported by Kopp *et al.* (117). This expression pattern indicates that miRNA-200c is negatively correlated with tumorigenesis (125) and is therefore an attractive tumor suppressor target. Clinical information show important relevance of miR-200c in breast cancer as the patient's survival is prolonged when the primary tumor displayed elevated levels of miRNA-200c (126, 127). This might be due to the finding that breast tumor tissues expressed lower levels of miRNA-200c compared to the marginal tissue as shown in the study of Mansoori *et al.* (128). miR-200c can also be used as a diagnostic and prognostic marker for instance in clear cell renal cell carcinoma as shown by Saleeb *et al.* who presented that high levels of miR-200c are associated with high overall survival and progression-free survival in these patients (129, 130). Controversially, high levels of circulating miR-200c in patients with colon cancer were correlated with poor overall survival (130, 131). These examples shall demonstrate that the mode of action of a miRNA and thus the impact on clinical application as therapeutic agent or diagnostic and prognostic marker depends on the cancer entity.

1.3.3 MicroRNA-200c in Chemoresistance and Migration

MiRNA-200c is an interesting and very attractive target microRNA involved in the two major hallmarks of cancer: resistance formation to chemotherapeutic agents and migration and metastasis formation, respectively. Many proofs have been collected over the past decades that miRNAs play an important role in both hallmarks by regulating the translation of different mRNAs (132). Important genes, which are known to alter the chemosensitivity of tumor cells, like tropomyosin receptor kinase B (TrkB), B-cell specific Moloney murine virus integration site 1 (Bmi1), Kirsten rat sarcoma viral oncogene homologue (Kras), and other oncogenes, were found to be controlled by miRNA-200c (115, 117, 118, 125, 133). In addition to that, miRNA-200c can also directly or indirectly inhibit ABC transporters, such as ATP Binding Cassette Subfamily B Member 1 (ABCB1), ATP Binding Cassette Subfamily G Member 2 (ABCG2), ATP Binding Cassette Subfamily G Member 5 (ABCG5), and the multidrug resistance protein 1 (MDR1), which are known to be responsible for resistance formation to various drugs (134-136). MiRNA-200c can consequently increase the susceptibility of cells to chemotherapeutic agents. This perception is supported by the study of Chen *et al*. reporting decreased expression levels of miRNA-200c in drug resistant breast cancer patients (137). Puhr *et al.* have demonstrated docetaxel-resistance of prostate cancer cells as a consequence of diminished miR-200c expression and in turn restoration of EMT and Liu *et al.* revealed enhanced cisplatin-sensitivity of ovarian cancer as miR-200c targets DNMT1 (130, 138, 139), to name but a few mechanism of how miR-200c can target chemoresistance. Nonetheless, classical chemotherapy is still the method of choice in advanced tumor stages (140).

That miR-200c is playing a crucial role in tumor progression, especially in metastasis formation was summarized in different reviews (76, 103, 141, 142). But whether sole miR-200c expression can alter the metastatic burden in xenograft mouse models and could therefore have a huge clinical significance was part of this thesis. Metastatic spread is a highly complex biological process consisting of several different cellular procedures that must be conducted correctly and completely in order to enable metastasis in distant organs (76, 77). These steps are summarized in the invasion-metastasis cascade. Research of previous years has shown that miRNA-200c can alter different steps of the invasion-metastasis cascade, like migration, tissue invasion, anoikis, and EMT of cancer cells (76, 98, 103, 125, 141, 143-145), as potential targets

of miR-200c are found in nearly every step of the cascade as described in Table 3. EMT is a multifaceted mechanism as it also influences drug resistance, as previously mentioned, utilizing for instance the Wnt and Hedgehog pathway (146-148). Moreover, miR-200c alters the induction of EMT-inducing transcriptional factors, i.e. Twist-related protein 1 (Twist), Snail Family Transcriptional Repressor 1 (Snail) and ZEB (145, 149, 150). Many targets of the miR-200c, like the aforementioned ZEB1 and ZEB2 but also Ubiquitin Specific Peptidase 25 (USP25), Moesin (MSN), and Fibronectin 1 (FN1) directly alter migration as presented in the review of Mutlu *et al.* (103). In previous cooperation work, we found Filamin A (FLNA), as a further target of miR-200c, to impair cell migration (114). As migration of the cells is the prerequisite of metastasis formation in distant organs, the effect of miR-200c on this process was evaluated in more detail. Moreover, changing the anoikis pathway with its targets Leptin receptor (LEPR) and Rho GTPase activating protein 19 (ARHGAP19), as well as the re-organization of the actin cytoskeleton with the miRNA-200c targets Formin homology domain-containing protein 1 (FHOD1) and Protein phosphatase 1F (PPM1F), can indirectly affect EMT/migration and invasion (103).

The multifaceted miR-200c with its various targets can affect tumor development and progression, which makes it an interesting target for improved breast cancer therapy in the future.

Process of the invasion-metastasis cascade	**Selection of possible miR-200c targets**
Tumor growth	Fms Related Receptor Tyrosine Kinase 1 (Flt1) also known as VEGFR1 (vascular endothelial growth factor receptor 1) and Vascular endothelial growth factor C (Vegfc) (151), Matrix Remodeling Associated 8 (MXRA8) (152)
Angiogenesis	VEGF receptor 2 (KDR) (153), Hypoxia-inducible factor 1-alpha (HiF-1α) (154)
Invasion	FHOD1 and PPM1F (155), Fucosyltransferase 4 (FUT4) (156)

EMT	ZEB1 (157), ZEB2 (158) (145, 159) BMI1 (102), USP25 (160), FN1 and moesin (161), zinc-finger protein 217 (ZNF217) (162)
Migration	Cofilin-2 (CFL2) (163), fascin (FSCN1), and myristoylated alanine-rich C kinase substrate (MARCKS), cofilin kinase LIM kinase 1 (LIMK1) and Protein Kinase cAMP-Dependent Regulatory Type I Alpha (PRKAR1A) and PRKACB (164), FLNA (114)
Intravasation	- (miR-200s reduce ability of cells to enter blood stream (165))
Cell survival in circulation	Phospholipase C, gamma 1 (PLCγ1) (via miR-200b/c/429 cluster) (166), Fibroblast activating protein 1 (FAP-1) (167), Phorbol-12-myristate-13-acetate-induced protein 1 (Noxa) (168), TrkB (169), LEPR and ARHGAP19
Extravasation	ZEB1 (170)
Metastatic colonization	CFL2, low-density lipoprotein receptor-related protein 1 (LRP1) and SEC23 homolog A, COPII coat complex component (Sec23a) (165)

Table 3: An overview on the different steps of the invasion-metastasis cascade with possible miR-200c targets. Targets were partly adapted from the reviews of Humphries *et al.* (76) and Mutlu *et al.* (103).

1.4 Aim of the Thesis

The focus of this thesis was to evaluate the two major hallmarks of cancer, chemoresistance and metastasis formation, in the context of breast cancer. Loss-of-function mutations in the tumor suppressor miRNA-200c, consisting of only 23 nucleotides, were shown to alter various target mRNAs at the post-transcriptional level, resulting in tumor development and progression. The goal of this thesis was to investigate novel functions of miRNA-200c in the aforementioned hallmarks of cancer.
The aim of the first part of this work was to combat resistance to chemotherapeutic drugs *in vitro* and *in vivo* via regulation of miRNA-200c expression. Acquired resistance to chemotherapy is a major obstacle for effective treatment. Whether miRNA-200c controls the detoxification of chemotherapeutic agents like doxorubicin and cisplatin via the phase II detoxification, particularly the glutathione pathway, and thus causes resistance, was to be evaluated.
To achieve this, on the one hand, the influence of miRNA-200c on the glutathione pathway and thus the phase II detoxification pathway should be investigated *in vitro*. On the other hand, miRNA-200c was to be assessed as a regulator of the expression of GSTs. Therefore, various *in vitro* and *in vivo* approaches were intended to reveal glutathione S-transferase mu 3 (GSTM3) as a novel target of miRNA-200c.
Finally, to identify a possible beneficial effect of a therapeutic application of miRNA-200c in combination with chemotherapeutic drugs different established approaches should be applied in diverse breast cancer cellular systems (including genetic knockouts, inducible overexpression and inducible decoy of miRNA-200c), but also including additional cancer entities like lung and bladder cancer, as well as in xenograft mouse models. With these investigations, the possible effective therapeutic application to circumvent resistance formation was to be identified, not only *in vitro* but also *in vivo.*
The aim of the second part of this thesis was to explore the metastasis formation of primary breast cancer tumors in distant mouse organs (lung, brain, liver, and spleen) depending on the exclusive miRNA-200c expression status of the TNBC primary tumor. If sole miRNA-200c expression was sufficient to prevent metastasis formation in the xenografts, the reason for this observation was to be elucidated *in vitro*. As migration of the cells is one of the prerequisites for metastasis, this biological process was to be analyzed to explain *in vivo* findings. A pleiotropy of diverse

in vitro approaches was to be performed to validate miRNA-200c as a migration and metastasis suppressor. The migratory behavior of breast cancer cells was to be analyzed on cell clusters, known as collective-cell migration, and on single-cell level. The diversity of all these experiments within this thesis was to be conducted to expand the knowledge of the role of miRNA-200c in chemoresistance and metastasis formation. This might strike new paths in the chemotherapeutic regimens for breast cancer patients to prolong survival and decrease relapse rates if miRNA-200c can be used as a biomarker for the co-application in personalized medicine.

2. Material and Methods

Parts of the material and methods chapter were directly adapted from the original publication, which was published as Köhler *et al.*, Cancers (Basel). 2022 Nov; 14(22): 5554 (see chapter 10.1 Articles).

Combating Drug Resistance by Exploiting miRNA-200c-Controlled Phase II Detoxification

Bianca Köhler, Sviatlana Dubovik, Elisa Hörterer, Ulrich Wilk, Jan Bernd Stöckl, Hande Tekarslan-Sahin, Bojan Ljepoja, Philipp Paulitschke, Thomas Fröhlich, Ernst Wagner, and Andreas Roidl

Author Contributions
Bianca Köhler, Conceptualization, Data curation, Formal analysis, Investigation, Methodology, Project administration, Resources, Validation, Visualization, Writing – original draft, Writing – review & editing, Sviatlana Dubovik, Resources, Elisa Hörterer, Methodology, Ulrich Wilk, Investigation, Jan Bernd Stöckl, Investigation, Hande Tekarslan-Sahin, Investigation, Bojan Ljepoja, Investigation, Philipp Paulitschke, Software, Thomas Fröhlich, Software, Ernst Wagner, Data curation, Funding acquisition, Project administration, Supervision, and Andreas Roidl, Conceptualization, Data curation, Funding acquisition, Methodology, Project administration, Supervision, Validation, Visualization, Writing – original draft, Writing – review & editing

Additionally, parts of this chapter were directly adapted from the original publication which was published as Köhler *et al.*, Mol Oncol. 2024 Oct 15 (see chapter 10.1 Articles).

Unraveling the Metastasis-Preventing Effect of miR-200c *In Vitro* and *In Vivo*

Bianca Köhler, Emily Brieger, Tom Brandstätter, Elisa Hörterer, Ulrich Wilk, Jana Pöhmerer, Anna Jötten, Philipp Paulitschke, Chase P Broedersz, Stefan Zahler, Joachim O Rädler, Ernst Wagner, and Andreas Roidl

Author Contributions

Bianca Köhler, Conceptualization, Data curation, Formal analysis, Investigation, Methodology, Resources, Validation, Visualization, Writing – original draft preparation, Writing – review & editing, Emily Brieger, Data curation, Investigation, Methodology, Resources, Software, Validation, Writing – original draft preparation, Tom Brandstätter, Data curation, Formal analysis, Investigation, Methodology, Resources, Software, Validation, Writing – original draft preparation, Elisa Hörterer, Methodology, Ulrich Wilk, Investigation, Methodology, Resources, Validation, Jana Pöhmerer, Investigation, Methodology, Resources, Validation, Anna Jötten, Data curation, Methodology, Validation, Philipp Paulitschke, Methodology, Supervision, Chase P Broedersz, Supervision, Stefan Zahler, Methodology, Resources, Supervision, Validation, Joachim O Rädler, Supervision, Ernst Wagner, Funding acquisition, Investigation, Methodology, Supervision, and Andreas Roidl, Conceptualization, Data curation, Funding acquisition, Methodology, Project administration, Supervision, Validation, Visualization, Writing – original draft preparation, Writing – review & editing, All authors have read and agreed to the published version of the manuscript.

2.1 Reagents

Doxycycline hyclate (cat. no. D9891), doxorubicin hydrochloride (cat. no. D1515) and cis-platinum(II)diamine dichloride (cat. no. P4394) were purchased from Sigma-Aldrich (St. Louis, MI, USA). Doxycycline hyclate (DOX) was resolved in sterile RNase/DNase-free water (Sigma-Aldrich, St. Louis, MI, USA, cat. no. 95284-1L), stored at -20 °C and used within the experiments at a final concentration of 5 µg/mL. Doxorubicin hydrochloride (DXR) was solved in dimethyl sulfoxide (DMSO) or 0.9 % sodium chloride solution (Deltamedica, Reutlingen, Germany) for animal experiments. Cis-platinum(II)diamine dichloride (CP) was solved in dimethylformamide (DMF). Lipofectamine 3000 was purchased from ThermoFisher Scientific (Waltham, MA, USA, cat. no. L3000008). Synthetic hsa-miR-200c was purchased from AxoLabs (Kulmbach, Germany) with the following sequence:

Sense: 5′ UAAUACUGCCGGGUAAUGAUGGA 3′;

Antisense: 5′ UCCAUCAUUACCCGGCAGUAUUA 3′.

The control siRNA duplex with a scrambled sequence was also obtained from AxoLabs:

Sense: 5′ AuGuAuuGGccuGuAuuAGdTsdT 3′;

Antisense: 5′ CuAAuAcAGGCcAAuAcAUdTsdT 3′.

Hoechst 33342 (cat. no. H1399) for nuclear staining of single cells on dumbbells for the 1D migration was acquired from Thermofisher (Thermofisher, Germany).

2.2 Cell Culture

MDA-MB 231 cells were acquired from DSMZ (Braunschweig, Germany), MDA-MB 231 Tripz 200c and MDA-MB 231 Tripz Ctrl were generated in our lab (114) by Dr. Bojan Ljepoja. All MDA-MB 231 cells were cultured at 37 °C and 0 % CO_2 in Leibovitz's L-15 medium (Sigma-Aldrich) supplemented with 10 % fetal calf serum (FCS, Gibco, ThermoFisher Scientific, Hanover Park, IL, USA). The activation of the inducible system with the tetracycline antibiotic doxycycline hyclate (at a final concentration of 5 µg/mL) results in the expression of either the miRNA-200c sequence (Tripz 200c) or a scrambled control sequence (Tripz Ctrl). Induction of the MDA-MB 231 Tripz 200c cells results in the expression of the miRNA-200c-3p and miRNA-200c-5p. Depletion of the DOX was prevented by adding fresh DOX to the medium every 48 to 72 hours.

The generation of MDA-MB 231 cell lines used for the analysis of metastases in a xenograft mouse model is described in the following section. A second lentiviral transduction was carried out with MDA-MB 231 Tripz 200c and MDA-MB 231 Tripz Ctrl cells in order to generate Luciferase tagged cell lines to enable *ex vivo* Luciferase analysis of the animals' organs. For this purpose, a third generation lentiviral system with the packaging plasmids pRSV-Rev (addgene plasmid #12253), pMDLg/pRRE (addgene plasmid #12251) and pCMV-VSV-G (addgene plasmid #8454) and the transfer plasmid pLenti CMV Puro LUC (w168-1) (addgene plasmid #17477) was transduced. The pRSV-Rev and pMDLg/pRRE plasmids were a gift from Didier Trono, pCMV-VSV-G was a gift from Bob Weinberg and the transfer plasmid was a gift from Eric Campeau & Paul Kaufman (171-173). Subsequently, cells were selected with puromycin dihydrochloride (Sigma-Aldrich, St. Louis, MI, USA, cat. no. P8833-10MG) for 48 hours. Polyclonal cell lines were generated to avoid clonal selection.

MCF7 wildtype (wt) cells were acquired from Cell Line Service (Eppelheim, Germany) and cultured at 37 °C and 5 % CO_2 in high glucose DMEM (Sigma-Aldrich) supplemented with 10 % FCS (Gibco, ThermoFisher Scientific). The MCF7 KO 200c clones M1, M2, and M3 were generated in our lab as previously described (115) by Jonathan García-Roman who performed this TALENs knockout. These cells were cultured according to parental MCF7 (wt) cells. For the analyses the monoclonal MCF7 KO 200c M2 cell line was used and termed MCF7 KO 200c throughout this thesis. This cell line is harboring a stably expressing RFP (red fluorescence protein).

To generate the inducible sponge, MCF7 wt cells were transduced with a 2nd generation lentiviral system comprised of the plasmids pCMV-dR8.2 dvpr (addgene plasmid # 8455) and pCMV-VSV-G (addgene plasmid # 8454). Both plasmids were a gift from Bob Weinberg (172). The transfer plasmid is a modification of the doxycycline-inducible Tripz-Ctrl (ThermoFisher Scientific, #RHS4743) plasmid. The control sequence in the Tripz construct was substituted by the sponge sequence (GCAGAATGGGCATCACAAACCAATT) which consists of 12 repeats. After successful transduction, cells were selected with 5 µg/mL puromycin (Sigma-Aldrich, cat. no. P8833) for 48 h. Subsequently, a monoclonal MCF7 Tripz 200c sponge cell line was generated by performing single-cell dilution. Like the parental MCF7 cell line the MCF7 Tripz 200c sponge was cultivated at 37 °C and 5 % CO_2 in high glucose DMEM (Sigma-Aldrich) supplemented with 10 % FCS (Gibco, ThermoFisher Scientific).

The inducible Tripz 200c construct was additionally stably transfected into A549 wildtype (wt) and T24 wt (purchased from ATCC) cells as previously described (114). A549 Tripz 200c and T24 Tripz 200c were cultured in low glucose DMEM (Sigma-Aldrich) supplemented with 10 % FCS (Gibco, ThermoFisher Scientific) at 37 °C and 5 % CO_2.

All cells were routinely tested for mycoplasm contamination.

2.3 Materials and Methods to Evaluate the Role of miR-200c in Chemoresistance and Migration *In Vitro*

2.3.1 Quantification of RFP Expression in the Inducible Cell Systems

Cells were seeded in triplicates in 96-well plates and subsequently induced with 5 µg/mL DOX per well. Red fluorescence protein (RFP) expression was measured using FACS analysis. The evaluation was performed using FlowJo 7.6.5.

2.3.2 Proteomics Sample Preparation

Twenty-four hours after cell seeding (n = 3), samples were treated with 5 µM DXR for 6 h. After washing the cells three times with cold PBS, they were lysed with 8 M urea in 400 mM ammonium hydrogen carbonate. Cell lysis was assisted with sonication, followed by homogenization using QIAshredder spin columns (Qiagen, Hilden, Germany). Briefly, 20 µg of protein was incubated for 30 min at a final concentration of 5 mM dithioerythritol (DTE) to reduce disulfide bridges. Cleaved disulfide bonds were then alkylated with iodoacetamide (final concentration 15 mM) for 30 min in the dark. After dilution with water to a concentration of 1 M urea, samples were digested over night with 400 ng porcine trypsin (Promega, Madison, WI, USA) at 37 °C. Samples were desalted using C18 spin columns (Pierce, ThermoFisher Scientific) following the manufacturer's recommended procedure.

2.3.3 Proteomics LC-MS/MS Analysis

1 µg of peptides, dissolved in 15 µL solvent A (0.1 % formic acid in water), were injected in an Ultimate 3000 (Thermo Scientific, Waltham, MA, USA) chromatography system and loaded on a capillary trap column (PepMap 100 C18, 100 µm × 2 cm, 5 µM particles, Thermo Scientific). Peptides were subsequently separated at 250 nL/min using an EASY-Spray column (PepMap RSLC C18, 75 µm × 50 cm, 2 µm particles, Thermo Scientific) with a two-step gradient: in the first step, ramping from 5 % solvent A to 25 % solvent B (0.1 % formic acid in acetonitrile) in 160 min, followed by a second ramp from 25 % to 40 % solvent B in 10 min. MS analysis was performed with a QExactive HF-X mass spectrometer. Using data-dependent acquisition, up to 15 MS/MS spectra per precursor scan were acquired. Precursor spectra were acquired

at a resolution of 60,000 (mass-range: 350–1600) and MS/MS spectra at a resolution of 15,000. MS data were deposited in PRIDE. Accessibility possible upon request.

2.3.4 LC-MS/MS Data Analysis

Mass spectrometry (MS) data were processed with MaxQuant (version: 1.6.5.0) using the human subset from Swiss-Prot (downloaded 2 May 2020) and the MaxQuant common contaminants database. The false discovery rate was set to be <0.01 and proteins that were only identified by site or potential contaminants were filtered out. For data analysis and evaluation, Perseus (version 1.6.5.0) was used (174). For label-free quantification (LFQ), samples were grouped and filtered for at least 70 % valid values per group. Missing values were imputed from a normal distribution (width, 0.3; down-shift, 1.8). To test for differentially abundant proteins, a modified two-sided Welch's t-test (s0 = 0.1) was employed. Multiple testing correction was performed with the permutation-based approach included in Perseus, resulting in a false discovery rate of <0.05. The gene set enrichment analysis was carried out using GSEA V4.0.2 (Broad Institute, Cambridge, MA, USA). As gene sets, the gene ontology database as well as the pathway databases REACTOME and KEGG were employed. The mass spectrometry proteomic data have been deposited to the ProteomeXchange Consortium (http://proteomecentral.proteomexchange.org, accessed on 14 October 2021) via the PRIDE partner repository (175) with the dataset identifier PXD029147.

2.3.5 Generation of 3′UTR GSTM3 Mutations in pISO

The 3′UTR fragment of GSTM3 was amplified and cloned downstream of a luciferase reporter system in the pISO vector (Addgene plasmid #12178). Amplification of the 3′UTR fragment of GSTM3 was performed with the following primers (Sigma-Aldrich):

5′-TTACAGAGCTCATCCTGTCCGTAAGGGGTCA-3′ (forward),
5′-TGTAATCTAGAAGTCTGAAATACTGCCTTTATCAC-3′ (reverse).

To generate part or full mutation of the binding site for hsa-miR-200c-3p at the 3′UTR of GSTM3, the reverse primers (Sigma-Aldrich) listed below that contained nucleotide mismatches were used:

Mut 1	5′-TGTAATCTAGAAGTCTGAAACACTGCCTTTATCAC-3′
Mut 2	5′-TGTAATCTAGAAGTCTGAAATACATCCTTTATCAC-3′
Full mutation	5′-TGTAATCTAGAAGTCTGATCACAATCCTTTATCAC-3′

Putative miRNA-mRNA seed-site interactions for hsa-miR-200c-3p were analyzed *in silico* using TargetScan (104, 176, 177). Sequences of 3′UTRs and the predicted site types of the different GSTs were also adapted from TargetScan.

2.3.6 Co-Transfection and Luciferase Reporter Assay

For co-transfection of pDNA and hsa-miR-200c, MCF7 KO 200c M2 cells were seeded in a 6-well plate. Then, 24 h after seeding, cells were transfected with 6 µL Lipofectamine 3000 and 75 pmol hsa-miR-200c or scrambled control siRNA and 1 µg pDNA per well at the same time. After 48 h of incubation, cells were lysed, and a luciferase assay was performed using standard protocol (178).

2.3.7 RNA Lysis and Purification

Cells were induced with 5 µg/mL DOX for 72 h where necessary. Subsequently, cells were treated with the indicated concentration of DXR (or solvent), when 80 % of confluency was achieved. After appropriate incubation with the treatment agent, cells were harvested and purified using the Micro RNA Kit (peqGOLD Micro RNA Kit Safety-Line, cat. no. 732-3088, VWR, Darmstadt, Germany) following the manufacturer's protocol. For RNA lysis of tumor samples, 20 mg of tumor tissue per animal was homogenized in the appropriate lysing buffer (Micro RNA Kit, Safety-Line, peqlab-VWR), using MP Biomedicals™ Lysematrix D, (ThermoFisher Scientific, cat. no. 11432420) in a homogenizer following manufacturer's protocol (peqGOLD Micro RNA Kit, cat. No. 732-3088, VWR).

2.3.8 cDNA Synthesis

Following RNA purification, cDNA was synthesized, according to the manufacturer's protocol, using 1 µg RNA. QScript cDNA Synthesis Kit (Quantabio, Beverly, MA, USA) for mRNA or qScript™ microRNA cDNA Synthesis Kit for miRNA (Quantabio) were used.

2.3.9 Quantitative Real-Time Polymerase Chain Reaction (qRT-PCR)

Messenger RNA expression values were analyzed using qRT-PCR. The LightCycler 480 (Roche, Basel, Switzerland), the Universal Probe Library (UPL, Roche Diagnostics Germany, Mannheim, Germany) and LightCycler 480 Probes Master (Roche Diagnostics Germany) were used. The sample composition was described previously (179). Briefly, 5 µL cDNA with a 1:10 dilution, after cDNA synthesis, were added per well. Primer probe pairs are specified in Table 4. MiRNA expression was also analyzed using qRT-PCR. The sample mixture was prepared according to the manufacturer's protocol (qScript™ microRNA cDNA Synthesis Kit for miRNA, Quantabio), and 10 µL microRNA cDNA (1:50 dilution after cDNA synthesis) was used per well.
The $2^{-\Delta Ct}$ or the $2^{-\Delta\Delta Ct}$ method was used for quantification. GAPDH or hsa-miRNA-191 were utilized as housekeepers.

Proteins	Left Primer	Right Primer	Probe
GSTA1	gagaactattgagaggaacaaagagc	tctcctggaggtttctctaagc	85
GSTA2	agaaacctccaggagactgcta	tctgccccgtatattggagt	53
GSTA3	ctgacattagcctggtggaac	tcagcagagggaagttggag	19
GSTA4	cttcctcttgtcctttgtcctc	tgctgccatgatagcttttc	58
GSTA5	tgcagaagatttggacaagttaag	ggttgtatttgctggcaatg	21
GSTP1	catctccctcatctacaccaacta	aggacctcatggatcagcag	62
GSTM1	aggacttcatctcccgcttt	cccagacagccatctttga	13
GSTM2	catgacactggggtactgga	tcctcgtagcttgagtctgtgt	68
GSTM3	ccaatggctggatgtgaaat	tccaggaggtagggcagat	85
GSTM4	tgacctctctgactgggaca	tctgaaggccagagaaccag	13
GSTM5	tggacgccttcctaaacttg	aaacaaaagacctcggaggaa	13
GSTT1	gtagccatcacggagctgat	gaagaggtcctcccccact	71
GSTT2	gctgtttcttgacctggtgtc	tcttgtgctgccctttgac	28
GSTZ1	cctgcagaacctgtctgtcc	ccacaagtgatggcgttct	55
GSTO1	gcacttttgagctaaggaggaa	caggggattcaggaagtaggt	12
GSTO2	gagatgtgggagagaatgcac	gaaggtggtgttctgatactcaag	8
GSTK1	tatttggctctgaccggatg	ggtatagggcccatccactt	62
MGST1	tcagcatccagttggctttt	aatgggtttaccccagttca	6
MGST2	gggtcaccagagtttgagaga	ccttgaagtgacgctgatga	85

MGST3	actggtgctgccagctttat	tttcagggtccgtgctgta	49
LTC4 S	accatgaaggacgaggtagc	tgcagggagaagtaggcttg	66
FLAP	catcagcgtggtccagaat	caagtgttccggtcctctg	52
GAPDH	tccactggcgtcttcacc	ggcagagatgatgacccttttt	45
hsa-miR−200c−3p	gcgtaatactgccgggtaat	PerfeCTa Universal PCR Primer	
hsa-miR−191	gcgcaacggaatcccaaaag	PerfeCTa Universal PCR Primer	

Table 4: Sequences of qRT-PCR primers and TaqMan qRT-PCR analysis.

For the analysis of the ABCB1 gene, the TaqMan assay (ThermoFisher Scientific) with the TaqMan® Fast Advanced Master Mix (ThermoFisher Scientific, cat. no. 4444557) was used (Table 5) and run on the LightCycler 480. Per sample, 5 µL of Master Mix was pre-mixed with 0.5 µL of the ABCB1 TaqMan assay. GAPDH was used as a housekeeper. Finally, 4.5 µL of a 1:10 dilution of cDNA was added to each well.

Proteins	**Assay ID**
ABCB1	Hs00184500_m1
GAPDH	Hs02758991_g1

Table 5: TaqMan assays for qRT-PCR analyses with the LightCycler 480.

2.3.10 Protein Lysis and Western Blot

Cells were lysed after individual treatment with cell lysis buffer containing cell culture lysis 5 × reagent (Promega, Madison, WI, USA, cat. no. E1531), cOmplete™, Mini, EDTA-free Protease Inhibitor Cocktail (Roche, cat. no. 11836153001) and Sodium orthovanadate (Sigma-Aldrich, cat. no. S6508). Briefly, 30 µg protein (determined via BCA assay, manufacturer's protocol, ThermoFisher Scientific, cat. no. #23228 and #23224) per sample was analyzed. PVDF-membranes were blocked with NET-gelatin prior to overnight incubation at 4 °C with GSTM3-antibody (ThermoFisher Scientific, cat. no. PA5-57191) solution (1:1000) in NET-gelatin or GAPDH-antibody (1:10,000, loading control, Sigma-Aldrich, cat. no. G9545-100 UL). After washing, membranes were incubated in horseradish peroxidase-conjugated anti-rabbit secondary antibody

(goat anti-rabbit-hrp, cat. no. PI-1000, Vector Laboratories, Newark, CA, USA) at room temperature. Desired proteins were detected utilizing enhanced chemiluminescence (Lumi-LightPLUS Western Blotting Substrate, Roche, cat. no. 12015196001) on X-ray films (Amersham Hyperfilm ECL, GE Healthcare, VWR cat. no. 28-9068-39, Darmstadt, Germany). For quantification contrast ratios were analyzed using ImageJ 1.53e. Briefly described, lane profile plots for GSTM3 and GAPDH and corresponding peak areas were measured. Subsequently, all sample areas and all loading-control areas were separately displayed as percent of the total size of measured peaks within the same protein. The relative density of the areas was calculated by ratio determination of the percent of the sample to percent control (always the first sample line of a blot, the corresponding value is 1.0). Final adjusted density values were calculated as the ratio of relative sample density to the relative loading-control density of each sample. Samples are normalized to the control sample (first sample line of a blot).

2.3.11 Analysis of Total Glutathione Using the GSH/GSSG-Glo Assay

Glutathione (GSH) and GSSG were measured using the GSH/GSSG-Glo assay (Promega Madison, WI, USA). Cells were treated with either 0.1 µM DXR for the MCF7 and 0.6 µM DXR or 50 µM CP for MDA-MB 231 in a 96-well format. Tripz-constructs were pre-induced for 72 h with 5 µg/mL DOX before DXR treatment. The assay was performed according to the manufacturer's protocol.

2.3.12 Evaluation of Cell Death Using Propidium Iodide Assay

Cells were treated with DXR or the appropriate solvent control for 72 h prior to FACS measurement. MCF7 cells were treated with 0.1 µM DXR, MDA-MB 231 cells with 0.6 µM DXR or 50 µM CP, A549 cells with 0.06 µM DXR or 8.5 µM CP and T24 cells with 0.05 µM DXR or 3.5 µM CP. The inducible constructs were 24 h pre-induced with 5 µg/mL DOX before DXR treatment. Propidium iodide (PI) staining was performed by harvesting the floating cells as well as the detached cells after trypsinization. Cells were incubated for three hours with intermittent shaking at 4 °C with 50 µg/mL PI solution. Subsequently, the cell cycle was analyzed using FACS. Evaluation of the cell cycle phases was performed using FlowJo 7.6.5.

2.3.13 Analysis of Long-Term Effects of hsa-miR-200c *In Vitro* Using the Cellwatcher System

The same number of MDA-MB 231 Tripz 200c cells was seeded and either induced with 5 µg/mL DOX or not. The medium was changed every 48 – 72 h (containing DOX or not). When the cells reached a confluency of 80 %, they were treated with 0.1 µM of DXR for 48 h followed by medium change. Confluency was monitored over a time of 800 h using the PHIO cellwatcher (PHIO scientific, Munich, Germany).
After termination, cells were washed with ice-cold PBS, fixed with methanol for 10 min and placed on ice, for colony formation assay. Briefly, 0.5 % crystal violet in 25 % methanol was applied at room temperature for 10 min to the cells and subsequently washed with water.

2.3.14 Proliferation Analysis Using the PHIO Cellwatcher

Cells were seeded and induced with 5 µg/mL DOX where indicated. Every 48 to 72 hours new DOX was added to the cells to compensate for depletion. The proliferation was determined as the doubling time value. The proliferation curve was analyzed by taking the confluency values between 30 % and 60 % into account. Doubling time was calculated using the equation of the best fit line and calculating the interval between 30 % and 60 % confluency.

2.3.15 Clinical Impact Using Kaplan–Meier Plotter

The clinical impact of hsa-miR-200c (gene symbol: hsa-miR-200c) (180) and GSTM3 (gene symbol: 202554_s_at) (181) was analyzed using the Kaplan-Meier plotter (https://kmplot.com/analysis/) (accessed on 3 November 2022) (182). Overall survival was depicted for the miRNA analysis, and for the mRNA analysis, the relapse-free survival is shown additionally restricted to the cohort of basal breast cancer subtype and neoadjuvant chemotherapy treatment. Further parameters used for the analysis can be found in the Supplementary Figure S8.

2.3.16 *In Vitro* Confined Cell Motility Analysis (1D Dumbbells)

Single-cell motility was monitored on 1D dumbbell micropatterns. For micropatterning the surface of the ibiTreat µ-dish (ibidi, Germany, cat. no. 81156) was passivated with a small drop of 0.01 % (w/v) PLL (Sigma-Aldrich, cat. no. P8920-100ML). After incubating the dish for 30 minutes with PLL at room temperature, it was rinsed with HEPES buffer (pH = 8.3, Thermo scientific, cat. no. J16924-AP) and subsequently 100 mg/mL of mPEG-SVA (LaysanBio, cat. no. NC0107576) diluted in 0.1 M HEPES were evenly distributed. The dish was further incubated at room temperature for at least 1 hour before rinsing with milliQ water. The passivated dish was then photopatterned using the PRIMO module (Alvéole, France) mounted on an automated inverted microscope (Nikon Eclipse Ti). After passivation, PLPP gel (Alvéole) was diluted in 99 % ethanol to distribute the gel evenly throughout the surface. The dumbbell-shaped pattern was placed on top of the dish via the Leonardo software (Alvéole) and illuminated with UV-light with a dose of 15 mJ/mm^2. Next, the dish is washed with milliQ water and rehydrated with PBS for 5 minutes followed by an incubation with 20 µg/mL of labelled Fibronectin-Alexa647 (Y-proteins cat. no. 663, Thermo Fisher, cat. no. A37573) for 15 minutes at room temperature. Once the dish was washed with PBS a total number of 10,000 cells, when appropriate 72 hours treated with DOX prior to seeding, were added and left to adhere for at least 4 hours. After that, the medium was exchanged to medium without phenol red containing Hoechst 33342 at a final concentration of 25 nM for nuclear staining. If necessary, medium was additionally supplemented with 5 µg/mL DOX. All confined motility measurements were performed in time-lapse mode for 48 hours on a Nikon Eclipse Ti microscope using a 10× objective. The experiments were carried out at cells' specific cultivating conditions using a heated chamber (Okolab) at 37 °C. Images (brightfield and DAPI) are acquired every 10 minutes. Cell tracking of the nuclei was performed by using TrackPy (Python Version 3.10.5). 89 tracks of the MDA-MB 231 Tripz Ctrl +DOX, 85 tracks of the MDA-MB 231 Tripz 200c -DOX and 94 tracks of the MDA-MB 231 Tripz 200c +DOX were analyzed. Each single measurement was conducted for at least 48 hours, but track length varied between 8 hours (minimum) and 48 hours (maximum). To quantify the dynamics of confined cell migration, we analyzed the stay probability (former also termed survival probability (183)) S(t). This is the probability that a cell has not transitioned from one island to the other after a time

interval of length t. The stay probability was calculated from the distribution of dwell times p(τ). The dwell time τ here is the time a cell spent on its own island before it transitioned to the other island. Transition events were detected in the cell trajectories, allowing the measurement of τ. The stay probability was then computed through:

$$(1) \qquad S(t) = 1 - \int_0^t p(\tau)\, d\tau$$

For more information, refer to Brückner *et al.* (183). Finally, from the trajectories, the speed of the cells on the bridge was measured through v=(x(t+Δt)-x(t))/Δt, where x(t) and x(t+Δt) are two consecutive positions of the cell nucleus and Δt is the measurement interval of tracking the cells. This results in an additional characterization of the hopping dynamics. The average of this speed was displayed, and error bars represent the error of the mean. To gain more detailed insight into the dynamics of cell hopping, a physical model for cell migration within our micropattern was inferred. The complexity of cell migration was reduced by employing a coarse-grained description of cell migration: we capture the dynamics for the nucleus position x and the nucleus velocity v using an underdamped Langevin equation, and used a previously developed method to directly infer such an equation from experimental data (183):

$$\frac{dx}{dt} = v$$

$$(2) \qquad \frac{dv}{dt} = F(x, v) + \sigma\eta(t)$$

Here $F(x, v)$ is an effective force that describes the deterministic component of how the cell nucleus is accelerated at a given position and velocity. This effective force encodes how the migrating cell interacts with the geometric confinement of the micropattern. To capture the stochasticity of cell migration, leading to a wide variety of different cell behaviors, a dynamical noise term ση(t) is included that adds to the acceleration of the nucleus, where σ is the noise amplitude and η(t) is a Gaussian white noise with ⟨η(t)⟩=0 and ⟨η(t)η(t')⟩=δ(t-t'). Using a statistical learning framework called Underdamped Langevin Inference (ULI) (184), the deterministic and the stochastic terms in the Langevin equation were inferred from our experimental trajectory data. This approach has the advantage that a specific form for $F(x, v)$ and a specific value for σ were not *a priori* assumed based on physical principles. Instead, the experimental rigorously constrained the form and value of these terms. We refer to Brückner *et al.* for more details (184). From the inferred model, the structure of $F(x, v)$ was analyzed,

which provided information on the underlying qualitative features of the hopping dynamics as represented.

For experiments with MCF7 10,000 cells were seeded on the micropatterned ibiTreat µ-dish (ibidi GmbH) and left to adhere for at least 4 hours. The further implementation of the experiments corresponds to the method already mentioned besides the size of the micropattern for MCF7 which was adjusted and 1.3x bigger than that of MDA-MB 231 cells. This was because MCF7 cells are approximately 1.3x bigger than MDA-MB 231 cells. 62 tracks of the MCF7 wt and 44 tracks of the MCF7 KO 200c cells were analyzed. Each single measurement was conducted for at least 48 hours, but track length varied between 8 hours (minimum) and 48 hours (maximum). Every 10 minutes one image was taken.

2.3.17 Analysis of Single- and Collective-Cell Motility Using Transwell Assays

Migration analysis was performed in a transwell assay using Falcon Cell Culture Inserts with a membrane pore size of 8 µm (Corning, Kaiserslautern, Germany, cat. no. 353097) in a 24-well format. Inserts (n = 3) were filled with 500 µl of appropriate medium supplemented with 0.5 % FCS and 100,000 cells. MDA-MB 231 Tripz 200c cells were either 72 hours pre-induced with DOX (5 µg/mL) before seeding and induced with DOX as mentioned or not. Wells were filled with 750 µl corresponding medium supplemented with 10 % FCS. Cells were incubated 18 hours and subsequently excess of the cell suspension was removed and the insert was carefully washed with PBS. For permeabilization, inserts were incubated 20 minutes with 100 % methanol. After washing, inserts were placed into 0.5 % crystal violet solution containing 25 % methanol for 15 minutes. Excess of the solution was removed by washing the inserts several times with water and subsequently the inserts were dried overnight. Microscopic pictures of migrated cells were taken with a 5× magnification of the central part of the membrane. These pictures were analyzed using the ImageJ 1.53e software. To determine the quantity of migrated cells, pictures were binarized and the “area” of black pixels was calculated. Relative migration is presented by normalization to the wildtype cell line.

2.3.18 Analysis of Undirected (Random Walk) and Directed Migration (Scratch Assay) in Cell Clusters

For the random walk experiments cells were seeded with a concentration of 50,000 cells per well (n = 3). MDA-MB 231 Tripz 200c and Ctrl were pretreated with DOX for 72 hours before seeding if appropriate. Alterations in the motility of the cells were monitored using a PHIO Cellwatcher M (PHIO scientific GmbH, Munich, Germany). Motility behavior of the cells was evaluated between 30 and 80 % confluency. Motility in µm/h was described for this condition as well as the mean motility of the triplicates for every specific confluency. Additionally, pictures of the MCF7 wt and KO 200c clusters formed after 50 hours of cultivation were taken using the Cellwatcher M.

Scratch assays were performed in 8-well coverslides (ibidi, Gräfelfing, Germany, cat. no. 80826) and cells were seeded 24 hours prior to performing the scratch in 100 % confluent cells. MDA-MB 231 Tripz 200c cells were pre-induced for 72 hours with DOX when appropriate. Nuclei of the cells were stained with the live cell imaging probe siR-DNA, Spirochrome (tebu-bio, Rodgau, Germany, cat. no. 251 SC007). Cells were stained with 1 µM siR-DNA solution and subsequently migratory behavior of the cells was recorded under a confocal-microscope (Leica SP8) for 24 hours. Microscope settings: A 10×/0.30 DRY objective and hybrid detector (Leica HyD 641 nm – 777 nm) for siR-DNA fluorescence detection and a photomultiplier (PMT) were applied. The Diode 638 laser for the laser line of 638 nm was used. Live cell imaging was conducted with a frame rate of 1 per 5 minutes. Data was obtained with the LAS X software 3.5.7.23225. Migration was quantified by determining the closure of the scratch. Therefore, occupied area by cells was defined at 0 and 10 hours after scratching for the MDA-MB 231 cells and 14 and 24 hours after scratching for the MCF7 cells. All cells were stained as mentioned previously and pictures show siR-DNA labeled cells at the indicated timepoints. The difference in area in % was quantified using the Fiji plug in “Wound healing size tool” (185). The blue lines define the boarders of the scratch which were automatically calculated with the same parameters within each live cell imaging sample. Additionally, the number of cells migrating into the free space as well as the confinement ratio were analyzed. To be able to identify cells entering the free area, blue lines were hand-drawn indicating the wound-boarder at 0 hour (MDA-MB 231) and 14 hours (MCF7) after scratch performance. The number of cells which

moved into the free area of the scratch was calculated manually after 10 hours. The confinement ratio of each cell was quantified by converting the images to 8bit, using bandpass filter and subtracting the background. Subsequently the Fiji plug in “TrackMate” (DOG detector 15 pix., LAP tracker 15 pix.) was utilized to obtain the tracks (186). Motility behavior of the MDA-MB 231 cells was further analyzed by dividing the cells within a scratch experiment in cells of the “migratory front” and the dense cell clusters named “bulk”. The migratory behavior of cells of these two regions (further subdivided into left and right side, n = 10) was quantified using the “Chemotaxis and Migration Tool” Version 2.0 from ibidi GmbH (Germany) by determining the directionality of the cells. To calculate the directionality of a cell the ratio of the Euclidian distance to the accumulated distance was used. Accumulated distance in µm was determined using the “Chemotaxis and Migration Tool” Version 2.0 (stand-alone) from ibidi GmbH (Germany). Position of the cells in X and Y axis was taken from the TrackMate analysis. Within each condition the movement of cells was summarized as the number of cells migrating to the right or left side (numbers indicated within the graphs). Red trajectories indicated movement of these cells into the scratch to close it. The difference between MDA-MB 231 cells with and without miR-200c expression was quantified by comparing the directionality of the front and bulk cells (n = 80 cells, 20 cells per biological replicate (4 replicates in total), right and left side were cumulated).

2.3.19 Quantification of Cluster Cell Migration in Cell Aggregates in Collagen

Cell solutions of 100,000 cells/mL (MDA-MB 231) or 20,000 cells/mL (MCF7) were prepared to generate 3D cell aggregates with the hanging drop method. Drops of 20 µl solution were pipetted into the lid of a petri dish and cultivated for 24 hours at the appropriate conditions. If necessary, cells were 72 hours pre-induced with DOX. A 2 mg/mL collagen (rat tail collagen I, ibidi, cat. no. 50201) base layer was distributed evenly into the wells and gelled at 37 °C. Aggregates were embedded in a final collagen concentration of 2 mg/mL following the manufacturer’s protocol using 10 x M199 medium and 1 x complete DMEM high glucose medium for MCF7 cells and 1 x complete L-15 medium (supplemented with DOX if needed) for MDA-MB 231 cells. Finally, medium was added on top of the embedded 3D aggregates and changed every 48 to 72 hours with fresh complete medium. Images of the 3D aggregates were taken with the inverted fluorescence phase microscope (Axiovert 200, Zeiss, Germany,

10x objective lens) at regular intervals as presented in this study. Quantification of the migratory behavior of 3D cell clusters in collagen matrix was achieved using ImageJ software analyzing the area of the aggregates at different time points. To calculate the total area of an aggregate, the outline of the entire aggregate was determined to scale (line shown in red). The core of the aggregate is the part that is characterized by dark contours that are caused by changes in the refraction of light in the object (displayed as a green line). The area of migrated cells is calculated as the difference between the whole and the core area of an aggregate in μm^2. Additionally, the perimeter of each cell aggregate was determined (red line). In total at least n = 4 aggregates per cell line were analyzed.

3D cell aggregates were further characterized using ImageJ. The perimeter of at least n = 4 cell aggregate was determined (red line) as well as the area of the aggregates. Both were normalized to the initial values of the aggregates at day 0. Finally, the coefficient of determination of a theoretically perfect circle was compared to the coefficient of determination of MCF7 KO 200c and wt cell aggregates. Therefore, the mean area in μm^2 and the mean perimeter in µm of the cell aggregates were plotted for each time point. To determine the values of the perfect circle pre-defined numbers for the area were inserted into the equation: $area = \pi * R^2$ and the radius (R) was calculated. Using the following equation: $perimeter = 2 * \pi * R$ the corresponding perimeter values were calculated and plotted (187, 188).

2.3.20 Cell Survival Quantified with an Anoikis Assay

One million cells with either miR-200c expression or without were seeded in uncoated culture dishes (100 mm growth area) and were incubated with intermitted shaking at 37 °C. MCF7 cells were incubated for 24 hours, and MDA-MB 231 cells were incubated for 96 hours in suspension prior to the analysis of cell survival. The percentage of live cells was determined performing trypan blue staining (1:1 dilution factor) and subsequent analysis with the TC20 automated cell counter from Bio-Rad (Bio-Rad Laboratories, Germany, cat. no. 145-0101). Living cells are bypassing anoikis pathways. Therefore, the effect of loss of cell-matrix contact was presented as the percentage of live cells.

2.4 Materials and Methods to Evaluate the Role of miR-200c in Chemoresistance and Metastasis Formation *In Vivo*

2.4.1 *In Vivo* Xenograft Studies of hsa-miR-200c as Genetic Biomarker for Chemoresistance

Five million human MDA-MB 231 Tripz 200c cells were injected s.c. into the left flank of 6-week-old female NMRI-nu mice (Janvier, Le-Genest-St-Isle, France). Tumor growth was monitored using caliper measurement ($a \times b^2 /2$; a = longest side of the tumor; b = widest side vertical to a) (189). Animal well-being and weight were monitored throughout the whole experiment. Mice were either fed continuously with a regular diet or with doxycycline containing diet (+ 625 mg/kg doxycycline, sniff Spezialdiäten, Soest, Germany, cat. no. A115 D70624) depending on the animal study.
Initial tumor growth was monitored from the day of tumor cell injection till the day when the first animal of each diet group reached the tumor volume of 150 to 200 mm^3.
At this tumor size, mice were randomized into four groups depending on the subsequent treatment regime for the animal experiment “(I) Treatment of hsa-miR-200c positive and negative tumors”. Each diet group was subdivided into a group of animals with either DXR treatment (5 mg/kg) or control treatment with saline (0.9 % sodium chloride solution). For the animal experiment “(II) Single or double treatment of hsa-miR-200c negative tumors” tumors grew *ab initio* under regular diet conditions. When tumors reached approximately 150 mm^3 mice were randomized into 4 groups: regular diet and control treatment (−DOX −DXR), regular diet and DXR treatment with 5 mg/kg (−DOX +DXR, single DXR treatment), DOX diet and control treatment (+DOX −DXR, single hsa-miR-200c treatment) and DOX diet and DXR treatment (+DOX +DXR, double treatment). A cohort of 5 mice per group was used for animal study I and 10 mice per group were used for the xenograft mouse model II. Treatment day 0 correlates with the day of reaching 150 to 200 mm^3 of tumor size. On days 0, 7, 14 and 21 each mouse was injected i.v. with the appropriate treatment. Where indicated mice diet was switched to the DOX diet on day 0 of the treatment. Mice were sacrificed by cervical dislocation once their tumor reached a tumor diameter bigger than 12 mm.
The control cell line MDA-MB 231 Tripz Ctrl was injected as described above into the left flank of 6-week-old female NMRI-nu mice. Mice were beforehand divided into two

diet groups (n = 5), normal or DOX diet. Mice were sacrificed by cervical dislocation once their tumor reached the critical size of 800 mm^3.
All animal experiments were performed according to the guidelines of German law for the protection of animal life and were approved by the district government of Upper Bavaria, Germany. Reference number: ROB-55_2-2532_Vet_02-19-20.

2.4.2 H&E Staining of *In Vivo* Tumors

H&E staining was performed as described earlier (190). Shortly, tumors were extracted upon euthanasia and fixed for at least 48 hours in 4 % paraformaldehyde (PFA). For histological evaluation the fixed tumors were embedded into cassettes and washed two hours thoroughly with water. After dehydration in a series of alcohol solutions and finally xylene using the Thermo Shandon Excelsior, a tissue processor, tumors were embedded into paraffin. With the microtome tumors were sliced into tissues of 2.5 µm thickness and transferred onto object slides. Finally, the H&E staining was performed including the following steps: immersion of slides in xylene twice for 15 minutes each, then 5 minutes in each ethanol concentration (100 % to 96 % to 70 %) and shortly in demineralized water. Thereupon, the slides were stained with haemalaun for 2 minutes, subsequently followed by a 5-minute wash with water. Next, tumors were stained with eosin for 5 minutes. After staining and washing with water, slices were incubated in each ethanol concentration (70 % to 96 %) and subsequently in 100 % for 5 minutes and lastly twice in xylene for 10 minutes each. Dry slides were capped off with mounting medium and covered with a glass slip for protection.

2.4.3 Analysis of Metastatic Formation in Distant Organs of Mice with or without miR-200c-Expressing Breast Cancer Tumors

A total number of five million human MDA-MB 231 Tripz 200c Luc cells were injected s.c. into the left flank of twenty 6-week-old female Rj: NMRI-Foxn1nu/Foxn1nu mice (Janvier, Le-Genest-St-Isle, France). Due to a mutation in the Foxn1 gene, the outbred strain exhibits T cell immunodeficiency and lack of body hair (191). Mice were kept in isolated ventilated cages (IVC type II long, Tecniplast, Hohenpeißenberg, Germany) under specific pathogen-free (SPF) conditions in an air-conditioned room with a 12-hour day/night cycle. Animal welfare, room temperature (24 - 26 °C) and humidity

(40 - 60 %) were controlled daily in accordance with §11 of the German Animal Welfare Act (192). Prior to the start of experiments, the animals were allowed to acclimate to their new environment for at least 7 days. Autoclaved feed (Ssniff Spezialdiäten, Soest, Germany) and water were provided *ad libitum*. Mice were randomized into two experimental groups when their tumor reached a size of approximately 200 mm^3. One group was kept with the original, normal feed, whereas the second group of mice was switched to doxycycline containing feed (+ 625 mg/kg doxycycline, sniff Spezialdiäten, Soest, Germany, cat. no. A115 D70624) in order to induce miR-200c expression. Mice were kept with their corresponding diet until the end of the study.

Additionally, a control study was performed to exclude DOX effects. Therefore, eighteen mice were randomized into two groups beforehand. One group was fed with normal feed (n = 7) and the second group of mice was nourished with DOX feed (n = 11) throughout the study. Five million MDA-MB 231 Tripz Ctrl Luc cells were injected into these mice. Tumor growth as well as animal well-being and weight were monitored over the entire period.

To analyze the impact of a chemotherapeutic treatment on the metastatic burden of mice with or without miRNA-200c expression in the primary tumor, two additional groups were added to the study. Five million MDA-MB 231 Tripz 200c Luc cells were inoculated into twenty mice. After reaching a tumor size of around 200 mm^3 mice were randomized into two groups with ten animals each. One group was further kept with the normal diet and was treated once a week with 5 mg/kg doxorubicin for four weeks. Treatment days have been day 0 (day of reaching a tumor size of 200 mm^3), day 7, 14 and 21. The second group of mice was switched to DOX feed *ad libitum* and treated additionally with doxorubicin as indicated in group one.

Tumor growth was monitored throughout the whole study using caliper measurement as described previously. Criteria for euthanasia were set to a critical tumor size which was achieved when the tumor diameter was bigger than 12 mm. Mice were sacrificed by cervical dislocation when they reached the critical tumor size. If necessary, mice were sacrificed also before reaching the critical tumor size due to animal well-being reasons.

All animal experiments were performed according to the guidelines of German law for the protection of animal life and were approved by the district government of Upper Bavaria, Germany. Reference number: ROB-55_2-2532_Vet_02-19-20.

Immediately after euthanasia, mice were dissected, and their organs removed for *ex vivo* Luciferase analysis. Brain, lung, liver, and spleen were further washed with PBS to remove any blood residuals and subsequently frozen overnight at -80 °C. Before luciferase activity measurement, organs were thawed and weight. Each organ was homogenized with a lysis solution containing a 1:5 dilution of Luciferase Cell Culture Lysis 5X Reagent (Promega, Madison, WI, USA, cat. no. E1531) in Millipore water supplemented with 1 % (v/v) protease and phosphatase inhibitor cocktail (Protease and Phosphatase Inhibitor Cocktail, Sigma-Aldrich, cat. no. PPC1010). Homogenization was carried out in different rounds: 4 times with 6 m/s and 2 times with 6.5 m/s intermitted by cooling on ice using MP Biomedicals™ Lysematrix D (ThermoFisher Scientific, Waltham, MA, USA, cat. no. 11432420) in a homogenizer (MP Biomedicals™ FastPrep-24, ThermoFisher Scientific, cat. no. 12079310). Samples were frozen overnight at -80 °C to allow further cell lysis. Test specimens were thawed and subsequently centrifuged at 13,300 rpm for 10 minutes at 4 °C. Luciferase activity was measured in 50 µl of the appropriate supernatant together with 100 µl of LAR buffer solution with 5 % (v/v) of a mixture of 10 mM luciferin and 29.375 mM glycylglycine. LAR buffer components: 20 mM glycylglycine, 1.0 mM $MgCl_2$, 0.10 mM EDTA, 3.3 mM DTT, 0.55 mM ATP, and 0.27 mM coenzyme A adjusted to a pH of 8 – 8.5. Measurements were carried out in triplicates. Relative light units per gram organ (RLUs/g) were calculated as mean with SD. The livers were measured in two separate runs due to their greater weight and RLUs were finally calculated for the whole organ. Values smaller or equal to the values of the control measurement (solely lysis buffer) were set to zero and the organ was termed metastases free.

2.5 Software

The Figure 10A and B, as well as the subfigure Figure 15C were created with BioRender.com.

2.6 Statistical Analysis

Statistical significance was calculated utilizing GraphPad Prism 7.04. To compare two samples an unpaired two-tailed Student’s t-test was used, and to compare more than

two samples the one-way ANOVA with Tukey's Multiple Comparison Test or 2 way ANOVA with Šídák's or Tukey's multiple comparison test was applied. Utilizing box and whisker plots the median with SD is displayed as well as the mean ("+") if not stated otherwise. * $p < 0.05$, ** $p < 0.01$, *** $p < 0.001$, **** $p < 0.0001$. Values are displayed as mean with SD if not stated otherwise.

3. Results Chapter I: MicroRNA-200c Prevents Drug Resistance by Downregulating Glutathione S-transferases

This chapter was directly adapted from the original publication, which was published as Köhler *et al.*, Cancers (Basel). 2022 Nov; 14(22): 5554 (see chapter 10.1 Articles).

Combating Drug Resistance by Exploiting miRNA-200c-Controlled Phase II Detoxification

Bianca Köhler [1], Sviatlana Dubovik [1], Elisa Hörterer [1], Ulrich Wilk [1], Jan Bernd Stöckl [2], Hande Tekarslan-Sahin [1], Bojan Ljepoja [1], Philipp Paulitschke [3], Thomas Fröhlich [2], Ernst Wagner [1] and Andreas Roidl [1,*]

[1] Pharmaceutical Biotechnology, Department of Pharmacy, Ludwig-Maximilians-Universität München, D-81377 Munich, Germany

[2] Laboratory of Functional Genome Analysis (LAFUGA), Gene Center, Ludwig-Maximilians-Universität München, D-81377 Munich, Germany

[3] PHIO Scientific GmbH, Esswurmstr. 16, D-81371 Munich, Germany

* Corresponding author

3.1 Proteomic Analysis of a hsa-miR-200c Knockout upon Doxorubicin Treatment Reveals a Higher Abundance of the Glutathione Pathway

Several reports and reviews state that hsa-miR-200c is involved in drug resistance (3, 54, 61, 76, 103). However, an in-depth analysis of the underlying mechanisms is lacking. Therefore, a proteome analysis was performed to evaluate the impact of altered hsa-miR-200c expression in the presence of chemotherapeutic treatment. Treated with doxorubicin (DXR), the wildtype (wt) epithelial luminal A breast cancer cell line MCF7 with high endogenous hsa-miR-200c expression was studied in comparison to three MCF7 hsa-miR-200c monoclonal knockout (KO) cell lines (M1, M2 and M3) (115). A total number of 3890 proteins was identified in this approach (Figure 3A). The principal component analysis (PCA) of protein profiles depicted a clear separation indicating prominent differences between the KO and the wt cell lines when treated with DXR (Figure 3B). To identify differentially expressed proteins among

the cell lines, a modified *t*-test (FDR < 0.05) was conducted, and the results were visualized in a volcano plot (Figure 3C). Here, 340 proteins were ascertained as significantly up- or downregulated in the KO cell lines compared to the unmodified parental MCF7 cell line. The top 10 most altered proteins are presented in Figure 3D. The majority of proteins, listed in Figure 3D, are part of cancer-relevant pathways such as proliferation (e.g., STX4, SCIN, TXNRD1), apoptosis (e.g., ESPL1, CD44, ATP2A3, RALB, SCIN, TIMP3) and migration (e.g., S100P, CD44, STX4, LCP1). Strikingly, glutathione S-transferase mu 3 (GSTM3), a protein that is involved in the detoxification of xenobiotics, such as doxorubicin, is highly upregulated in the hsa-miR-200c KO cell lines. Glutathione S-transferases (GSTs) convert xenobiotics to less toxic derivates and help to excrete them from the cells by conjugating glutathione to the drugs (65) and therefore play a crucial role in drug resistance of tumors (71). To further identify affected pathways, a gene set enrichment analysis (GSEA) was performed. Here, overexpression of the Gene Ontology (GO) term “glutathione metabolic process” was detected. Besides GSTM3, three other altered glutathione S-transferases were identified, namely GSTK1, GSTZ1 and MGST1 (Supplementary Figure S1A) and depicted in a heat map (Supplementary Figure S1B). Additionally, unsupervised hierarchical clustering was accomplished on the proteins included in the GO term. (Supplementary Figure S1C). Summarizing the performed proteomic analysis, evidence is shown that MCF7 KO cells, lacking hsa-miR-200c expression, upregulate a number of resistance-relevant proteins, amongst them several of the glutathione pathway, which are important for the detoxification of drugs.

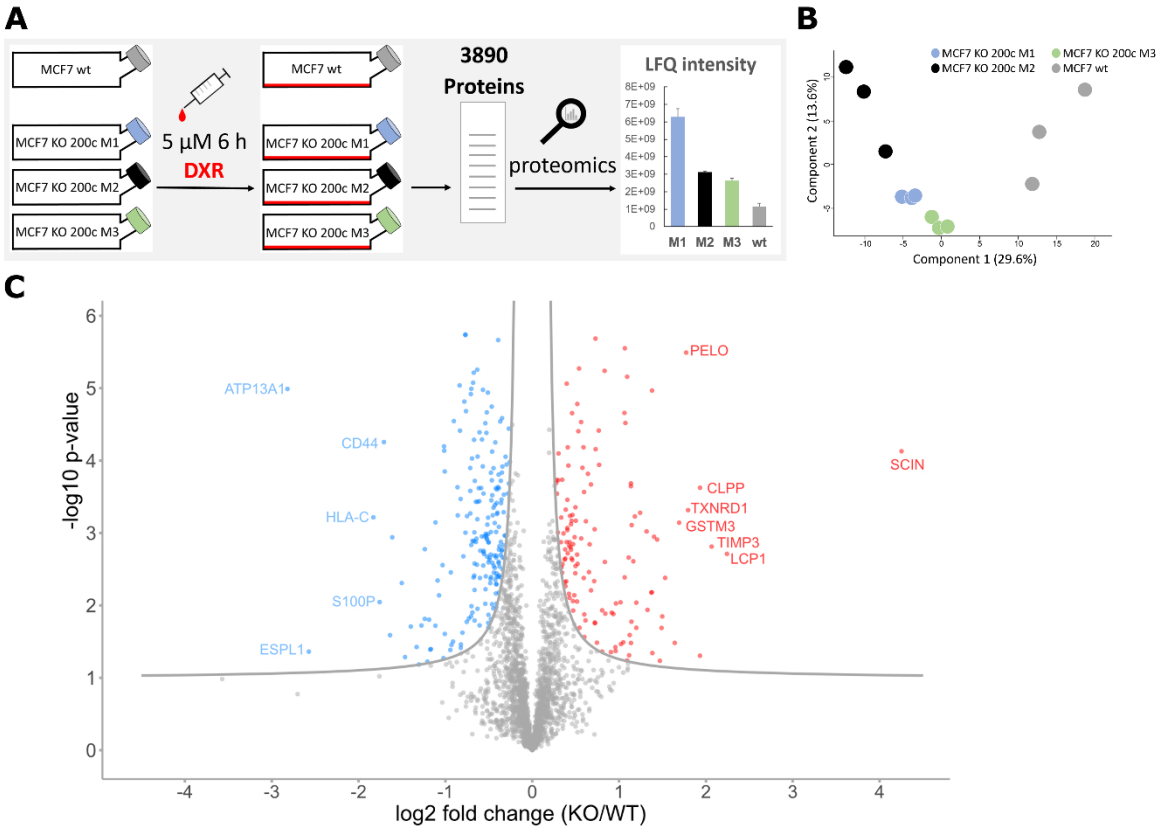

D

Rank	Protein names	Gene names	-Log (p-value)	Difference
1	Adseverin	SCIN	4.13	4.25
2	Plastin-2	LCP1	2.71	2.24
3	Metalloproteinase inhibitor 3	TIMP3	2.81	2.07
4	ATP-dependent Clp protease proteolytic subunit, mitochondrial	CLPP	3.62	1.93
5	Cysteine and glycine-rich protein 1	CSRP1	1.30	1.93
6	Thioredoxin reductase 1, cytoplasmic	TXNRD1	3.32	1.79
7	Protein pelota homolog	PELO	5.49	1.77
8	Glutathione S-transferase Mu 3	GSTM3	3.14	1.69
9	NADH dehydrogenase [ubiquinone] iron-sulfur protein 5	NDUFS5	1.48	1.64
10	Nuclear pore complex protein Nup133	NUP133	2.38	1.53

Rank	Protein names	Gene names	-Log (p-value)	Difference
1	Manganese-transporting ATPase 13A1	ATP13A1	4.99	-2.82
2	Separin	ESPL1	1.36	-2.57
3	HLA class I histocompatibility antigen, Cw-7 alpha chain	HLA-C	3.22	-1.83
4	Protein S100-P	S100P	2.05	-1.76
5	CD44 antigen	CD44	4.25	-1.71
6	Rab11 family-interacting protein 1	RAB11FIP1	1.59	-1.64
7	Sarcoplasmic/endoplasmic reticulum calcium ATPase 3	ATP2A3	2.94	-1.61
8	Ras-related protein Ral-B	RALB	2.31	-1.50
9	Heme oxygenase 2	HMOX2	1.29	-1.46
10	Syntaxin-4	STX4	1.71	-1.40

Figure 3: A proteomic analysis revealed novel hsa-miR-200c targets and altered signaling pathways in the field of detoxification from chemotherapy. **(A)** Experimental design of the proteomic approach of three monoclonal hsa-miR-200c knockout (KO) cell lines (M1: blue, M2: black and M3: green) vs. the parental MCF7 wt cells (gray) upon 6 h of 5 µM doxorubicin (DXR) treatment (n = 3). **(B)** Principal component analysis (PCA) of the hsa-miR-200c KO clones and MCF7 wt proteome profiles. Numbers in parentheses indicate the percentage of variation each component explains. **(C)** Volcano plot showing regulated proteins upon doxorubicin treatment in hsa-miR-200c positive MCF7 breast cancer cells vs. hsa-miR-200c KO cells. Significantly regulated proteins are indicated in red (upregulated) or blue (downregulated). **(D)** Top 10 list of proteins being significantly upregulated (upper table) or downregulated (bottom table) in DXR-treated MCF7 KO 200c cells compared

to DXR-treated MCF7 wt. All genes are ranked for the biggest difference to MCF7 wt cells.
Sample preparation was generously performed by Dr. Ann-Katrin Sommer-Joos (Pharmaceutical Biotechnology, Department of Pharmacy, Ludwig-Maximilians-Universität München, Germany). Data collection of the proteomics experiment including LFQ intensity, principal component analysis, volcano plot and the Top 10 protein lists was performed by Dr. Jan Bernd Stöckl and Dr. Thomas Fröhlich (Laboratory of Functional Genome Analysis (LAFUGA), Gene Center, Ludwig-Maximilians-Universität München, Germany). The principal component analysis figure was adapted from, and the volcano plot figure was directly designed by Dr. Jan Bernd Stöckl and Dr. Thomas Fröhlich (Laboratory of Functional Genome Analysis (LAFUGA), Gene Center, Ludwig-Maximilians-Universität München, Germany). Writing of the corresponding text was generously performed by Dr. Jan Bernd Stöckl (Laboratory of Functional Genome Analysis (LAFUGA), Gene Center, Ludwig-Maximilians-Universität München, Germany) and adapted when appropriate.

3.2 Glutathione S-Transferase mu 3 Is a Novel Target of hsa-miR-200c-3p

Next, glutathione S-transferases as potential targets of hsa-miR-200c-3p were investigated in more detail. The family of GSTs can be classified into eight subgroups, consisting of one to five members (Figure 4A). Potential hsa-miR-200c-3 p target sites were found *in silico* throughout all GST families. Eight transferases show either a 7mer-m8, 8mer or a 7mer-A1 predicted binding site for hsa-miR-200c in their 3′UTR region (Figure 4B and Supplementary Figure S2A). To analyze whether the identified sites are crucial for the regulation by hsa-miR-200c, the GSTM3 3′UTR was chosen as an exemplary target sequence and validated by a luciferase reporter assay. Part of the wt 3′UTR of GSTM3 was cloned downstream of a luciferase sequence and transfected into the MCF7 KO 200c cell line (Figure 4C). Synthetic hsa-miR-200c was co-transfected and thus a reduction in the relative light units (RLUs) was detected. Subsequently, the impact of sequence mutations of the hsa-miR-200c target site of the GSTM3 3′UTR was examined. The more the sequence of the target site was modified the higher was the ability to reconstitute the luminescence signal towards the initial level (Figure 4D). Further, a scrambled control siRNA was co-transfected with different GSTM3 3′UTR plasmids (Supplementary Figure S2D) confirming that the 3′UTR of glutathione S-transferase mu 3 is a direct target of hsa-miR-200c.

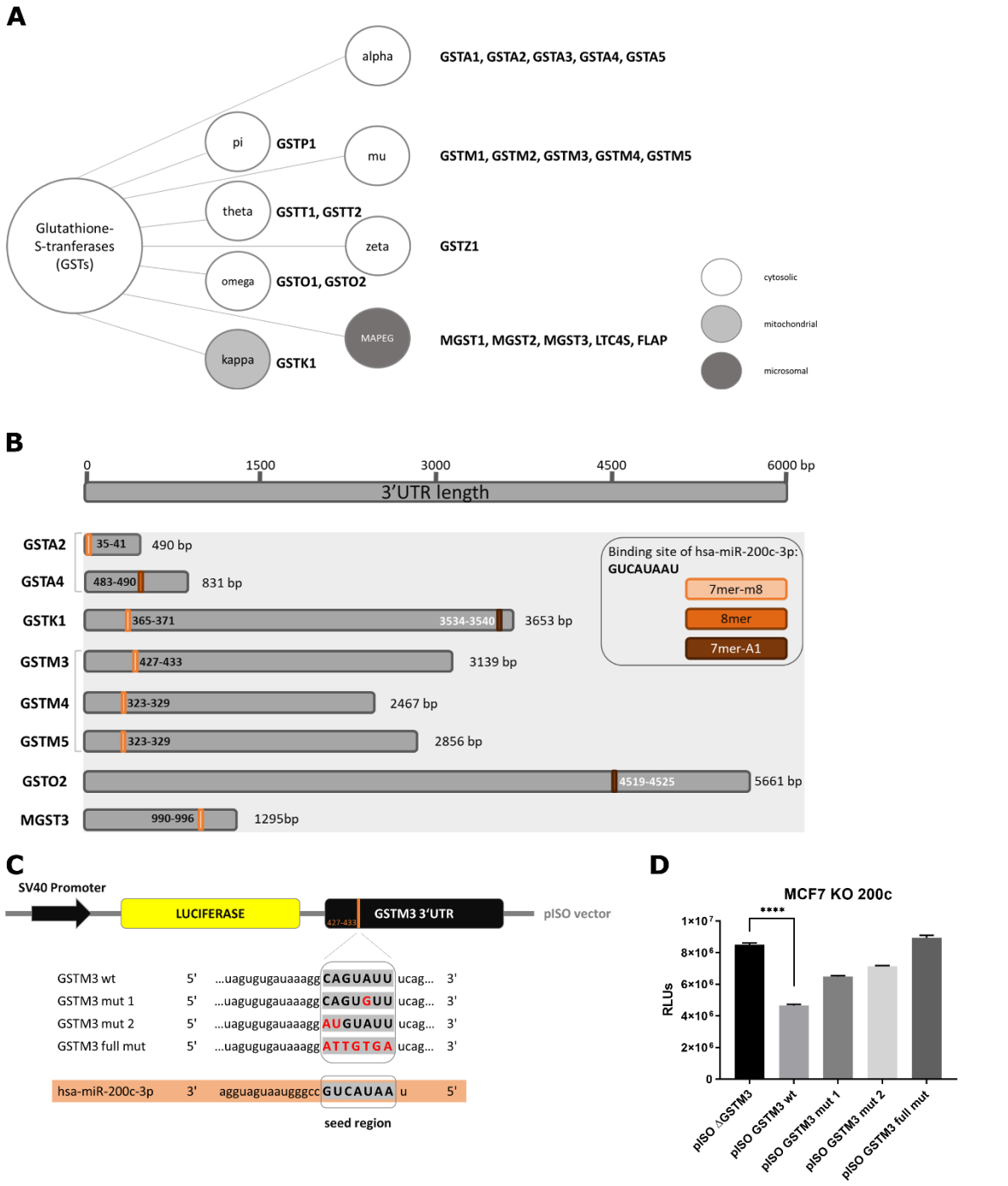

Figure 4: Validation of hsa-miR-200c-3p target site in the 3′UTR of glutathione S-transferases. **(A)** Glutathione S-transferases can be classified into 8 different families. **(B)** The 3′UTR regions and their length in base pairs (bps) are indicated for the glutathione S-transferases which show a target site for hsa-miR-200c. The orange/brown-colored bars display the localization of the hsa-miR-200c target site. **(C)** Schematic layout of the luciferase reporter plasmid. The unmodified (wt), as well as three different mutations (indicated with red letters) of the GSTM3 3′UTR, are shown in comparison to the seed region of hsa-miR-200c. **(D)** Luciferase assay of the different GSTM3 3′UTR constructs. Hsa-miR-200c and the plasmids were co-transfected into MCF7 KO 200c cells. One representative diagram out of three is displayed. A two-tailed Student's t-test for pISO ΔGSTM3 and pISO GSTM3 wt was performed. **** $p < 0.0001$. Values are displayed as mean with SD.

The generation of the plasmids was generously performed by Sviatlana Dubovik (Pharmaceutical Biotechnology, Department of Pharmacy, Ludwig-Maximilians-Universität München, Germany) who additionally partly conducted the co-transfection study.

3.3 Hsa-miR-200c Controls the Expression of Additional Glutathione S-Transferases

For a comprehensive analysis of the expression changes of all GSTs mediated by hsa-miR-200c, three different model cell lines were utilized. Besides the previously generated hsa-miR-200c KO cell line (115), a doxycycline-inducible MCF7 sponge cell line was generated for the current study to scavenge the endogenous mature miRNA. Furthermore, a third cellular system, MDA-MB 231 Tripz 200c, was generated, in which the hsa-miR-200c and the red fluorescent protein (RFP) expression can be induced simultaneously in an hsa-miR-200c-null background (Figure 5A) (114). Analyses of the expression levels and kinetics of the respective constructs and cell lines can be found in the Supplementary Figure S3A–C. Deactivating hsa-miR-200c in our two MCF7 cell systems led to the consistent upregulation of seven glutathione S-transferases (GSTM3, GSTM4, GSTK1, MGST1, MGST3, GSTO2, GSTT2) compared to the wt and uninduced cells, respectively (Figure 5B,C, Supplementary Figure S2B and Table S1). When hsa-miR-200c was overexpressed in the doxycycline-induced MDA-MB 231 Tripz 200c cell line, GSTM1, GSTM3, GSTO1, GSTP1 and GSTZ1 were downregulated (Figure 5D, Supplementary Figure S2B and Table S1). Comparing the eight GSTs harboring an *in silico* identified target site to the GSTs identified with quantitative RT-PCR (Table 4) revealed three GSTs resembling the expected changes in expression pattern (GSTM3, GSTM4, MGST3) consistent in all cell systems. Three GSTs were not at all expressed in the investigated cell lines. GSTK1 and GSTO2 show, as expected, increased expression upon hsa-miR-200c downregulation in MCF7 cells but also enhanced expression upon hsa-miR-200c induction in the cancer cell line MDA-MB 231. Despite no obvious target sites for hsa-miR-200c, both MGST1 and GSTT2 seemed to be regulated by hsa-miR-200c in MCF7 cells (Supplementary Figure S2B). As enlightened in the luciferase reporter assay (Figure 4D), point mutations in the hsa-miR-200c binding site may still lead to the degradation of the targeted mRNA. Therefore, the 3′UTR sequences of these GSTs were re-analyzed and potential binding sites of hsa-miR-200c were found *in silico* (Supplementary Figure S2C).

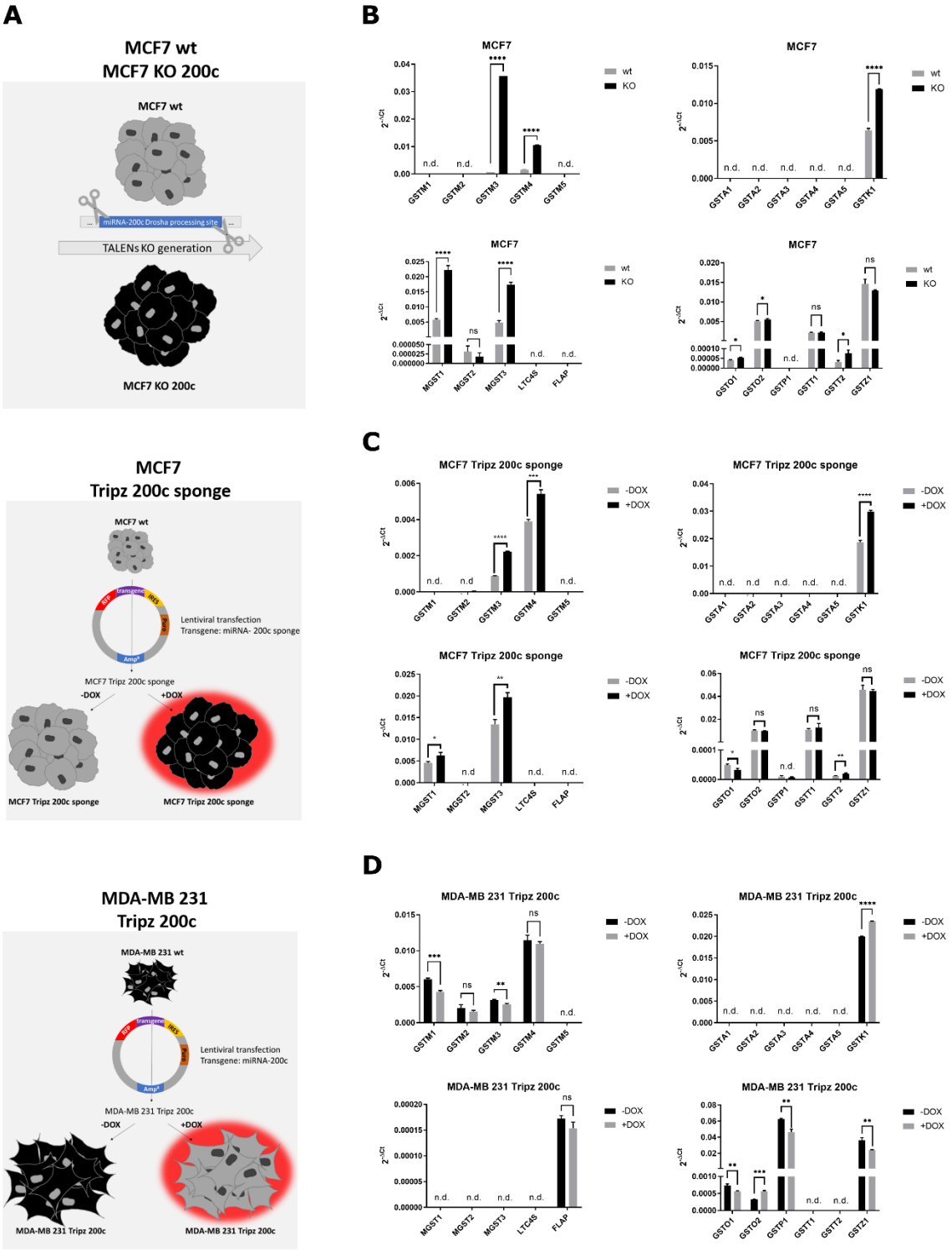

Figure 5: Expression of glutathione S-transferases (GSTs) in different hsa-miR-200c expression systems. **(A)** Overview of the generation of cell systems. Corresponding qRT-PCR analysis of all glutathione S-transferases in the **(B)** MCF7 wildtype and MCF7 KO 200c, **(C)** MCF7 Tripz 200c sponge and **(D)** MDA-MB 231 Tripz 200c cell line. Both Tripz construct systems were induced (or not) with 5 µg/mL doxycycline (DOX) for 72 h. An unpaired two-tailed Student's t-test was performed. * $p < 0.05$, ** $p < 0.01$, *** $p < 0.001$, **** $p < 0.0001$. Values are displayed as mean with SD. ns = not significant, n.d. = not detected.

3.4 GSTM3 as Target of the hsa-miR-200c Is Differentially Expressed upon Chemotherapeutic Treatment

Further studies were carried out with GSTM3 only, as its hsa-miR-200c binding site was previously validated and because GSTM3 showed the most prominent expression change in the GST screen. We investigated the direct effect of doxorubicin and hsa-miR-200c on GSTM3 expression on mRNA (Figure 6A,C,E) and protein levels (Figure 6B,D,F and Supplementary Figure S4) in all three cell systems mentioned before. Generally, DXR treatment enhanced GSTM3 expression in all examined cell lines. The KO of hsa-miR-200c in MCF7 and the MCF7 sponge construct enhanced GSTM3 expression which was even elevated when cells were treated with DXR. On the contrary, hsa-miR-200c induction in MDA-MB 231 Tripz 200c cells led to a decreased expression of GSTM3. Thus we show, that when hsa-miR-200c expression is lost in cancer cells, GSTs will become upregulated. As a consequence, the increased number of GST enzymes promotes the binding of glutathione (GSH) to the drugs when patients' tumors are treated with chemotherapy. Thereby, tumor cells become more resistant to chemotherapeutics as the drug is more rapidly inactivated and excreted. Hence, less accumulation of the chemotherapeutic drug in the cells will take place.

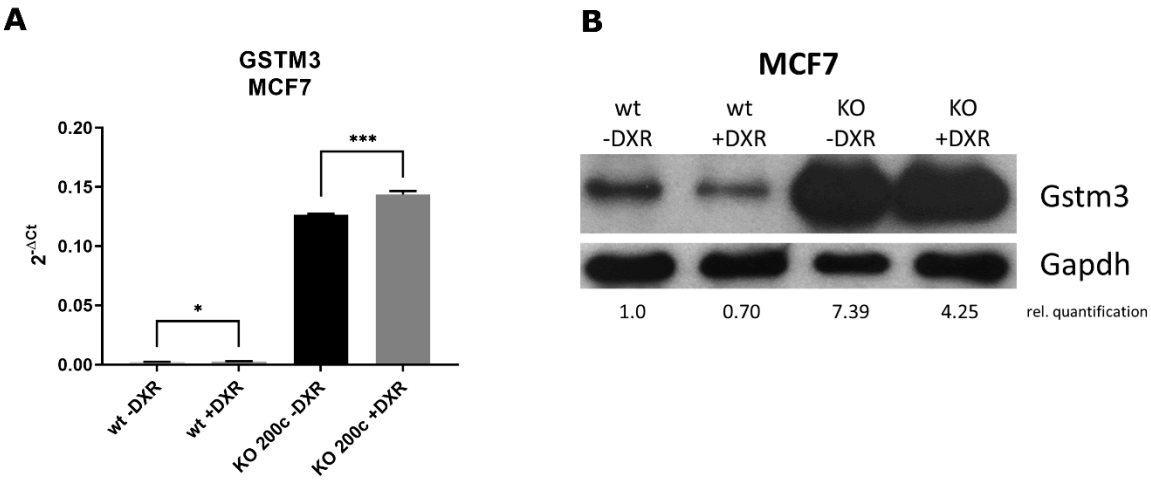

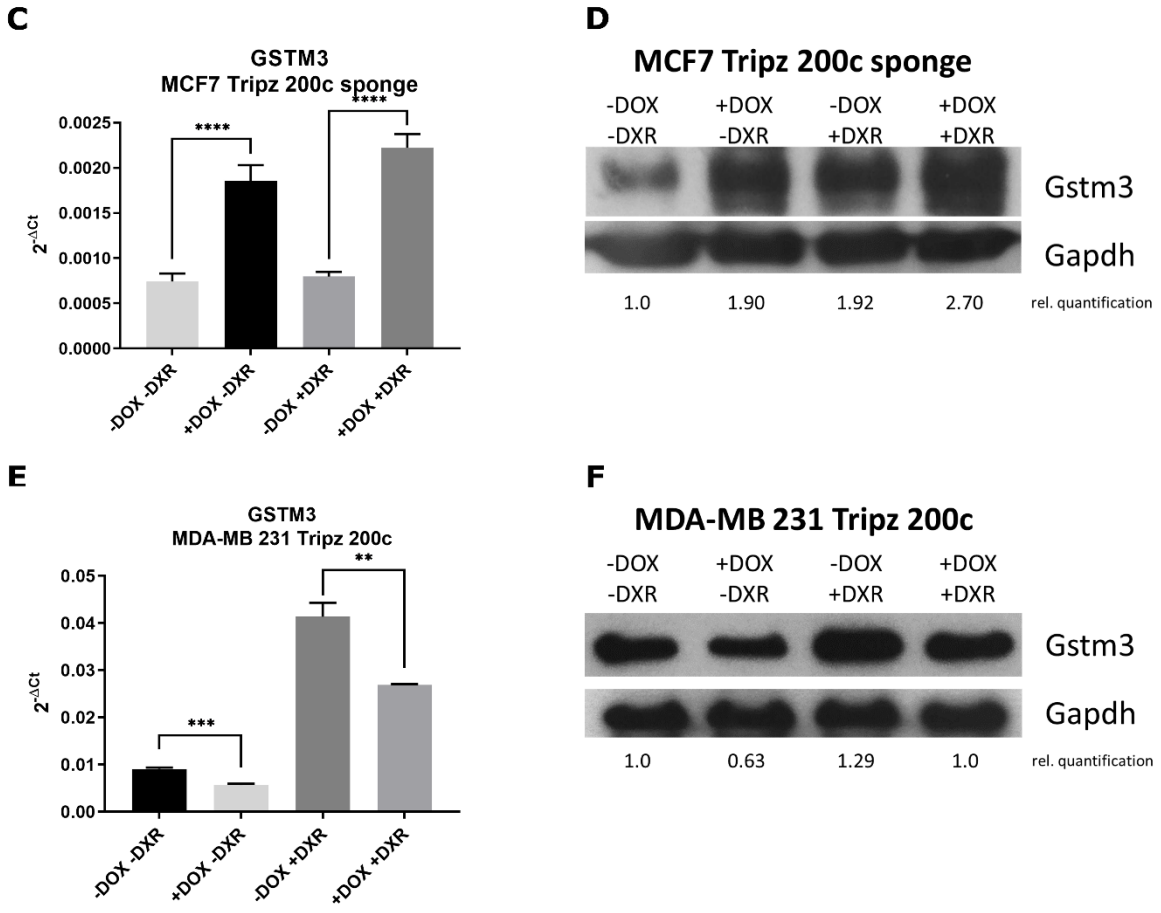

Figure 6: qRT-PCR and Western blot analysis of GSTM3 upon chemotherapeutic treatment. **(A, B)** MCF7 wt vs. MCF7 KO 200c cell line treated with 5 µM DXR for 6 h. **(C, D)** MCF7 Tripz 200c sponge cell line with or without DOX induction for 72 hours and subsequent DXR treatment with 0.1 µM for 24 h. **(E, F)** MDA-MB 231 Tripz 200c cells with or without DOX induction (72 h) and subsequent DXR treatment with 0.6 µM for 24 h. For Western blot quantification, contrast ratios were analyzed. An unpaired two-tailed Student's t-test was performed for qRT-PCR statistics. One representative replicate out of three is shown. * $p < 0.05$, ** $p < 0.01$, *** $p < 0.001$, **** $p < 0.0001$. Values are displayed as mean with SD.

3.5 Hsa-miR-200c Influences the GSH Pool and Mediates Drug Resistance *In Vitro*

To verify this hypothesis, different physiological assays were performed. A GSH/GSSG-Glo assay was carried out, as GSTs reduce the pool of GSH present in a cell by conjugating it to xenobiotics. Consistent in all three cell systems, the number of total glutathione is reduced when hsa-miR-200c is absent and the cells were stressed with DXR at the same time (Figure 7A). A second chemotherapeutic drug, i.e., cisplatin (CP), was utilized to show general validity. Similar to the treatment with DXR, the GSH/GSSG assay revealed a decrease in the total glutathione amount when

hsa-miR-200c was absent and cells were treated with CP (Figure 7B). The analysis of the subG1 population, representing the rate of cell death in general, disclosed that the highest proportion of apoptotic cells can be observed when cells express hsa-miR-200c and are treated with DXR simultaneously (Figure 7C). Similar results were obtained in all cell systems. Likewise, when cells were treated with CP, the highest subG1 levels, and therefore the most abundant rate of cell death was observed with high hsa-miR-200c expression levels (Figure 7D). To expand these findings from breast cancer to other tumor types, the A549 Tripz 200c lung cancer cell line and the T24 Tripz 200c bladder cancer cell line were generated. Upon hsa-miR-200c induction, chemosensitivity to DXR and CP was increased (Supplementary Figure S5A–D). These data demonstrate on the one hand that tumor cells expressing hsa-miR-200c are more sensitive to chemotherapeutic treatment. On the other hand, by losing the hsa-miR-200c expression, tumor cells can acquire drug resistance.

To analyze the long-term effects of hsa-miR-200c expression, where drug resistance is even more evident, MDA-MB 231 Tripz 200c cells, whether induced with doxycycline (DOX) or not, were treated once with DXR and the cell confluency was monitored for six weeks. This live cell imaging can be retraced in the videos of both cell lines (Supplementary Video S1 and Video S2). In line with the literature, we observed a retarded cell proliferation in hsa-miR-200c expressing cells, which is depicted by an increased doubling time and a flatter proliferation curve (Supplementary Figure S6). The one-time chemotherapeutic treatment led to the expected decrease in confluency, however, in hsa-miR-200c expressing cells this effect was significantly stronger. While in the experimental setting without hsa-miR-200c expression, different resistant clones started to regrow, no viable cells were detected when hsa-miR-200c expression had been induced (Figure 7E). This effect can also be illustrated by a colony formation assay where crystal violet staining represents regrown clones only in hsa-miR-200c negative cells (Figure 7F).

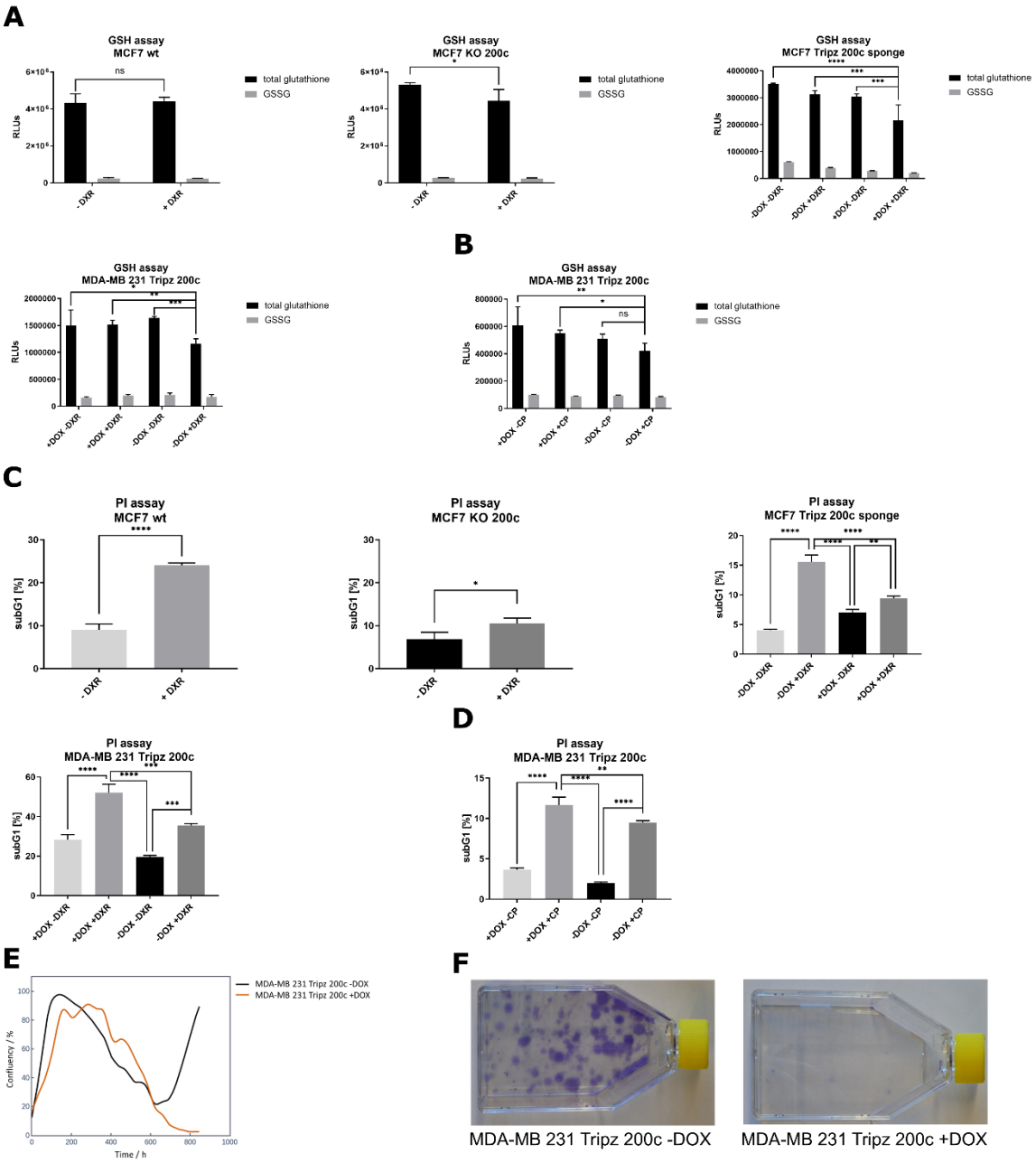

Figure 7: Effect of hsa-miR-200c expression on the glutathione (GSH) pathway and cell death. *In vitro* long-term effect of hsa-miR-200c expression. **(A, B)** GSH/GSSG assay in MCF7 wt vs. KO 200c, MCF7 Tripz 200c sponge and MDA-MB 231 Tripz 200c (doxorubicin left, cisplatin right). Total GSH and GSSG were measured after 24 h of DXR or CP treatment (0.1 µM DXR for MCF7 and 0.6 µM DXR and 50 µM CP for MDA-MB 231 cells). Tripz-constructs were pre-incubated with 5 µg/mL doxycycline or not for 72 h before chemotherapeutic treatment. **(C, D)** PI assay analysis using propidium iodide (PI) and measurement of subG1 population in MCF7 wt vs. KO 200c, MCF7 Tripz 200c sponge and MDA-MB 231 Tripz 200c. Either an unpaired two-tailed Student's t-test, an ordinary one-way ANOVA with Tukey's multiple comparison test or a 2 way ANOVA with Šídák's or Tukey's multiple comparison test was performed for statistics. One representative replicate out of three is shown. * $p < 0.05$, ** $p < 0.01$, *** $p < 0.001$, **** $p < 0.0001$. Values are displayed as mean with SD. **(E)** Confluency monitoring and corresponding **(F)** colony formation of MDA-MB 231 Tripz 200c cells

induced (orange lines) or not (black lines) with DOX (every 48 to 72 h) and single treatment with 0.1 µM DXR at 80 % of confluency.
The GSH/GSSG-Glo assay was partly performed by Sviatlana Dubovik (Pharmaceutical Biotechnology, Department of Pharmacy, Ludwig-Maximilians-Universität München, Germany). The figure of the confluency monitoring was generously prepared by Dr. Philipp Paulitschke and his team from PHIO (PHIO Scientific GmbH, Esswurmstr. 16).

3.6 Xenograft Mouse Models Present Drug Resistance *In Vivo* upon Modulation of hsa-miR-200c Expression

As hsa-miR-200c positive and negative tumors exist in the clinics, we investigated, on the one hand, the growth of these tumors, and on the other hand, tested our hypothesis of drug resistance by loss of hsa-miR-200c, in a xenograft mouse model. Therefore, we utilized the inducible MDA-MB 231 Tripz 200c cell model and an inducible MDA-MB 231 Tripz Ctrl cell line, expressing a control RNA sequence upon DOX administration. Respectively, one group of mice was fed with DOX feed continuously from the day of tumor cell injection on to induce the expression of the hsa-miR-200c transgene in all tumor cells (Figure 8A, I) “Treatment of hsa-miR-200c positive and negative tumors”). No difference in tumor growth was detected in both control cell lines (Figure 8B) which indicates that the steady DOX diet does not affect tumor growth. As expected, the hsa-miR-200c expressing group showed delayed and strongly decelerated tumor growth compared to the control group (Figure 8B). After reaching a tumor size of 150–200 mm^3 two additional groups of mice were introduced to the study. From each diet group (with or without DOX feed, n = 10) mice were either treated i.v. with 5 mg/kg DXR (n = 5) or with NaCl-solution (n = 5). After mice had been sacrificed, the expression of hsa-miR-200c and GSTM3 was analyzed. In the control groups (MDA-MB 231 Tripz Ctrl), where hsa-miR-200c cannot be expressed, GSTM3 was constantly expressed, irrespective of the DOX diet. In mice where hsa-miR-200c was induced in the tumors by DOX (MDA-MB 231 Tripz 200c), cells expressed hsa-miR-200c to a high level and, in line with the *in vitro* results, did not express GSTM3 (Figure 8C). Sections of hsa-miR-200c positive tumors did not show histological differences compared to hsa-miR-200c negative tumors, and no loss in body weight could be observed in any groups independent of the cell line, the induction or treatment (Supplementary Figure S7A–D). When analyzing the effect of chemotherapy on tumor growth and survival, reduced tumor size was measurable in both groups treated with the chemotherapeutic drug (Figure 8D). Of note, mice only

harboring hsa-miR-200c expressing tumor cells, which did not receive the anti-cancer treatment, revealed a strong reduction in tumor growth. However, these results are strongly influenced by the long-term effect of decelerated proliferation in hsa-miR-200c positive cells. To level these effects, we normalized the tumor growth of all mice to the starting day of chemotherapeutic treatment. Here, a cytostatic effect of the chemotherapeutic treatment was measurable whereas a cytotoxic effect was only observed in hsa-miR-200c expressing and DXR-treated tumors (Figure 8E). Increasing tumor volumes were measured in all groups until the euthanasia of the mice except for the DXR-treated group of hsa-miR-200c positive tumors. The latter group comprised of mice with slowly growing tumors (n = 1), with static tumors (n = 3) and with completely reduced tumors (n = 1) till euthanasia of mice, reflecting the cytostatic effect of doxorubicin in hsa-miR-200c positive tumors. Thus, hsa-miR-200c-positive tumors are more chemosensitive than tumors without hsa-miR-200c expression. When evaluating the survival rate from the start of the treatment, most mice had to be sacrificed within 41 days (Figure 8F left). Only in the case of hsa-miR-200c positive tumors and DXR treatment a prolonged survival was observed, and mice had to be sacrificed due to different animal health care reasons. When taking also the days before treatment into account, the Kaplan–Meier analysis indicates that hsa-miR-200c negative tumors were growing faster and reached the critical tumor size earlier (Figure 8B). Consequently, the treatment of these mice had to start approximately 60 days prior to the treatment of the first mice with hsa-miR-200c positive tumors. Mice without hsa-miR-200c expression showed the worst overall survival compared to hsa-miR-200c expressing mice (Figure 8F right). Concluding from these data, the expression of hsa-miR-200c in cancer cells shows a dramatic delay of tumor growth onset and an increased sensitivity to chemotherapy.

In a second experiment (Figure 8A, II) “Single or double treatment of hsa-miR-200c negative tumors”) mice without hsa-miR-200c induction were randomized after the tumors reached a volume of 150–200 mm^3. To investigate whether hsa-miR-200c could sensitize tumor cells to DXR treatment, groups (n = 10) of mice were formed that were either only DXR treated, or only hsa-miR-200c induced with DOX, and a cohort of mice with a combination of both was formed. We observed a clear beneficial effect of the double (+ DOX + DXR) treatment in tumor growth (Figure 8G). Survival analysis revealed that mice without hsa-miR-200c expression, irrespective of DXR treatment, had to be euthanized within the first 73 days after the beginning of the treatment,

whereas mice with the induction of hsa-miR-200c during the tumor growth were partially still alive at the end of the study. Drug treatment showed a beneficial survival rate for both diet groups but an impressive increase when combined with hsa-miR-200c expression (Figure 8H). A detailed analysis of the tumor growth of single mice in the cohort of hsa-miR-200c treatment versus the double treatment group revealed different tumor growth after the initial response to both treatments (Figure 8I). Mice, treated with DOX showed a tumor growth progression after a while. Only two mice of this group were observed with tumor regression followed by a recurrence of the tumor. In comparison, mice additionally being treated with doxorubicin showed delayed tumor progression (n = 3) or recurrence after a while (n = 1). The remaining animals from the double treatment group (n = 6) displayed no recurrence until this study was terminated 250 days after tumor cell injection.

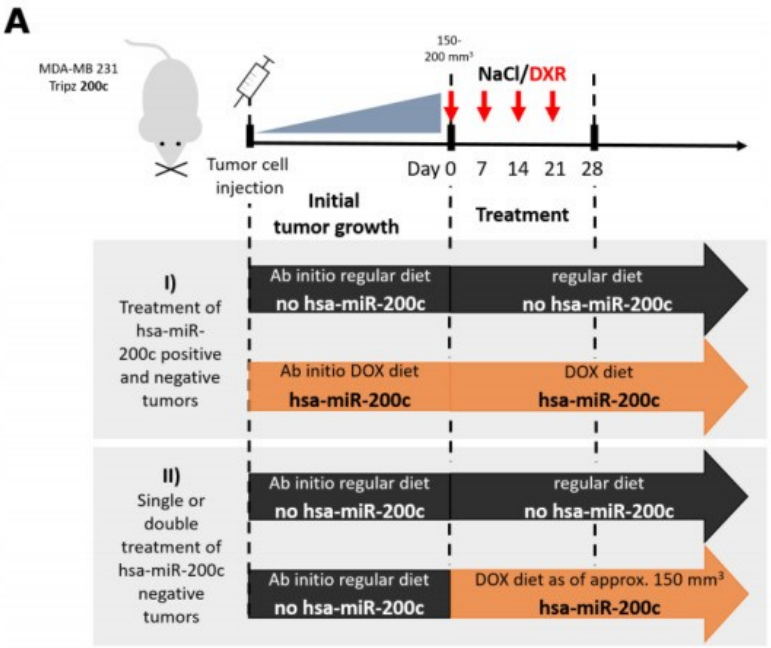

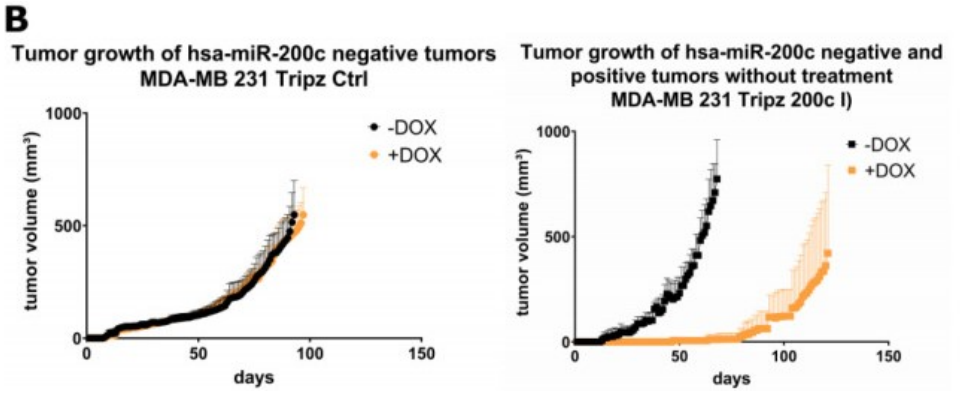

C

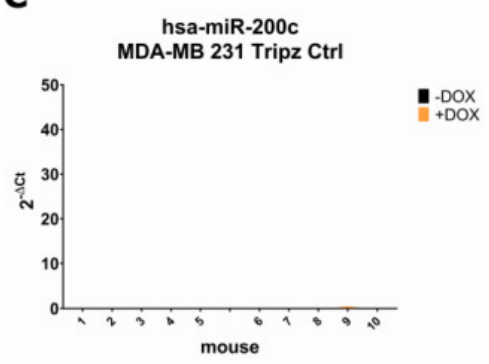
hsa-miR-200c
MDA-MB 231 Tripz Ctrl
-DOX
+DOX
$2^{-\Delta Ct}$
mouse

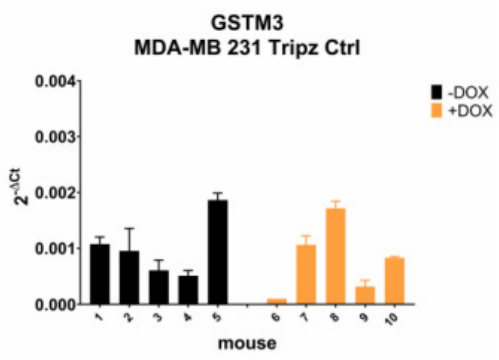
GSTM3
MDA-MB 231 Tripz Ctrl
-DOX
+DOX
$2^{-\Delta Ct}$
mouse

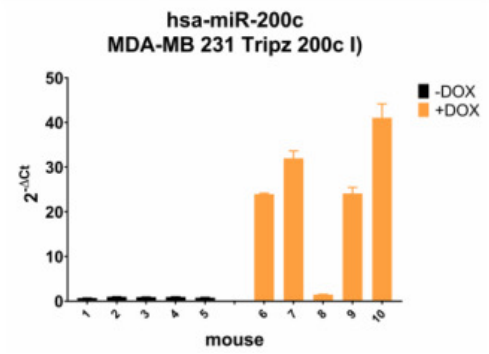
hsa-miR-200c
MDA-MB 231 Tripz 200c I)
-DOX
+DOX
$2^{-\Delta Ct}$
mouse

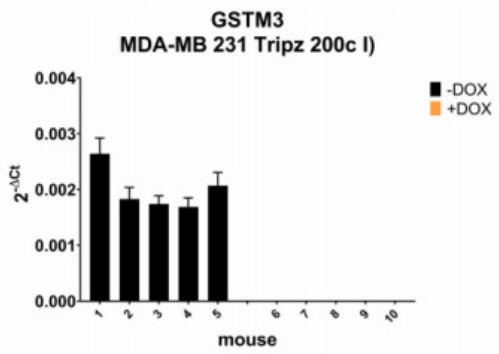
GSTM3
MDA-MB 231 Tripz 200c I)
-DOX
+DOX
$2^{-\Delta Ct}$
mouse

D

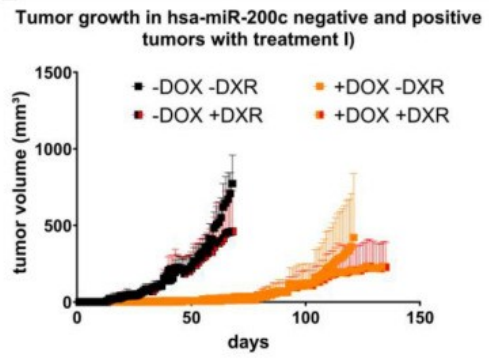
Tumor growth in hsa-miR-200c negative and positive tumors with treatment I)
-DOX -DXR
+DOX -DXR
-DOX +DXR
+DOX +DXR
tumor volume (mm³)
days

E

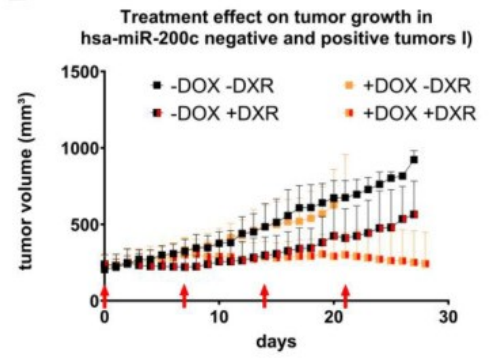
Treatment effect on tumor growth in hsa-miR-200c negative and positive tumors I)
-DOX -DXR
+DOX -DXR
-DOX +DXR
+DOX +DXR
tumor volume (mm³)
days

F

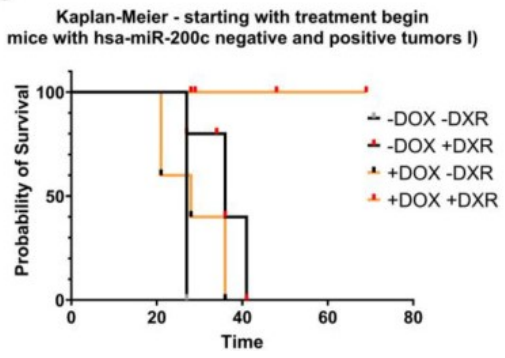
Kaplan-Meier - starting with treatment begin
mice with hsa-miR-200c negative and positive tumors I)
Probability of Survival
Time
-DOX -DXR
-DOX +DXR
+DOX -DXR
+DOX +DXR

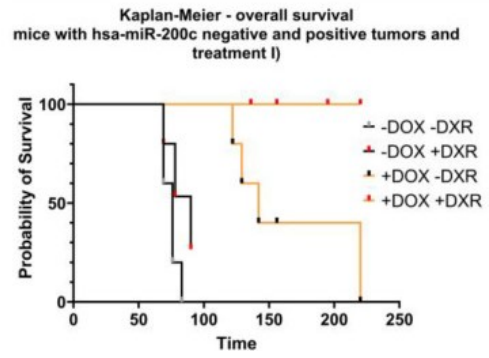
Kaplan-Meier - overall survival
mice with hsa-miR-200c negative and positive tumors and treatment I)
Probability of Survival
Time
-DOX -DXR
-DOX +DXR
+DOX -DXR
+DOX +DXR

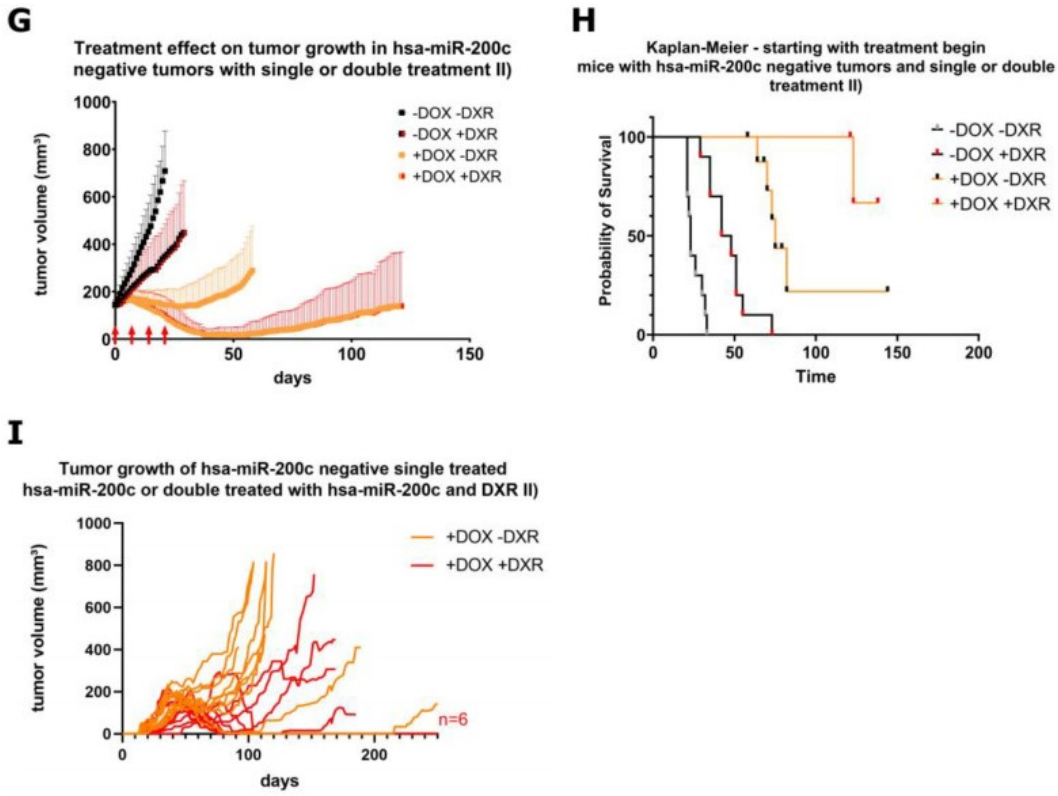

Figure 8: Long-term effect of hsa-miR-200c expression *in vivo* on tumor growth and resistance. **(A)** Two xenograft mouse models to investigate tumor growth: (I) Scheme for the analysis of hsa-miR-200c positive and negative tumors and additional chemotherapeutic treatment. (II) Xenograft mouse model of MDA-MB 231 Tripz 200c tumors to examine single doxorubicin (DXR) or hsa-miR-200c treatment and their combination. **(B)** Tumor growth of MDA-MB 231 Tripz Ctrl (control sequence expressing tumors) vs. MDA-MB 231 Tripz 200c (n = 5 per group) under regular (black) or DOX diet (orange). **(C)** Corresponding molecular analysis of the control (top) and hsa-miR-200c (bottom) inducible xenograft mouse model. Quantitative RT-PCR analysis of the expression levels of GSTM3 and hsa-miR-200c. DOX induction is indicated in orange. **(D)** Evaluation of the development of hsa-miR-200c positive (n = 5, orange curves) and negative tumors (n = 5, black curves) and their treatment with DXR (red-filled squares) based on tumor growth. **(E)** Tumor growth analysis normalized to treatment begin (set as day 0) in hsa-miR-200c positive and negative tumors with or without DXR treatment. Red arrows indicate treatment days (days 0, 7, 14 and 21). **(F)** Kaplan–Meier analysis of mice with hsa-miR-200c positive or negative tumors starting at treatment begin (left). Second Kaplan–Meier (right) displays the overall survival of mice with or without hsa-miR-200c expression and treatment. **(G)** The analysis of tumor growth of xenograft mouse model II). The development of tumor volume in hsa-miR-200c deficient mice upon only treatment with DXR or hsa-miR-200c or the combinatorial treatment (n = 10 per group). Red arrows indicate treatment days. **(H)** Kaplan–Meier survival analysis of mice with single or combinatorial treatment of hsa-miR-200c negative tumors (black curves). All tumor growth graphs terminate when the first animal of the group had to be euthanized. **(I)** Tumor growth curves displaying resistant, regrowing tumors of single mice from either the hsa-miR-200c treated (orange curves) or the hsa-miR-200c and DXR double-treated group (red curves). Red n = 6 presents the number of mice with complete regression in the double-treatment cohort at day 250 after tumor cell inoculation.

Tumor growth and survival data were collected by the veterinarians Dr. Elisa Hörterer and Dr. Ulrich Wilk (Pharmaceutical Biotechnology, Department of Pharmacy, Ludwig-Maximilians-Universität München, Germany). The grinding of the tumors for subsequent RNA isolation was also generously performed by these veterinarians.

Whether the *in vivo* results are reflected in the clinics, an *in silico* study on breast cancer patients was performed. The Kaplan–Meier analysis revealed a significant increase (p = 0.0067) in the overall survival of patients with tumors displaying high hsa-miR-200c levels compared to patients with low hsa-miR-200c expression (Figure 9A and Supplementary Figure S8). To analyze the hsa-miR-200c target GSTM3, a patient cohort with neoadjuvant chemotherapy treatment and displaying a basal subtype was plotted. Comparing the 5-year relapse-free survival, a reduction in the probability of survival in the GSTM3 overexpressing cohort could be seen (Figure 9B and Supplementary Figure S8).

Taking all results into account, we establish the hypothesis that hsa-miR-200c positive tumors suppress GSTs' expression, which is beneficial for a successful chemotherapy by increasing the overall survival of cancer patients. In this case, xenobiotics remain longer in the tumor cells and cause greater damage, which results in enhanced tumor cell death. On the contrary, loss of hsa-miR-200c leads to increased expression of glutathione S-transferases resulting in better drug export, drug-resistant tumors and eventually reduced overall survival of the patients (Figure 9C, D).

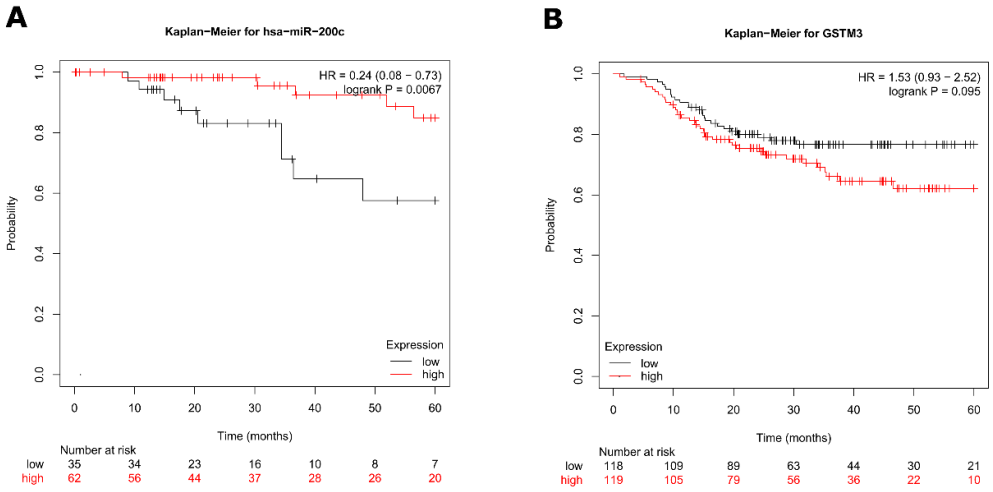

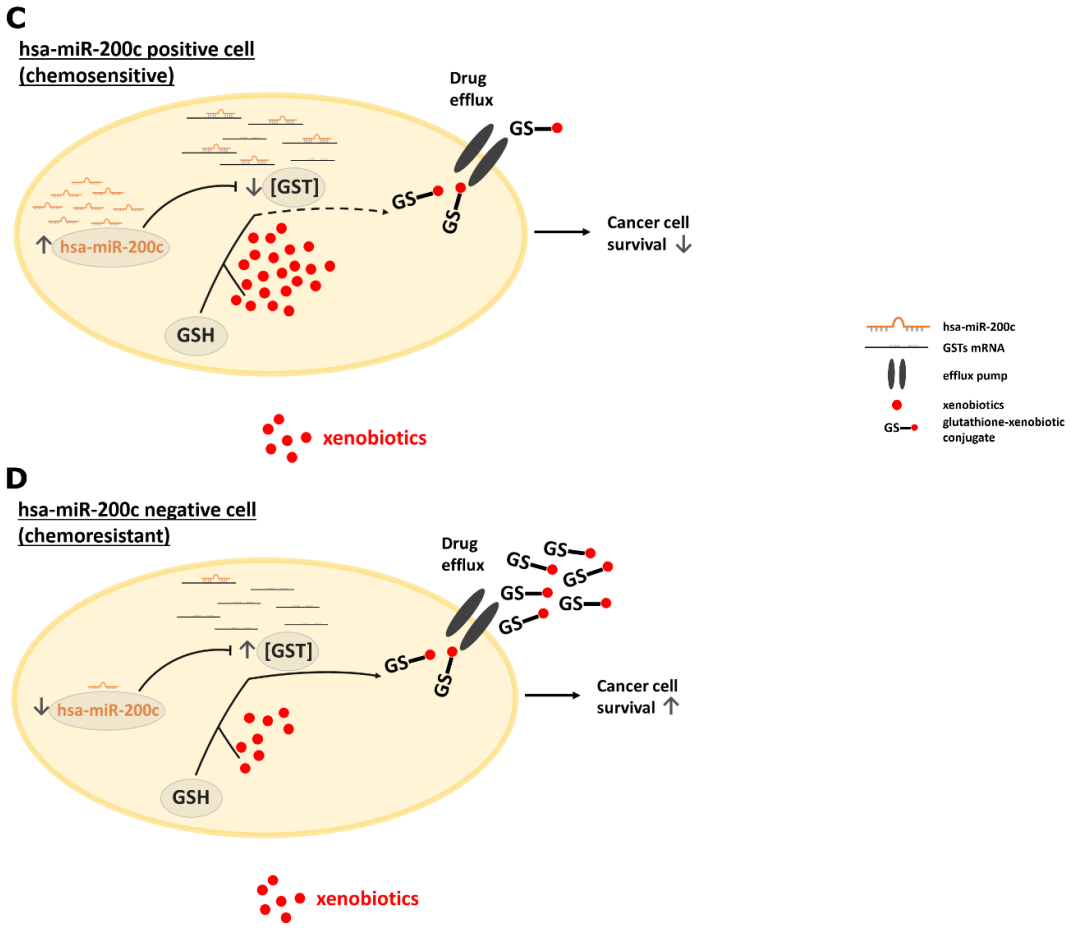

Figure 9: Analysis of clinical relevance. **(A)** Kaplan–Meier analysis for hsa-miR-200c expression in breast cancer patients. Overall survival is depicted. **(B)** Kaplan-Meier plot for the relapse-free survival of GSTM3 expressing patients. Neoadjuvant chemotherapy and basal subtype were used as cohort. **(C)** Graphical summary and hypothesized mechanism of action of hsa-miR-200c and its target GSTM3 in cancer cells. Potential detoxification pathway of a hsa-miR-200c positive cell upon treatment with xenobiotics such as doxorubicin. **(D)** Putative mechanism of resistance formation in hsa-miR-200c negative cells.

4. Results Chapter II: Unraveling the Metastasis-Preventing Effect of miR-200c *In Vitro* and *In Vivo*

This chapter was directly adapted from the original publication which was published as Köhler *et al.*, Mol Oncol. 2024 Oct 15 (see chapter 10.1 Articles). Additional sections were included.

Unraveling the metastasis-preventing effect of miR-200c *in vitro* and *in vivo*

Bianca Köhler [1], Emily Brieger [2], Tom Brandstätter [3, 4], Elisa Hörterer [1], Ulrich Wilk [1], Dr. Jana Pöhmerer [1], Anna Jötten [2], Philipp Paulitschke [2, 5], Chase P Broedersz [3, 4], Stefan Zahler [6], Joachim O Rädler [2], Ernst Wagner [1], and Andreas Roidl [1,*]

[1] Pharmaceutical Biotechnology, Department of Pharmacy, Ludwig-Maximilians-Universität München, D-81377 Munich, Germany.

[2] Faculty of Physics and Center for NanoScience, Ludwig-Maximilians-Universität München, D-80539 Munich, Germany.

[3] Department of Physics and Astronomy, Vrije Universiteit Amsterdam, 1081HV Amsterdam, Netherlands.

[4] Arnold-Sommerfeld-Center for Theoretical Physics, Ludwig-Maximilians-Universität, D-80333, Munich, Germany.

[5] PHIO Scientific GmbH, Esswurmstr. 16, D-81371 Munich, Germany.

[6] Pharmaceutical Biology, Department of Pharmacy, Ludwig-Maximilians-Universität, D-81377 Munich, Germany.

* Corresponding author

4.1 miR-200c Lowers the Metastatic Burden *In Vivo*

To investigate whether the expression of miR-200c alone is sufficient to prevent metastases, we utilized the triple negative breast cancer (TNBC) cell line MDA-MB 231, which was genetically modified with a Tripz-construct to selectively induce miR-200c expression upon treatment with doxycycline (DOX) (114). In order to monitor disseminated cells from the primary tumor this cell line was additionally

transduced with a luciferase tag (Figure 10A). These cells were injected into mice and after initial tumor growth to a size of 200 mm^3, mice were randomized into two diet groups (n = 10) (Figure 10B). Mice were either kept with their normal diet, where the inducible construct was not activated, or fed with DOX-containing diet to express miR-200c in the inoculated cells. We analyzed the metastatic spread of the primary tumor of each mouse *ex vivo* in the distant organs lung, liver, brain, and spleen. Except for the spleen, these organs are predominant sites for metastasis formation of primary breast cancer in patients, also known as “organotropic metastasis” (193, 194). Additionally, we conducted a xenograft mouse experiment with a control cell line (MDA-MB 231 Tripz Ctrl Luc), which expresses a scrambled sequence after DOX administration. We performed this approach in order to exclude DOX effects on metastasis formation. The expression of miR-200c was validated in both *in vitro* cell systems (Supplementary Figure S11A and B and (113, 115)). In vivo, upon doxycycline feed MDA-MB 231 Tripz 200c Luc tumors expressed miR-200c compared to the scrambled control (Tripz Ctrl Luc) tumors (Supplementary Figure S11C and D and (113)). A DOX effect which coincidentally could induce miR-200c expression can be excluded *in vivo* and *in vitro* upon this data. Regardless of the treatment group, all control mice showed metastases in the lung, liver, brain, and spleen to a similar extent (Figure 10C) and therefore no effect of the doxycycline administration was detectable. Subsequently, we measured luciferase activity in the organs of mice with the inducible MDA-MB 231 Tripz 200c Luc primary tumors (Figure 10D). While in 90 % of the animals with tumors lacking miR-200c expression (gray) metastases were found in the lungs, only 40 % of the mice with miR-200c-expressing tumors (orange) developed pulmonary metastases. Moreover, we found statistically significant differences in the metastatic spread for all remaining organs. 80 % of the mice without miR-200c expression showed metastases in the liver while only 10 % of miR-200c-positive tumors spread into this organ. miR-200c-negative primary tumors formed metastases in 70 % of the cases in the brain and in 8 out of 10 mice in the spleen. Of note, all mice with miR-200c-positive tumors were free of metastases in these two organs. Additionally, we evaluated the mean-difference in survival time, tumor volume and metastatic burden in mice bearing miR-200c-depleted or expressing primary tumors. While we found no substantial difference in the control mice (with or without DOX diet, Figure 11A), considerable difference was detected when comparing the two groups from the miR-200c xenograft mouse model. The mean survival time of mice with

miR-200c-positive primary tumors was almost doubled compared to mice with miR-200c-non-expressing tumors (Figure 11B left). Despite the increased survival time of miR-200c-positive tumor bearing mice the tumor volume at day of euthanasia is significantly decreased (Figure 11B middle). Finally, the metastatic burden defined by the number of organs affected by metastases was analyzed. miR-200c-positive tumors spread on average into one distant organ whereas miR-200c-non-expressing tumors affected three organs (Figure 11B right). To determine whether the elevated survival time or tumor size influences the metastasis capacity, we evaluated and compared these parameters across all four experimental animal groups (Supplementary Figure S12A to D). Both control groups, (MDA-MB 231 Tripz Ctrl -DOX and +DOX), show comparable survival times documented by no significance in the mean values, and the corresponding metastatic burdens are evenly distributed indicated by non-significant evaluation (Figure 11A and Supplementary Figure S12A). The same applies to the comparison of tumor volume and metastatic burden in these two groups (Figure 11A and Supplementary Figure S12B). In contrast, while the survival time of mice with miR-200c-positive tumors was on average twice as high as of miR-200c-negative animals, the metastatic burden showed an inverse correlation (Figure 11B). This means, although miR-200c-positive animals lived longer and thus there was more time for tumors to metastasize, many animals did not show any metastases (the metastatic burden mostly equaled zero). Comparing the tumor volume of miR-200c-negative or positive tumors in relation to the metastatic burden, smaller tumors (miR-200c-positive tumors) generally tend to show a lower metastatic burden (Supplementary Figure S12D). However, by comparing similar tumor sizes of miR-200c-negative and positive tumors, only miR-200c-expressing ones displayed a low metastatic burden. In summary, the xenograft experiment clearly showed that miR-200c reduces the metastatic burden and thus is able to prevent metastasis formation *in vivo*.

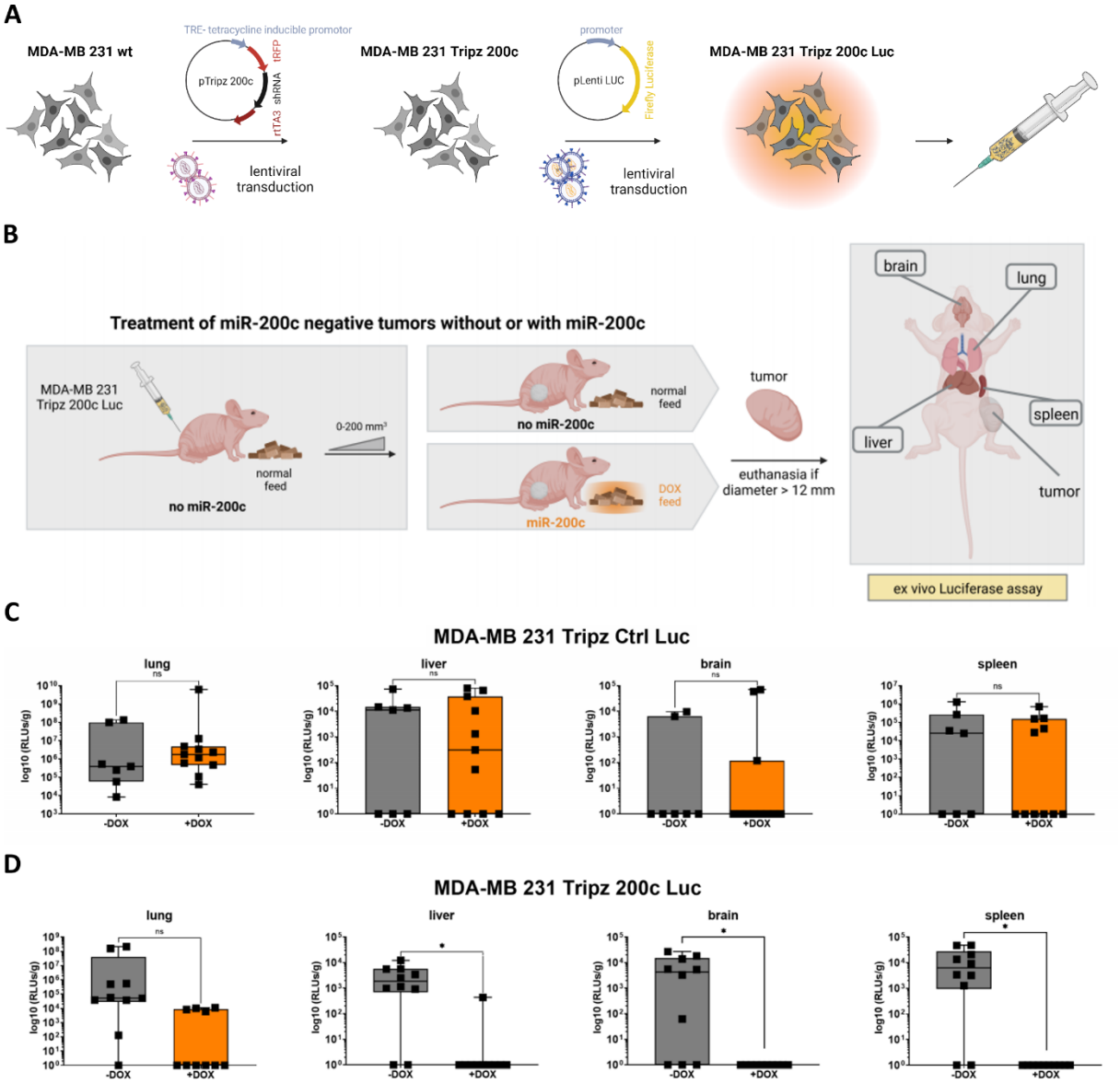

Figure 10: Metastasis formation in mice is reduced when microRNA 200c (miR-200c) is expressed in the primary tumor. **(A)** Generation of the doxycycline (DOX) inducible MDA-MB 231 Tripz 200c cell line from MDA-MB 231 wildtype (wt) cells. This inducible cell line was further transduced with a luciferase (Luc) tag, using a lentiviral system, for injection into mice. Figure was created with BioRender.com. **(B)** Experimental procedure for the treatment of inoculated MDA-MB 231 Tripz 200c Luc cells in mice. After initial tumor growth with normal feed until approximately a size of 200 mm^3, mice were randomized into two diet groups: doxycycline containing or further normal feed. Mice were euthanized as indicated and different organs were analyzed for metastasis formation performing an *ex vivo* luciferase assay. Figure was created with BioRender.com. **(C)** Quantification of luminescence (relative light units, RLUs) and therefore metastasis formation in lung, liver, brain, and spleen of mice of a control (Ctrl) group. MDA-MB 231 Tripz Ctrl Luc cells were injected into the mice of this control group. These breast cancer cells express a scrambled control sequence upon doxycycline induction. Cell generation was conducted as described in Figure 10A. Mice were either fed with normal (gray, n = 7) or doxycycline feed (orange, n = 11) *ab initio*. Values are displayed on a logarithmic scale as RLUs per gram organ (RLUs/g). Each

data point represents one mouse. For statistical evaluation an unpaired, two tailed student's t-test was performed. ns = not significant. **(D)** Quantification of luminescence (relative light units, RLUs) and therefore metastasis formation in lung, liver, brain, and spleen of mice of MDA-MB 231 Tripz 200c Luc cells without (gray, n = 10) or with miR-200c expression (orange, n = 10). Change of diet was conducted, if necessary, when tumors reached a size of approximately 200 mm^3. Values are displayed on a logarithmic scale as RLUs/g organ. Each data point represents one mouse. For statistical evaluation an unpaired, two tailed student's t-test was performed. ns = not significant, * $p < 0.05$. Data in (C) and (D) are presented as box and whiskers plots with minimal to maximal values. The median is plotted with a line.
The processing of the tumors with subsequent ex vivo luciferase assay performance was generously conducted by the veterinarians Dr. Elisa Hörterer, Dr. Ulrich Wilk, and Dr. Jana Pöhmerer (Pharmaceutical Biotechnology, Department of Pharmacy, Ludwig-Maximilians-Universität München, Germany).

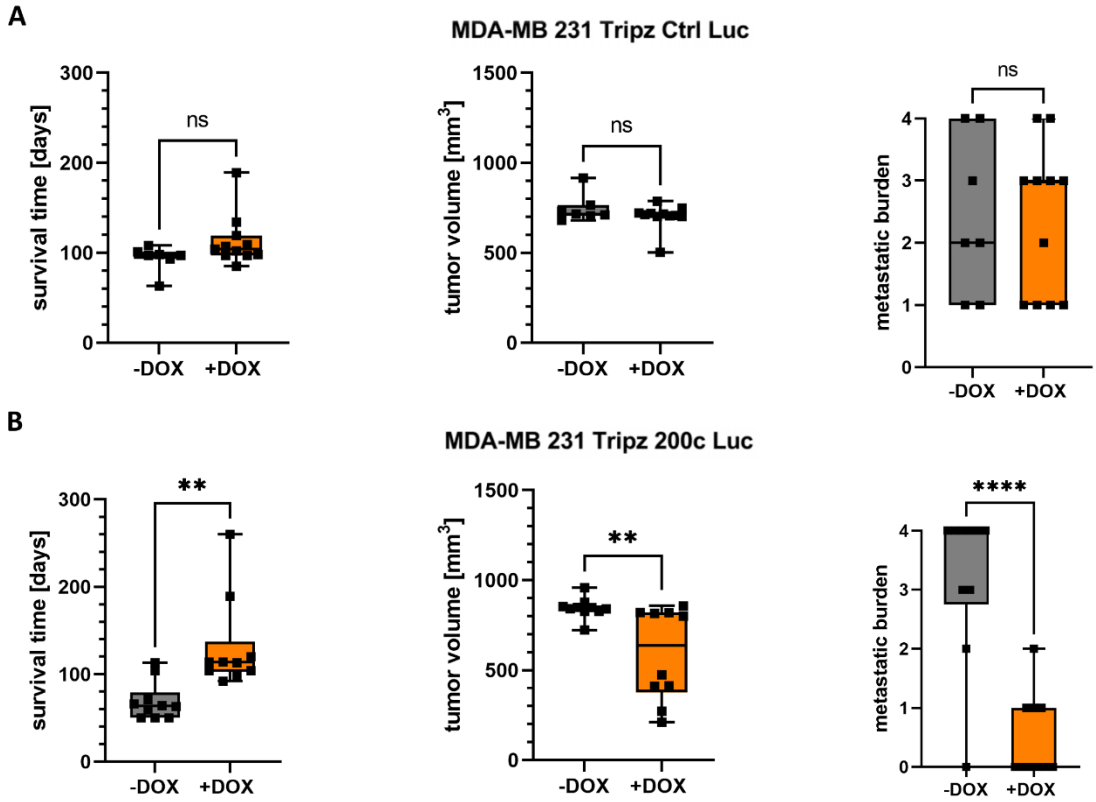

Figure 11: MicroRNA 200c (miR-200c) positively alters survival time of mice whereas it negatively influences tumor volume and metastatic burden. The term "metastatic burden" refers to the number of affected organs. **(A)** Survival time, tumor volume and metastatic burden of control (Ctrl) mice injected with MDA-MB 231 Tripz Ctrl Luc cells. Mice were either fed with normal feed (gray, n = 7) or with doxycycline (DOX) containing feed (orange, n = 11) *ab initio*. For statistical evaluation an unpaired, two tailed student's t-test was performed. ns = not significant. **(B)** Survival time, tumor volume and metastatic burden of mice injected with MDA-MB 231 Tripz 200c Luc cells. Mice were either fed with normal feed (gray, n = 10) or switched to DOX containing feed (orange, miR-200c positive, n = 10) when tumor reached a size of approximately 200 mm^3. For statistical evaluation an unpaired, two tailed student's t-test was performed. ** $p < 0.01$ and **** $p < 0.0001$. Data in (A) and (B) are presented as box

and whiskers plots with minimal to maximal values including all data points. Each data point represents one mouse. The median is plotted with a line.
Data collection of the survival time and tumor growth of the mice was generously performed by the veterinarians Dr. Elisa Hörterer, Dr. Ulrich Wilk, and Dr. Jana Pöhmerer (Pharmaceutical Biotechnology, Department of Pharmacy, Ludwig-Maximilians-Universität München, Germany).

In addition, the impact of chemotherapeutic treatment i.e., i.v. application of doxorubicin treatment into tumor-bearing mice with miRNA 200c-positive or negative primary tumors, on metastasis formation was investigated. The *ex vivo* luciferase assay of lung, liver, brain, and spleen revealed an immense benefit on the metastatic burden of the double treated experimental group (Figure 12A). No metastases were measured in any of the analyzed organs in this group whereas all mice treated with doxorubicin only showed pulmonary metastases and two animal displayed further metastases in the three remaining tissues. Compared to the previous study (Figure 11B) the mean survival time of animals receiving either miRNA-200c (via DOX-feed induction) or chemotherapy as single treatment was comparable. While all animals treated with doxorubicin formed pulmonary metastases only four mice did so in the miRNA-200c treatment group. Additionally, comparing the remaining potential metastatic sites in the miRNA-200c positive with the doxorubicin treated group, only one mouse was detected with hepatic metastases in the group receiving miRNA-200c induction whereas two animals in the single doxorubicin treated group showed metastases in all examined organs. Coming back to the chemotherapeutic study, the survival time of animals with miRNA-200c and combined doxorubicin treatment was tripled compared to doxorubicin treated mice (Figure 12B). Even within this expanded lifetime animals did not express any measurable metastasis in the organs and the metastatic burden in this group equals zero (Figure 12B). On the contrary, in the doxorubicin treated group at least one organ per animal was infiltrated with luciferase positive breast cancer cells. Animals with chemotherapeutic treatment were euthanized because their tumors reached a diameter of more than 12 mm which is the criteria for euthanasia. Hardly any of the animals in the double treatment group had to be sacrificed because of reaching the critical tumor size. Reasons for euthanasia before reaching the critical tumor volume included other life-threatening circumstances i.e., auto-mutilation, open wounds, etc. and finally the termination of the study. Interestingly, 50 % of the animals treated with miRNA-200c and chemotherapy at the same time did not show any measurable primary tumor. After initial tumor onset the

size of the breast cancer tumors dropped beneath the detection limit and these animals can be termed tumor-free. This animal experiment clearly depicts the benefit of combining chemotherapeutic treatment with miRNA-200c expression which can affect both hallmarks of cancer: avoiding resistance and decreasing or even preventing metastasis formation.

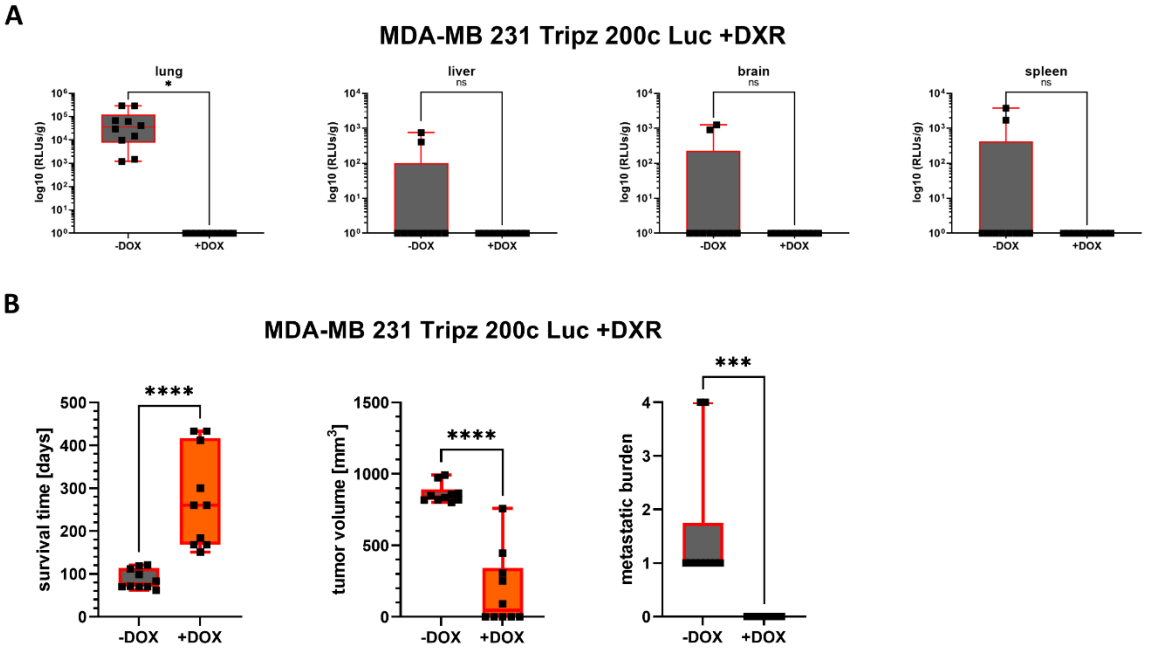

Figure 12: The combination of a chemotherapeutic treatment using doxorubicin with additional miRNA-200c expression hampered the metastasis formation. **(A)** *Ex vivo* luciferase assay to detect metastasis in lung, liver, brain, and spleen in mice with single doxorubicin treatment (-DOX group, gray, n = 10) and in the group with additional miRNA-200c treatment (+DOX, orange, n = 10) with subsequent quantification of light signal (relative light units, RLUs) and therefore metastasis formation. Values are displayed on a logarithmic scale as relative light units (RLUs) per gram organ. Each data point represents one mouse. For statistical evaluation an unpaired, two tailed student's t-test was performed. ns = not significant, * $p < 0.05$. **(B)** Survival time, tumor volume and metastatic burden of mice injected with MDA-MB 231 Tripz 200c Luc cells. Mice were either fed with normal feed (gray, n = 10) or with doxycycline containing feed (orange, miR-200c positive, n = 10) as indicated previously. Red framed bares indicate doxorubicin treatment. For statistical evaluation an unpaired, two tailed student's t-test was performed. *** $p < 0.001$ and **** $p < 0.0001$. Data in (A) and (B) are presented as box and whiskers plots with minimal to maximal values including all data points. Each data point represents one mouse. The median is plotted with a line. *The processing of the tumors with subsequent ex vivo luciferase assay performance and data collection of the survival time and tumor growth of the mice was generously performed by the veterinarians Dr. Elisa Hörterer, Dr. Ulrich Wilk, and Dr. Jana Pöhmerer (Pharmaceutical Biotechnology, Department of Pharmacy, Ludwig-Maximilians-Universität München, Germany).*

4.2 miR-200c Expression Modulates Undirected Collective Migration

A prerequisite for metastasis formation is the motility of cells and thus cellular migration. One can discriminate between single-cell migration and collective-cell migration, where the movement of a single cell in a cell cluster is influenced by factors like cellular surface adhesion, cell-cell contacts or collisions, and gradients of chemoattractants. Our first *in vitro* assay sought to determine the impact of miR-200c on the random walk of the triple negative breast cancer cell line (MDA-MB 231) and the Luminal A breast cancer cells (MCF7) growing under regular culture conditions. While cells at low confluence migrate nearly unaffected by other cells, similar to single-cell migration, higher confluence leads to cluster formation of cells resulting in collective-cell migration behavior. By live imaging we were able to monitor cell migration during different confluence rates. A significant difference in the average motility was measured in the epithelial Luminal A breast cancer cell lines MCF7 wt and MCF7 KO 200c (Figure 13A). We observed MCF7 KO 200c cells having a higher motility rate when the confluence was lower (Figure 13B, Video 1 and Video 2), but this motility rate decreased when these cells became denser and finally approximated the motility rate of the MCF7 wt cells. Other than MCF7 wt, the mean motility of the MCF7 KO 200c cells seems to be dependent on the confluence. Moreover, pictures of the naturally formed cell clusters show big clusters in MCF7 wt cells while MCF7 KO 200c cells have smaller clusters and display more frequently single cells (Figure 13C). In contrast, the mesenchymal triple negative breast cancer cell line MDA-MB 231 Tripz 200c shows an opposite effect in its migratory behavior. The overall motility rate is slightly increased when these cells express miR-200c (Tripz +DOX) (Figure 13D, Video 3 and Video 4). When correlating motility rates with the confluence over time, miR-200c-positive cells show increased motility compared to miR-200c-negative cells with increasing cell density (Figure 13E). Overall, MDA-MB 231 cells show a higher motility rate compared to MCF7 cells and display an elevated motility rate the denser the cells grow (Figure 13E). These observed effects are not DOX induced as in MDA-MB 231 Tripz Ctrl cells no differences in the motility behavior of these two states were detected (Figure 13F and G). Altogether, in these experiments we observed that miR-200c-positive cells in both cell systems behaved differently. Thus, it is very likely that the collective migration is influenced by factors as cell-cell-

contacts, adhesion or the epithelial or mesenchymal phenotype, all parameters potentially affected by miR-200c.

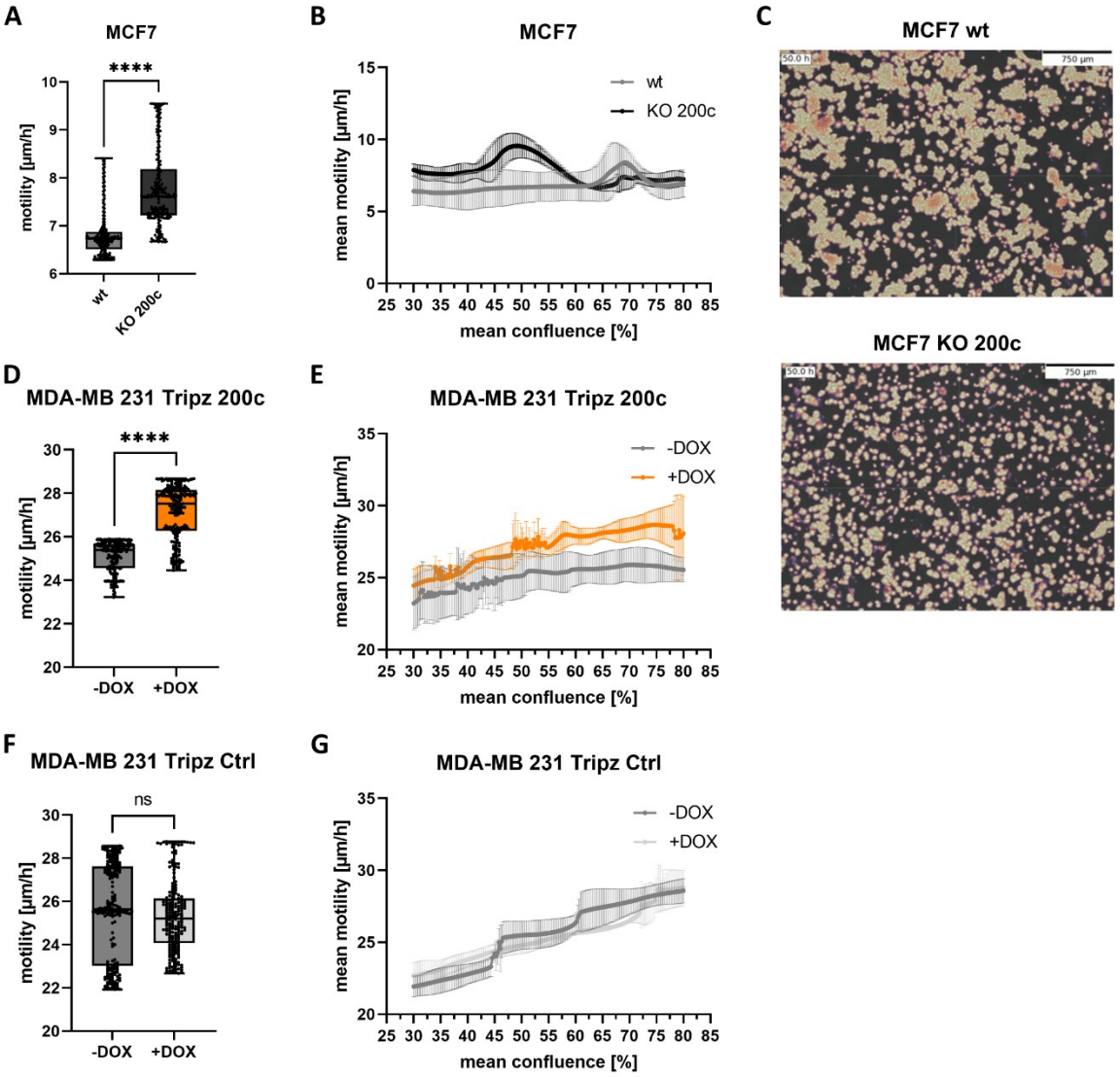

Figure 13: Mean motility is modulated by microRNA 200c (miR-200c) expression dependent on the cellular phenotype. Motility behavior in random walk experiments of epithelial MCF7 wildtype (wt) and knockout (KO) 200c cells. **(A)** Average motility in µm per hour [µm/h] (n = 3) and **(B)** mean motility [µm/h] at a specific confluence ranging from 30 to 80 % (n = 3). **(C)** Formed cell clusters of MCF7 wt (top) and MCF7 KO 200c cell (bottom) after 50 hours post seeding for the random walk analysis. Scale bar equals 750 µm. Pictures were taken with a Cellwatcher M device. **(D)** Average motility of MDA-MB 231 Tripz 200c cells with or without doxycycline (DOX) induction in [µm/h] (n = 3) and **(E)** mean motility [µm/h] over a confluence rage of 30 to 80 % (n = 3). Control experiments to exclude any DOX effect were performed using MDA-MB 231 Tripz Ctrl cells. **(F)** Average motility of MDA-MB 231 Tripz Ctrl cells with or without DOX induction in [µm/h] (n = 3) and **(G)** mean motility [µm/h] over the confluence rage of 30 to 80 % (n = 3). Data of the average motility in (A), (D) and (F) are presented as box and whiskers plots with minimal to maximal values. The median is plotted with a line and the mean with “+”. Values in (B), (E) and (G) are displayed as mean with SD.

For statistical evaluation an unpaired, two tailed student's t-test was performed in (A), (D) and (F). ns = not significant, **** $p < 0.0001$.
Data analysis of cell motility and mean motility was conducted by Dr. Philipp Paulitschke and Dr. Anna Jötten (PHIO Scientific GmbH, Esswurmstr. 16, Germany; Faculty of Physics and Center for NanoScience, Ludwig-Maximilians-Universität München, Germany).

4.3 The Migratory Behavior in Directed Collective Migration Assays Revealed Enhanced Predisposition of miR-200c Non-expressing Cells to Leave Cell Clusters

To analyze collective-cell migration in more detail, we performed scratch assays and measured the migration of cells from dense clusters into the free space. Wound closure, which is the increase of the occupied area within 10 hours, was significantly hampered in miR-200c induced MDA-MB 231 cells (Figure 14A, Video 5, Video 6, Video 7 and Video 8). Furthermore, MCF7 KO 200c cells inclined to close the wound faster than miR-200c-expressing MCF7 wt cells (Supplementary Figure S13A, Supplementary Video S3, Video S4, Video S5 and Video S6). In both cellular systems significantly more cells moved into the scratch when miR-200c was not expressed (Figure 14B and C and Supplementary Figure S13B and C). Additionally, the confinement ratio of miR-200c-expressing and non-expressing cells was determined (Figure 14D and Supplementary Figure S13D). This ratio is defined as the cell's net-distance divided by the total-distance traveled and represents the straightness of cell tracks (195, 196). MDA-MB 231 Tripz 200c -DOX cells (without miR-200c expression) show a significantly enhanced straightness compared to miR-200c induced cells (Figure 14D and Supplementary Figure S13D). Of note, MDA-MB 231 Tripz 200c -DOX cells showed a two-parted distribution of the confinement ratio. This indicates a possible bilateral motility behavior, which might depend on the location of the cells within the scratch assay. For this reason, we performed a detailed evaluation of the cellular directionality at the front and the bulk regions (Figure 15A to D). We validated the trajectories of the MDA-MB 231 cells (Video 6 and Video 8) and observed an enhanced directionality of the MDA-MB 231 cells without miR-200c expression (Tripz 200c -DOX) at the front and bulk regions compared to miR-200c-expressing cells (Figure 15A). Moreover, significant differences in the accumulated distance were observed only in the front region comparing miR-200c-expressing and non-expressing cells (Figure 15B). As an example, the movement of 10 cells per region (Figure 15C) visualizes the difference in how cells are closing the scratch (Figure 15D). As indicated

by the significantly enhanced directed movement in the bulk region of miR-200c-non-expressing cells, 100 % of measured cells at both fronts of the uninduced (-DOX) MDA-MB 231 Tripz 200c cell line moved into the scratch, whereas only 50 % of miR-200c-positive cells contributed to the wound closure (Figure 15D). In summary, our data show an elevated intrinsic potential of cells without miR-200c to leave cell clusters making them more prone to disseminate into distant tissues.

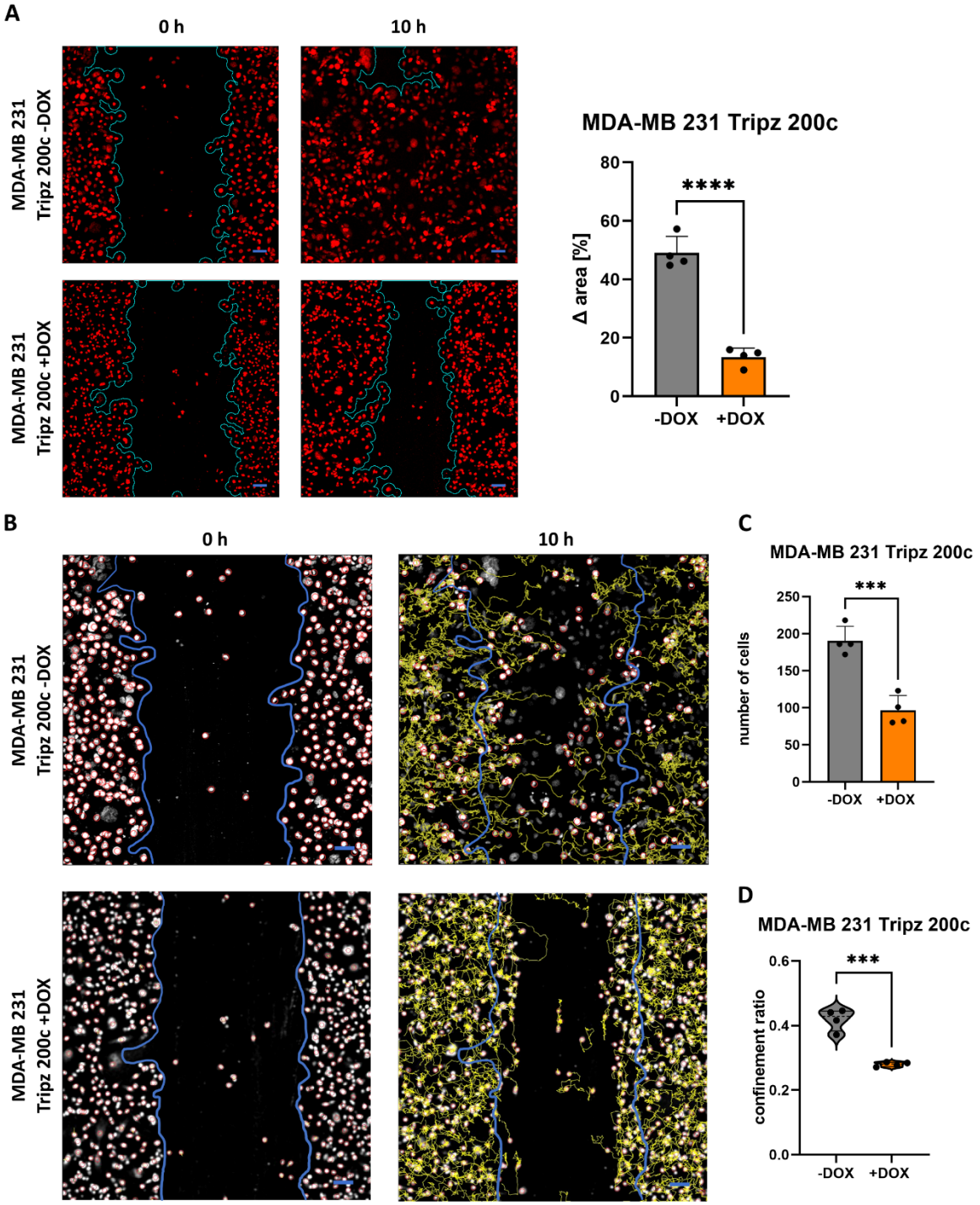

Figure 14: MDA-MB 231 breast cancer cells without microRNA 200c (miR-200c) expression leave cell clusters more frequently. **(A)** Wound closure of MDA-MB 231

Tripz 200c cells with (doxycycline treated, +DOX) or without (not doxycycline treated, -DOX) miR-200c expression. Blue lines in the microscopic pictures (left) indicate the borders of the wound at 0- and 10-hours post scratching. The difference in the area in [%] (right) is used to quantify the scratch closure (n = 4). Cells are stained with siR-DNA. Values are displayed as mean with SD. For statistical evaluation an unpaired, two-tailed student's t-test was performed. **** $p < 0.0001$. **(B)** Microscopic pictures of MDA-MB 231 cells with different miR-200c expression and their corresponding trajectories representing temporally resolved migratory behavior of individual cells. Scale bar equals 50 µm and applies to both (A) and (B). These pictures were additionally used for the analysis of **(C)** the number of cells closing the scratch and **(D)** the confinement ratio (n = 4). Blue lines present the border of the scratch at 0 hours. Yellow lines represent the trajectories of the cells after 10 hours. Values in (C) are displayed as mean with SD. The dashed line shows the median and the full lines the quartiles of the violin plot in (D). For statistical evaluation an unpaired, two-tailed student's t-test was performed in (C) and (D). *** $p < 0.001$.
The data collection of the scratch assay was performed by Dr. Andreas Roidl and Lorina Bawej (both from Pharmaceutical Biotechnology, Department of Pharmacy, Ludwig-Maximilians-Universität München, Germany) and Prof. Dr. Stefan Zahler (microscopy, Pharmaceutical Biology, Department of Pharmacy, Ludwig-Maximilians-Universität, Germany). The raw analysis with TrackMate was partly performed by Dr. Andreas Roidl (Pharmaceutical Biotechnology, Department of Pharmacy, Ludwig-Maximilians-Universität München, Germany).

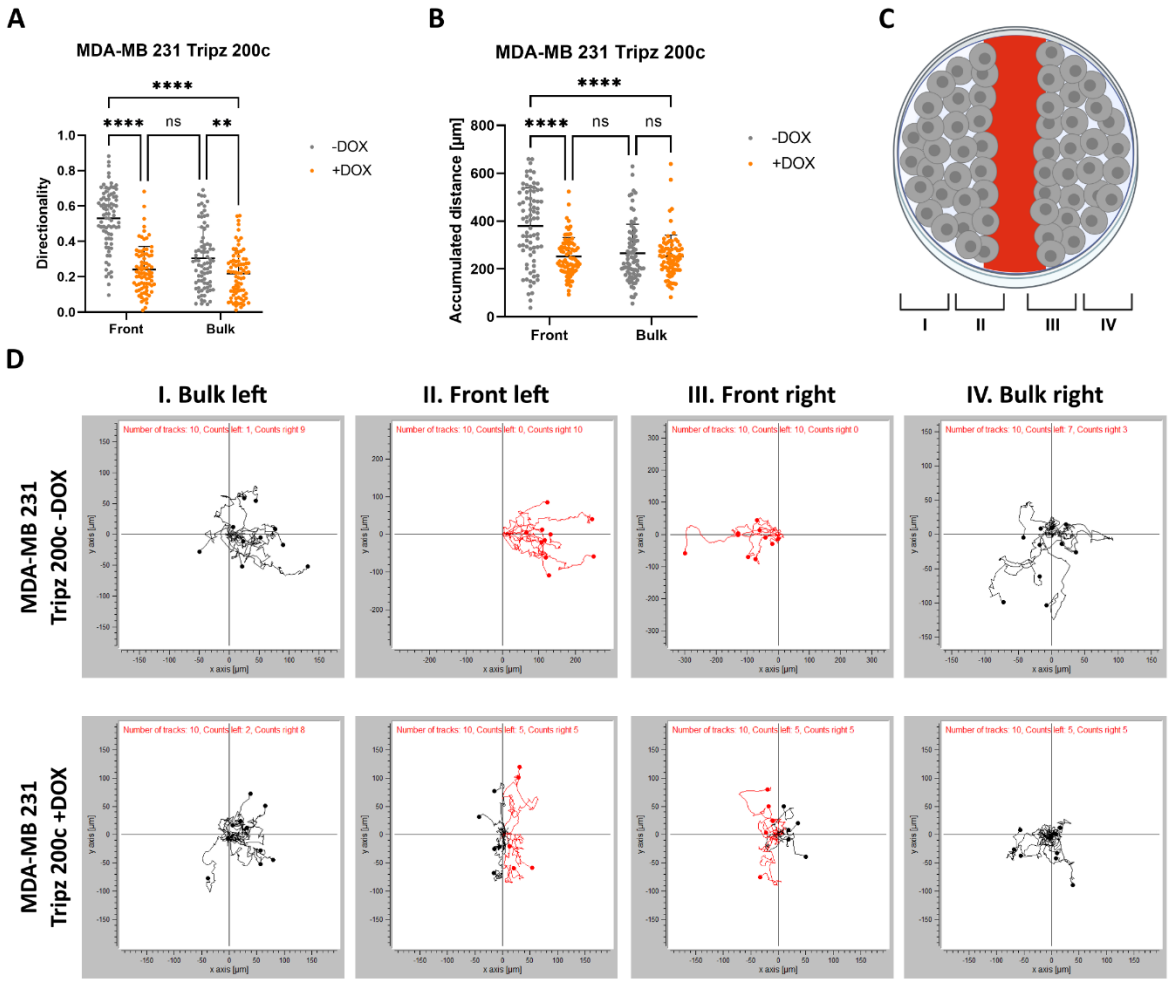

Figure 15: Enhanced directionality and accumulated distance of the microRNA 200c (miR-200c) non-expressing MDA-MB 231 cells in the front region. **(A)** Quantification of the directionality of MDA-MB 231 Tripz 200c doxycycline- uninduced (-DOX) and induced (+DOX) cells in the front and in the bulk region (n = 80 cells, 20 cells per biological replicate (4 replicates in total), right and left side were cumulated). Values are displayed in a scatter dot plot as mean with SD. For statistical evaluation a two-way ANOVA with multiple comparison and Šidák correction was performed. ns = not significant, ** $p < 0.01$, **** $p < 0.0001$. **(B)** Quantification of the accumulated distance of MDA-MB 231 cells with altered miR-200c expression (n = 80 cells, 20 cells per biological replicate (4 replicates in total), right and left side were cumulated). Values are displayed in a scatter dot plot as mean with SD. For statistical evaluation a two-way ANOVA with multiple comparison and Šidák correction was performed. ns = not significant, **** $p < 0.0001$. **(C)** Analysis of migration behavior of cells in different regions of the scratch (front or bulk cells). Schematic presentation of the different areas within a scratch. Figure was created with BioRender.com. **(D)** Motility plots of cells (from experiment displayed in Figure 14B) in the bulk region left (I), front left (II), front right (III) and bulk right (IV) using the “Chemotaxis und Migration Tool” software from ibidi GmbH (Germany). Red trajectories represent migratory behavior into the scratch.

To further investigate if miR-200c-positive cells are also less frequently leaving cell clusters in 3D structures, cell aggregates were formed and embedded into collagen. Cluster cell migration and outgrowth of the aggregates were analyzed. The MDA-MB 231 cell system was unable to be quantified for cluster cell migration in 3D as no aggregates, but only loose formations of cells developed (Figure 16A and Supplementary Figure S14A). The development of the cell aggregates of MCF7 wt and KO 200c was monitored over 16 days post embedment into collagen. Cell aggregates with perimeter and size from specific time points are shown exemplarily in the supplementary Figure S14B-D. MCF7 wildtype and miR-200c KO cell aggregates on day 4 are shown in Figure 16B. The subsequent analysis of the spreading area revealed an approximately 2-fold higher area in miR-200c-negative MCF7 aggregates compared to the parental ones (Figure 16B bottom). To analyze the shape of the aggregates with and without miR-200c expression, we plotted the perimeter to area ratio (Supplementary Figure S14E). A second-grade polynomic function of a perfect circle was applied as a reference and the coefficient of determination obtained from this function was specified. This function was used with the two MCF7 cell lines. Each data point corresponds to the ratio of perimeter to area on a given day. The comparison of the curves and the coefficients showed that MCF7-aggregates with miR-200c expression follow an almost perfect circle in their temporal development whereas MCF7 KO-aggregates show a frayed shape. This irregular shape of the miR-200c KO cell aggregates together with the significantly increased spreading area (“area of migrated cells”) in these cells suggest higher motility within these aggregates and therefore a higher chance to leave cell clusters.

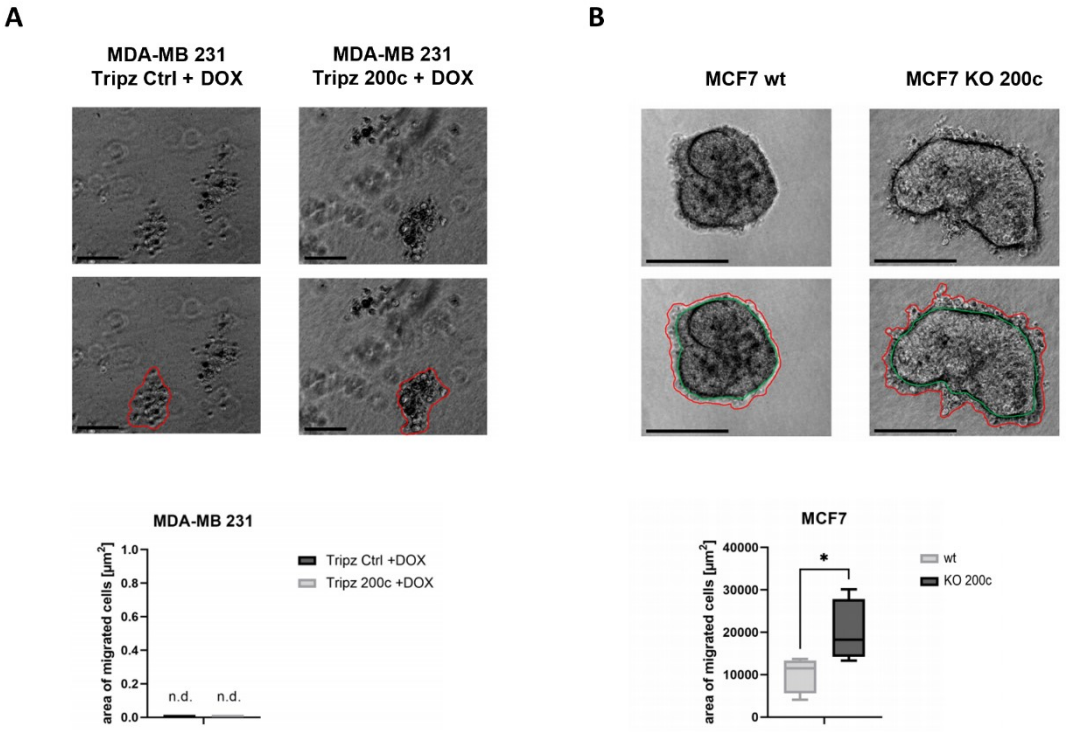

Figure 16: miR-200c-negative MCF7 cells tend to leave 3D aggregates more frequently compared to MCF7 wildtype cells. Quantification of cluster cell migration and outgrowth in 3D cell aggregates with different miR-200c expression. Cell aggregates of **(A)** MDA-MB 231 cells and **(B)** MCF7 wt and KO 200c embedded into collagen. Pictures show aggregates at day 4 after embedment into collagen. The area of the whole aggregate (red) was analyzed and compared to the core are (green). The difference is termed “area of migrated cells” in 3D. Scale bars are 200 µm for MCF7 and 100 µm for MDA-MB 231, respectively. For statistical evaluation an unpaired, two-tailed student’s t-test was performed. * $p < 0.05$, n.d. = not detected.

Detached cells from the primary tumor have the ability to disseminate into distant organs to form metastases. As we have observed elevated outgrowth rates of miR-200c depleted cells in 3D aggregates, we next simulated the survival (also called anoikis) of these shed cancer cells. Regulation of cell survival is of importance as anoikis resistant cells can attach to different matrices and facilitate the colonization to distant organs (197, 198). MCF7 and MDA-MB 231 cell lines were seeded into low attachment plates to prevent cell-matrix adhesion and cell survival as a measurable value for anoikis was measured. The expression of miR-200c in both cell systems resulted in a significant decrease in cell survival compared to miR-200c non-expressing cells (Figure 17A and B). This implicates that loss of miR-200c acquires anoikis resistance and the mesenchymal phenotype of breast cancer cells (MDA-MB 231 cells) facilitates anoikis resistance.

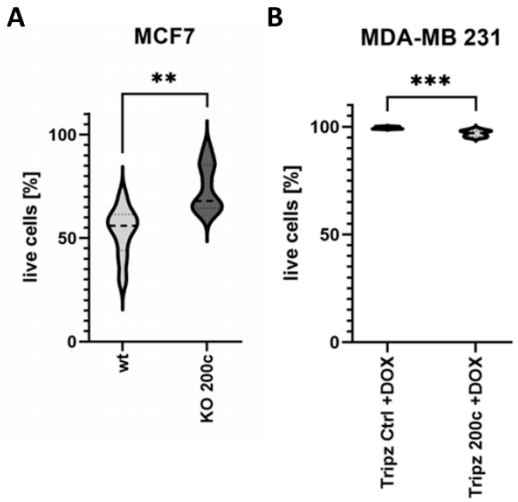

Figure 17: An increased rate of anoikis in miR-200c-expressing cell systems. Measurement of live cells (%) in **(A)** MCF7 (n = 3) 24 hours post-seeding and **(B)** MDA-MB 231 cells (n = 3) 96 hour after cultivation. Values are displayed as a violin plot with median (dashed pattern) and quartiles (dotted pattern). For statistical evaluation an unpaired, two-tailed student's t-test was performed. ns = not significant, ** $p < 0.01$, *** $p < 0.001$.

4.4 Migration is Reduced in miR-200c-Positive Cells in Transwell Assays

Metastasis formation involves single cells disseminating from a cluster of cells, e.g., the primary tumor. Analogously, in a transwell assay a cell needs to disassociate from the cellular cluster and subsequently squeeze through a pore of a membrane. Therefore, this assay analyzes migration of both stages: collective-cell migration and single-cell migration. In order to pass through the pores cells are forced to alter their plasticity. The motility ability of cells in the transwell assay was determined by quantifying the number of cells which migrated through the pores of the membrane. The epithelial MCF7 wildtype cells migrated less frequently compared to the MCF7 KO 200c cells (Figure 18A). The quantitative analysis shows that the relative migration of MCF7 cells significantly increased by 1.5-fold when these cells did no longer express miR-200c (MCF7 KO 200c) (Figure 18B). Furthermore, the second cell system MDA-MB 231 Tripz 200c (-DOX) showed a higher migratory capacity, which was inhibited by 40 % when switching on miR-200c expression (+DOX) (Figure 18C and D). These data show, that besides an miR-200c-effect on collective migration, miR-200c acts negatively on single-cell plasticity and motility.

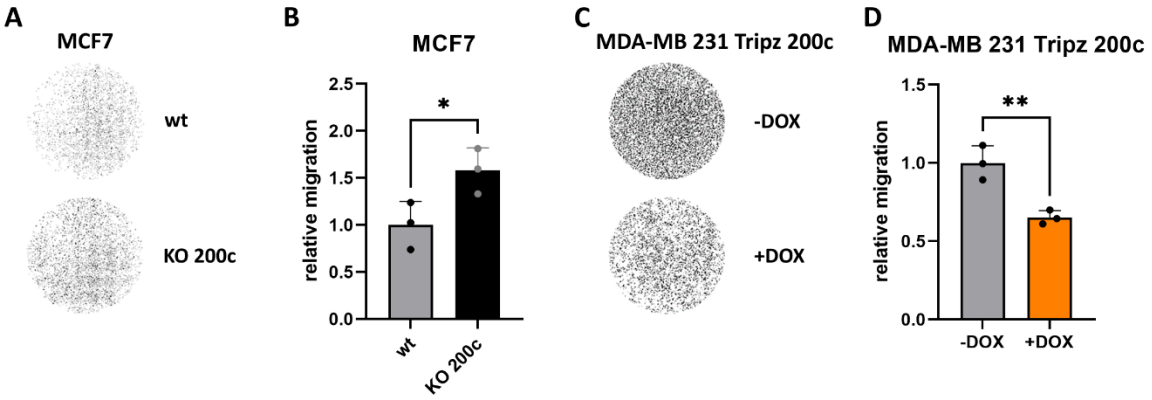

Figure 18: MicroRNA 200c (miR-200c) expression negatively modulates relative migration in a transwell assay. Pictures of the membranes with crystal violet stained, migrated **(A)** MCF7 wildtype (wt) and knockout (KO) 200c cells and **(B)** the calculated relative migration (normalized to MCF7 wt cells, n = 3). Values are displayed as mean with SD. For statistical evaluation an unpaired, two-tailed student's t-test was performed. * $p < 0.05$. With crystal violet stained **(C)** MDA-MB 231 Tripz 200c cells with and without doxycycline (DOX) induction and **(D)** the corresponding quantification of the relative migration (normalized to MDA-MB 231 Tripz 200c -DOX, n = 3). Values are displayed as mean with SD. For statistical evaluation an unpaired, two-tailed student's t-test was performed. ** $p < 0.01$.

4.5 miR-200c Critically Determines Confined Cell Motility

To study a potential impact of miR-200c on single-cell migration, we used a micropattern assay, consisting of two square islands connected by a thin bridge (Figure 19A and B). On this dumbbell-shaped assay, single cells repeatedly have to overcome the constricting bridge while they migrate. Therefore, with this assay, we gain quantitative insight into confined single-cell migration, which is a key aspect of metastasis. On the micropattern, MDA-MB 231 cells were highly motile and repeatedly hopped between the two islands (Figure 19A and B, Video 9 and Video 10). Because this process is variable between repeated experiments (199), we imaged a large amount of micropatterns simultaneously (n> 85). To quantitatively study this inherently stochastic migration behavior, we tracked the cell nuclei in all micropatterns (Figure 19C and D). Using these trajectories, we analyzed the hopping behavior of both miR-200c-negative (untreated, -DOX) and positive (treated with doxycycline, +DOX) MDA-MB 231 Tripz 200c cells. To quantify transition dynamics between the islands, we computed the stay probability $S(t)$ that a cell was not performing a transition between islands after a certain time t. Upon induction of the miR-200c (+DOX), cells showed an approximately two-times higher probability not to make a transition (Figure 19E). This indicates less frequent transitions after induction of miR-200c, which

correlates with the significant decrease in relative migration in our transwell assay (Figure 18D). Furthermore, we quantified the average speed of a cell when it is making a transition on the bridge. We found an approximately two-fold decrease of the transition speeds upon induction of miR-200c (Figure 19F). Taken together, these results showed that both transition frequency and transition speed of migrating MDA-MB-231 cells decreased due to miR-200c expression, indicating that miR-200c negatively affects the efficiency of confined cell migration.

To further obtain a quantitative understanding of the hopping behavior, we aimed to describe cells in our micropattern using a dynamical model. We made use of a previously developed approach to directly infer from finite experimental trajectory data a Langevin equation of motion describing the stochastic nucleus trajectories (184). The key advantage of this inference procedure is that it can separate stochastic features from deterministic features of cell behavior. Specifically, we find an effective force $F(x, v)$ for MDA-MB 231 cells with and without miR-200c expression. This effective force describes the deterministic part of the acceleration of the nucleus of these cells due to the average active cell migration behavior in our micropattern. The learned models can accurately predict the different stay probabilities (Figure 19E, dotted lines) and the average transition speeds of the cells (Figure 19F, dotted lines). Interestingly, we observed a clear difference in the effective force $F(x, v)$ of the two different miR-200c expression states of the MDA-MB 231 Tripz 200c cells which allows us to explain the higher stay probability in the miR-200c-positive MDA-MB 231 cells (Figure 19G): From a dynamical systems point of view, MDA-MB 231 cells without miR-200c expression, perform so-called “limit cycle oscillations”, which means that cells repeatedly and deterministically hop between the two islands (Figure 19H). In this case, the stochasticity only affects the hopping speed. In contrast, the miR-200c-positive MDA-MB 231 cells (Tripz 200c +DOX) displayed a qualitatively different behavior. Instead of deterministic oscillations, they are bistable and thus require fluctuations to hop between the islands (Figure 19I). This gave rise to less frequent and slow random transitions as observed (Figure 19E, F). Similar behavior has also been observed in the previously analyzed non-cancerous human epithelial breast cell line MCF10A (183), which endogenously expresses high levels of miR-200c (128), indicating that induction of miR-200c in the MDA-MB-231 cells fundamentally changed the phenotypic migratory behavior in our confining microenvironment. With the

induction of miR-200c the motility of the breast cancer MDA-MB 231 cells converged to the motility behavior of the non-cancerous MCF10A cells (183).

Additionally, an effect of the miR-200c-inducer DOX on confined cell motility needed to be excluded. Therefore, induced MDA-MB 231 control cells (Tripz Ctrl) were examined under similar conditions. As expected, we found that the behavior of induced control cells (Tripz Ctrl +DOX, Supplementary Figure S15A to C, Supplementary Video S7) is comparable with the behavior of miR-200c-negative cells (Tripz 200c -DOX) which is well described by limit cycle oscillations and is additionally comparable with wildtype MDA-MB 231 cells (183). The analysis of the effective force $F(x, v)$ of induced control cells revealed a similar pattern as the uninduced MDA-MB 231 Tripz 200c cell line (Figure 19G, Supplementary Figure S15D). Thus, the administration of DOX had in general no influence on the migratory profile of MDA-MB 231 cells. In our second cell system neither MCF7 wildtype nor miR-200c knockout (KO) cells were able to perform any form of cell hopping in this dumbbell assay (Supplementary Figure S15E and F, Supplementary Video S8 and Video S9) and therefore an evaluation of this cell system was not possible. Taken together, our dumbbell-micropatterns provide conceptual insight into the hopping dynamics altered due to miR-200c activation: From a dynamical systems perspective, miR-200c qualitatively changed the behavior of MDA-MB 231 from deterministic hopping to stochastic and less frequent hopping within our two-state micropatterns. This indicates that miR-200c hampers the ability of cells to efficiently migrate in confining microenvironments.

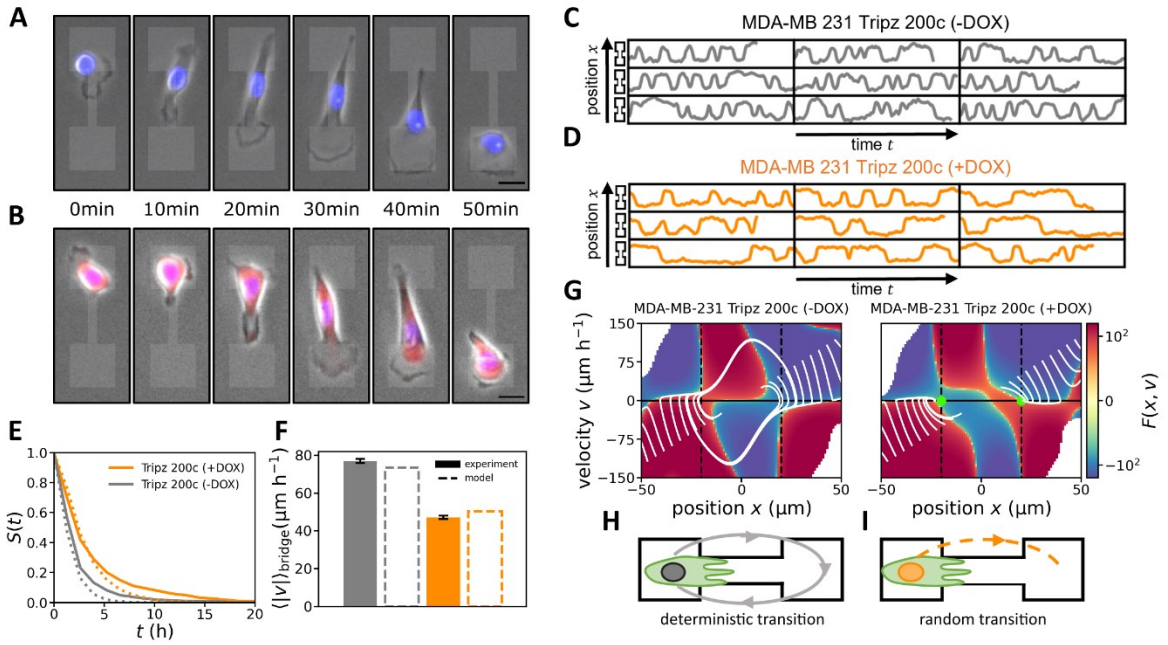

Figure 19: MicroRNA 200c (miR-200c) negatively affects the efficiency of confined cell migration. **(A)** Time series of brightfield images of a MDA-MB 231 Tripz 200c cell without miR-200c expression performing hopping behavior in a two-state micropattern. **(B)** Time series of brightfield images of a MDA-MB 231 Tripz 200c cell with miR-200c expression. Nuclei are stained in blue. Scale bar equals 20 µm and applies to both (A) and (B). Red fluorescence shows the red fluorescence protein (RFP) which is simultaneously expressed with miR-200c upon effective doxycycline (DOX) induction. Selection of nucleus trajectories for **(C)** MDA-MB 231 Tripz 200c (-DOX) (n = 85) and **(D)** MDA-MB 231 Tripz 200c (+DOX) cells (n = 94). Small dumbbell symbols next to the trajectories indicate the location of the cell. **(E)** Stay probability of the two cell lines which describes how likely it is that a cell has not made a transition after a certain time t. Both in (E) and (F) MDA-MB 231 Tripz 200c (-DOX) (n = 85) and MDA-MB 231 Tripz 200c (+DOX) cells (n = 94) are evaluated and dotted lines indicate model results. **(F)** Average speed of the MDA-MB 231 Tripz 200c cells while making a transition on the bridge. Values are displayed as mean with SEM. Legend of (E) also applies here. **(G)** Inferred effective force $F(x, v)$ describing the deterministic part of the hopping dynamics of the two states of the cells. White lines show the deterministic behavior in the two-dimensional phase space of the cells for the MDA-MB 231 cell line in both states. Green dots indicate the fix points of the dynamics in the (+DOX) case. Schematics in **(H)** and **(I)** show the qualitatively different dynamics of cells in the micropattern. Gray loop indicates deterministic transition dynamics where cells without miR-200c repeatedly oscillate between two islands. Dotted line indicates that cells with miR-200c only perform transitions into the opposite island when they are randomly excited to do so.

The data collection and analysis of the 1D dumbbell assay as well as the figure layout was performed by Emily Brieger (under the supervision of Prof. Dr. Joachim Rädler, Faculty of Physics and Center for NanoScience, Ludwig-Maximilians-Universität München, Germany) and Tom Brandstätter (under the supervision of Prof. Dr. Chase Broedersz, Department of Physics and Astronomy, Vrije Universiteit Amsterdam, Netherlands; Arnold-Sommerfeld-Center for Theoretical Physics, Ludwig-Maximilians-Universität, Germany). The corresponding text was written by Emily Brieger (under the supervision of Prof. Dr. Joachim Rädler, Faculty of Physics and Center for

NanoScience, Ludwig-Maximilians-Universität München, Germany) and Tom Brandstätter (under the supervision of Prof. Dr. Chase Broedersz, Department of Physics and Astronomy, Vrije Universiteit Amsterdam, Netherlands; Arnold-Sommerfeld-Center for Theoretical Physics, Ludwig-Maximilians-Universität, Germany) and adapted when appropriate.

5. Discussion

The following two chapters are based on the content from the original publication which was published as Köhler *et al.*, Cancers (Basel). 2022 Nov; 14(22): 5554 as well as the original publication which was published as Köhler *et al.*, Mol Oncol. 2024 Oct 15 y (see chapter 10.1 Articles). While there are partial overlaps text sections have been expanded with new and more detailed insights.

5.1 Discussion Chapter I: MicroRNA-200c Prevents Drug Resistance by Downregulating Glutathione S-Transferases

To investigate the role of miR-200c on drug resistance *in vitro* three cell systems differentially regulating miR-200c expression in breast cancer were utilized, including a genetic knockout of miR-200c in the epithelial MCF7 cell line, an inducible overexpression of miR-200c in the mesenchymal TNBC cell line MDA-MB 231 and an inducible miR-200c decoy system in the MCF7 cell line to scavenge the mature miRNA strand. Of note, comparing MCF7 wildtype and miR-200c KO cells (the expression of both strands, the 3p and 5p strand is hampered as the pri-miR is not further processed (200)) only targets are expected to be identified that are regulated under physiological settings. On the contrary, the MDA-MB 231 Tripz 200c cell line shows endogenously low levels of miR-200c which is reversed upon induction. This overexpression of miR-200c may consequently additionally affect targets with lower abundancy under physiological conditions. This approach is of interest when a wide range of highly expressed oncogenes needs to be altered simultaneously.

Aside from others, GSTM3, a glutathione-S transferase, and the glutathione pathway were identified in the proteome analysis of the MCF7 wildtype and miR-200c knockout cells to be differentially expressed. This identified pathway belongs to the cellular phase II detoxification (63-65) in which the glutathione-S transferases play a key role. In general, enhanced activity of GSTs foster drug resistance via decreasing the intracellular drug levels (63, 67, 201). Besides GSTM3 also other GSTs, e.g., GSTO1, GSTP1, GSTK1 and GSTA4, are known to induce resistance in cancer in various ways (202-204). As an example, GSTP1, an already well-studied resistance inducer in breast cancer (205, 206), utilizes two approaches to contribute to drug resistance formation. First, GSTP1 overexpression causing elevated drug efflux and secondly,

GSTP1 additionally being able to target the MAP kinase pathway (63, 206). This GST, besides others, was also found to be regulated upon miR-200c expression in the present work. As GSTM3 was the most differentially expressed GST in all cellular systems, the miR-200c binding site (a 7mer-m8) in its 3′UTR was validated. In seven further GSTs the same binding site (5 times) or similar sites (2 times) were found. The mRNA expression check of GSTs upon miR-200c expression partly confirmed the *in silico* results. The additional regulation of other GSTs could have several reasons including on the one hand the possibility that the sequence of the binding sites is not strictly determined, and on the other hand that miRNAs can also bind to the 5′UTR, the coding sequence, and to gene promoters (108) resulting in altered GST expression.
This study showed for the first time that miR-200c directly regulates the expression of GSTs and thus promotes the phase II detoxification via catalyzing the conjugation of GSH to xenobiotics. A significantly higher cellular GSH pool as well as an increase in cell death, demonstrated by higher subG1 levels, was measured when miR-200c was expressed and cells were simultaneously treated with chemotherapeutics. To exclude potential contribution to resistance formation upon other targets in the utilized cellular systems, the expression of ABCB1, a p-glycoprotein enhancing the drug efflux through elevated expression, was validated (207) and revealed no significant regulation upon miR-200c expression (Supplementary Figure S9, Table 5).

Besides utilizing three cellular breast cancer systems with differentially expressed miR-200c, the study was extended to additional types of cancer including lung cancer (A549 cell line) and bladder cancer (T24 cell line) to broaden the significance of miR-200c as a chemosensitizing miRNA. Similar to the MDA-MB 231 cells both cell lines endogenously express low miR-200c (Supplementary Figure S10A) which though can be induced upon DOX administration (Supplementary Figure S10B) after lentiviral transduction of the Tripz 200c construct. The miR-200c sensitized these cells to chemotherapeutic treatment and therefore can also be termed chemosensitizer for breast, lung and bladder cancer. In accordance with our observations the miR-200 family was published to sensitize pancreatic cancer cells to gemcitabine (208), head and neck cancer to taxol via a miR-200c/SSFA2/IP3R1 axis (209) and to play a role in multi drug resistance in A549 cells (210).

To evaluate whether the *in vitro* findings can be resembled *in vivo,* a more complex experimental environment, two mouse xenograft experiments with MDA-MB 231

Tripz 200c tumors were conducted. The first experimental attempt mimicked the clinical situation of patients, with miR-200c positive and negative tumors. Thus, mice developed tumors either with or without miR-200c expression *ab initio*. A late tumor growth onset and the reduced proliferation are similar to previously published data (114, 128, 151, 211-215) and clearly reflect the presented *in vitro* studies. As miR-200c can regulate also proliferation-associated proteins, most important Kras (117, 212) this observed effect on proliferation can be explained. Furthermore, miR-200c can directly target the Jagged1 receptors which is involved in Notch signaling and results in anti-proliferative effects in metastatic prostate cancer (103, 216). Also, chemotherapeutic treatment alone was able to reduce tumor growth in miR-200c positive and negative tumors. Nevertheless, the additive effect of the combinatorial miR-200c and DXR treatment resulted in reduced tumor growth and prolonged survival *in vivo*. This can be exploited by reducing the dose of chemotherapeutics, i.e. relieving doxorubicin side effects such as cardiotoxicity (217).

The second *in vivo* experiments evaluated if miR-200c expression can affect the efficacy of chemotherapeutic treatment. miR-200c negative tumors were either treated with chemotherapy, with miR-200c via induction using DOX administration or the combination of both. A clear beneficial effect of the miR-200c expression together with chemotherapeutic treatment was observed as all mice showed a decline in tumor volume and even 60 % of mice no measurable tumors as the result of a complete response to the administered therapy until the end of this study (day 250 after tumor cell inoculation). In the first study mice are differently responding to the treatment compared to the second animal study which could be explained by the adaptive effect of mice towards miR-200c expression in study one. Tumor growth rates of miR-200c-negative and positive tumors at later stage of the first study support this effect (Figure 8E).

So far, only *in vitro* studies investigated the combinational application of miR-200c and drug treatment (218). Though, the combinational strategy was already applied with other miRNAs like miR-101 or siRNAs like siEG5 in several cancer entities like hepatocellular carcinoma (219, 220), melanoma (221), cervix carcinoma (222) etc. (223) over the past few years. Up to now, the present *in vivo* studies on the combination of miR-200c and chemotherapeutic drugs are the first one being performed and reflect a tremendous improvement of chemotherapy when combined with miR-200c.

Therefore, novel approaches like the non-invasive detection of circulating miRNAs in liquid biopsies could be utilized in clinical settings in order to apply appropriate therapeutic approaches (224).

Consequently, chemotherapeutics show less efficacy on miR-200c depleted tumors which acquired drug resistance. This is also reflected by worse overall survival of breast cancer patients with low miR-200c expression in the Kaplan–Meier plots (Figure 9A). Loss or reduced miRNA expression levels might have many causes and in the following the most common are named and extended by specific regulatory mechanisms. Loss of miR-200c is known to be related to p53 mutation which in turn can increase Moesin expression, an oncogene considered to play a role in drug resistance (130, 225). Some mechanisms affecting miR-200c expression include besides miR-200c gene deletion also epigenetic processes like histone modifications of miRNA genes and the aberrant methylation of DNA (54) as of CpG island in the promoter region of the miR-200c/141 cluster (226) and TGF-β1 which can increase the methylation rate of miR-200c (119, 227). Differentially expressed transcription factors also contribute to the altered regulation and expression of miR-200c (54), i.e. ZEB1 binding alone or together with the transcription factors: C-terminal binding proteins (CtBPs) and Brahma-related gene-1 (BRG1) (103) suppress miR-200c expression. ZEB2 as well as p53 transcription factor regulate the expression of miR-200c (228). In addition, the basic helix-loop-helix transcription factor Achaete Scute-like 2 (Ascl2) and Twist are known to be a potential transcriptional repressor of miR-200c (103, 229, 230). The altered expression of miR-200c can also be caused by the expression of competitive endogenous RNAs (ceRNAs) (54) exemplarily via the expression of long non-coding RNAs (lncRNAs) such as TMPO-AS1 (231) and XIST (232). Additionally, circular RNA, i.e. circ-ZEB1, can act as a sponge on miR-200c resulting in chemoresistance formation in colorectal cancer as described by Chen *et al.* (233). The miR-103/107 family can inhibit the dicer activity and lead to a misregulation of miR-200c biogenesis (54) resulting in decreased expression levels (119, 234).

Whether GST inhibitors like Ethacraplatin-containing micelles, TLK199, Auranofin, TLK286 and Brostallicin are beneficial for the treatment of (breast) cancer is under investigation in several clinical trials as reviewed by Pljesa-Ercegovac *et al.* (235). Moreover, upstream regulators of GSTM3 such as GAS5 (236), a lncRNA which has

a mechanism of action comparable with a GST inhibitor, could contribute to chemosensitization describe promising subjects for further research.

5.2 Discussion Chapter II: Unraveling the Metastasis-Preventing Effect of miR-200c *In Vitro* and *In Vivo*

The interrelated steps of the invasion-metastasis cascade are the best to summarize the complex process of metastasis formation, and include the steps of cell motility, EMT, invasion, intra- and extravasation, anoikis and metastatic colonization (90). Whether the 23 nucleotides of miR-200c, a miRNA with a pleiotropy of targets within this cascade, can control the complex process and impede metastasis formation was to be elucidated. Currently, less evidence is reported in literature that sole miR-200c expression can modulate metastasis *in vivo*, most of these *in vivo* studies focused on cancer hallmarks like tumor growth, chemoresistance or immune-modulatory effects (151, 152, 212, 213, 237-240). Only Knezevic *et al.* studied metastasis formation upon miR-200c expression in more detail by analyzing lung metastases in claudin-low breast cancer (213). Therefore, to investigate the role of miR-200c on the formation of metastases *in vivo*, a mouse xenograft model with inducible miR-200c TNBC tumors, which were additionally tagged with luciferase, was utilized in the here presented animal experiment. Since the bone, lung, brain and liver are the major metastatic sites of breast cancer (78, 241-243) these organs, except for the bone, were evaluated together with the spleen for metastases *ex vivo*. Upon the induction of miR-200c expression in the primary tumor of the mice the metastatic burden, defined as the number of organs infiltrated with metastases, was diminished. This indicates that exclusive miR-200c expression leads to decreased rates of metastasis formation. As opposed to that, other reported studies which were also dealing with cell spreading used either the whole miR-200c/141 cluster, miR-200b or functional families including three different miRNAs (152, 165, 169, 244-247), but not sole miR-200c expression. Noteworthy the study of Simpson *et al.* in which the effect of the expression of the miR-200c/141 cluster was analyzed, revealed MXRA8 as a miR-200 target, and a factor in basal-like breast cancer metastasis (152). Clinical impact was demonstrated by the study of Song *et al.* who analyzed distant metastasis in 134 breast cancer patients and observed more patients with distant metastases in the cohort of patients with low levels of miR-200c (212). Furthermore, enhanced lymph node invasion in breast cancer patients was associated with decreased miR-200c expression (127, 248, 249). As known from the previous chemoresistance study presented also in this thesis, low miR-200c expression is correlated with a decreased overall survival of breast cancer

patients, which in turn is connected with metastasis formation in mammary carcinoma (113). Therefore, miR-200c is proposed to be a metastasis suppressor *in vivo*.

Experimental findings indicated sole miR-200c expression to impede the complex process of metastases formation by potentially affecting several important targets like XIAP, FOXF2, ZEB1, E-Cadherin, HMGB1, MXRA8, ZEB2, FN1, LEPR, FHOD1, PPM1F, Moesin, NTRK2, BMI-1, KRAS, PDE7B, USP25 and further as reviewed by i.e., Humphries *et al.* (76, 103, 152, 155, 158, 161, 212, 240, 245, 250-252).
miR-200c is known to inhibit EMT as it binds directly to ZEB1 and ZEB2 and subsequently decreases their expression which in turn leads to an increase of E-cadherin expression (76, 98). In this case, cancer cells undergo MET and maintain an epithelial, non-migratory behavior. Though, the transcription factors ZEB1 and ZEB2 themselves can reverse this transition by binding to the E-box sites of miR-200c and then again impede the transcription of E-cadherin resulting in mesenchymal-like, highly motile cancer cells (76).
Genes like BMI-1 and TrkB are both miR-200c targets but show a dual role as they are concurrently altering EMT and resistance formation (103). Cochrane *et al.* demonstrated in their study that exclusive restoration of miR-200c expression can hamper invasiveness (via suppression of ZEB1 and restoration of E-cadherin) and enhance chemosensitivity to microtubule-targeting agents at the same time (253). Due to the multispecificity of miR-200c, the metastasis formation driven by miR-200c was additionally analyzed in combination with administration of doxorubicin in this work. With this combinatorial treatment metastasis formation in mice was successful hampered making it a favorable treatment strategy for preventing metastases in miR-200c depleted breast cancer patients. Even pulmonary metastases were not detectable, which are often the cause of treatment failure in metastatic breast cancer. Upon the diagnosis of breast cancer with lung metastasis patients usually have a median survival of about 25 months, only (254, 255), which depicts the urgent need of an improved therapy for metastatic breast cancer.
Nonetheless, miR-200c has also been published earlier to foster lymph node and lung metastasis, and enhanced lung colonization in mouse models (256, 257).
However, the presented *in vivo* study clearly depicts the reduced metastatic burden in mice expressing miR-200c positive breast cancer tumors. Data from Xue *et al.* additionally support the hypothesis of miR-200c as a metastasis suppressor also in lung cancer (258).

To evaluate *in vitro* explanations for the observed *in vivo* findings one step of the invasion-metastasis cascade was validated in more detail namely the migration of cells, as it is the prerequisite of metastasis. Collective as well as single-cell migration were elucidated starting with more complex cellular systems and ending up with single-cell movement in confined spaces. The undirected migration analysis with the novel tool entitled “Cellwatcher M” revealed a confluence-dependent effect of miR-200c on cell motility. When higher confluence rates were achieved cell-cell contacts as well as cellular adhesion possibly influence migratory speed and can lead to its reduction as depicted in the MCF7 KO 200c cells. These cells grow in tight clusters when confluence is increased which in turn contribute to the reduction in migratory speed to the level of the wildtype MCF7 cells.

Unlike, the motility speed is increased when miR-200c is expressed in the mesenchymal MDA-MB 231 and when cell confluence is increased. A possible explanation for this observation is the expression of cell surface molecules like E-Cadherin (259) upon miR-200c which might enable and support the sliding behavior of cells instead of their unrestricted collisions. The analysis of undirected migration in different cellular models displayed the importance of the cellular phenotype on collective migration. Kopp *et al.* demonstrated that mesenchymal breast cancer cells show low or no expression of miR-200c, whereas epithelial cells are described by elevated expression of miR-200c (118). Using a stable knockout or the inducible overexpression system of miR-200c phenotypes were switched within single breast cancer cell lines.

The effect of miR-200c on direct migration was measured using scratch assays. An elevated rate of wound closure and an increased number of cells unrestrictedly closing the free area of the scratch was observed in miR-200c non-expressing breast cancer cells. Further parameters like confinement ratio (which is also known in literature as the straightness index or the persistence (260, 261)) and directionality, indicating the efficiency of a cell to move from its initial point in a direction, were analyzed to additionally characterize the role of miR-200c on migration. Both of these motility indicators were increased in miR-200c-negative cells resulting in enhanced directed movements (262). This observation was even clearer when separately analyzing the front region of the scratch assay in miR-200c-negative cells. These cells demonstrated elevated cell motility into the wound area, whereas the tendency of miR-200c-positive

cells to stay in their cellular clusters might once again be ascribed to cell contacts. Interestingly, no significant difference in migration speed between the two miR-200c expression states was observed. Habitually an epithelial monolayer, represented here by miR-200c-positive MDA-MB 231 cells, moves in a coordinated way (263). This was not observable, which leads to the conclusion that miR-200c impedes motility but does not evoke formation of collectively moving monolayers.

If miR-200c-positive cells incline to stay within their cellular clusters also in 3D was evaluated in a collagen assay. miR-200c could hamper the ability of MCF7 cells to leave the association of cells and subsequently migration into the collagen matrix was also impaired. No MDA-MB 231 breast cancer cell aggregates were formed upon the performance of the hanging drop method with subsequent embedment into collagen. An optimized protocol for a liquid overlay technique as shown e.g. by Froehlich *et al.* may result in MDA-MB 231 spheroids (264). The phenomenon that MDA-MB 231 in general but especially MDA-MB 231 cells with forced miR-200c expression do not form spheroids can also be related to impaired cytoskeletal arrangements. In cooperation, filamin A, an actin filament crosslinker, was uncovered to be inhibited upon miR-200c expression (114) which potentially might cause the inability to form spheroids in miR-200c positive cells.

miR-200c depleted cells showed a higher tendency to leave cell clusters which would be then more susceptible to recolonization. A process preventing detached cells to colonize at distant regions and form new secondary tumors is anoikis (198). It is a programmed cell death and characterized to occur after loss of cell-matrix adhesion (198). Elevated anoikis rates were detected in both miR-200c-positive breast cancer cell systems. The link between miR-200c and anoikis is EMT and loss of E-cadherin, respectively, as this transition is known to be associated with anoikis resistance (198, 265). As miR-200c can inhibit EMT in breast cancer these cells are sensitive for anoikis (197, 266). A predicted direct target of miR-200c which is able to restore anoikis sensitivity is TrkB (161, 169). Bringing these findings into clinical context, it can be stated that circulating tumor cells (tumor cells which entered the blood stream) (76) with miR-200c expression are less common to survive in the circulatory system.

Besides collective movement cells can migrate also as single cells. To analyze the crossover from collective-cell to single-cell movement a transwell assay was used in which cells need to leave their cellular cluster and to squeeze through a pore of a

membrane. This mimics the movement of cells through small cavities which can be found throughout the body as cells need to squeeze through e.g. vasculature of the blood system. miR-200c-positive cells displayed less migratory behavior and possibly altered cellular plasticity. Transwell data from Jurmeister *et al.* on invasion upon miR-200c mimic transfection and Park *et al.* on migration upon miR-200a/c transfection support these results (155, 267).

Finally, the movement of single cells in complex confining environments was investigated using 1D dumbbell assays. This experimental procedure is mimicking the cells' movement behavior after dissociating from the initial tumor site (97). Consistent with the transwell assay, cells must squeeze through a thin constricting obstacle (here a bridge). Herein, cellular plasticity is once again a prerequisite for this process and quantitative determination with the dumbbell assay revealed that miR-200c-negative cancer cells perform deterministic hopping, while miR-200c-positive cancer cells only hop randomly between the islands resulting in less frequent and slower transitions. This leads to the assumption that miR-200c alters migration also on single-cell level by negatively affecting the cancer cell's capability to squeeze through constricting cavities. As proposed by the motility behavior in the undirected migration analysis MDA-MB 231 cells with miR-200c expression should show elevated motility. This did not take place as single-cells on the dumbbell-shaped geometry lack cell-cell interactions.

The bridge of the dumbbell-shaped geometry acts as a cue for the MDA-MB 231 wildtype cells (183). The underlying mechanism might comprise the increased polymerization of actin fibers at the cell front whenever the cell's outward extension also known as protrusion is inside the bridge as suggested by Flommersfeld *et al.* and Brückner *et.al.* (268, 269). This, in turn, might be the consequence of increased alignment of actin fibers (270) or changes in the spreading of polarity cues (271) when the protrusion is limited in its sideways movement. Thus, miR-200c alters the cytoskeleton and subsequently reduces cellular motility in several ways. On the one hand, miR-200c expression is hypothesized to result in decreased cellular protrusions on the bridge. Additionally, the force on the cell's nucleus to follow the movement of the protrusions onto the bridge might be diminished. And on the other hand, the crosslinker of the actin cytoskeleton, filamin A, can indirectly be inhibited by miR-200c causing morphological changes (114). In addition, miR-200c can alter vimentin expression, an intermediate filament (IF) protein (272). Vimentin is expressed when

miR-200c is depleted (273, 274) and elevated vimentin levels were recently discovered to promote cell migration (272).
In contrast to the mesenchymal MDA-MB 231 cells, the epithelial MCF7 cells did not show any movement on the dumbbells, where the bridge might be even a more insuperable obstruction. This finding was supported by Mathieu *et al.* who measured only little velocity values of MCF7 cells on microlines (275) indicating no active movement or cytoskeletal dynamics of single MCF7 cells.

To bring the present findings into clinical use, miRNA delivery strategies (223) like viral and non-viral delivery systems need to be investigated for a successful application of miRNA-200c targeted therapies. Clinical trials for the replacement of miRNAs are already ongoing and include e.g., the delivery of miR-34, miR-16 and miR-193a-3p to reduce and prevent cancer metastasis (276) and the *in vitro* delivery of miR-200c loaded nanoparticles to inhibit proliferation (215) or the usage of mesoporous nanoparticles to deliver miR-200c as described by Garrido-Cano *et al.* (238). Administration of such multispecific miRNA nucleic acids to regulate a pleiotropy of targets might be more effective than altering individual targets. Further investigations on the role of miR-200c in additional cancer entities might extend the area of application for miR-200c targeted therapies.

6. Summary

This doctoral thesis deals with miRNA-200c and its crucial role in chemoresistance and metastasis in breast cancer.

The first part of the thesis revealed that miRNA-200c is regulating the glutathione pathway and hence facilitates the detoxification of xenobiotics like doxorubicin. Upon miRNA-200c expression this naturally occurring phase II detoxification is hampered increasing the susceptibility of cancer cells to classical chemotherapeutic treatment.
The underlying mechanism of action is the altered abundance of glutathione S-transferases (GSTs). The expression of various GSTs was impeded when cells expressed miRNA-200c, in particular the ones with *in silico* predicted miRNA-200c binding sites. Notably, the cytosolic glutathione S-transferase mu 3 (GSTM3) was detected to be a direct target und therefore upregulated in miRNA-200c depleted breast cancer cells *in vitro* and *in vivo*.
The *in vitro* treatment of different cancer entities with miRNA-200c and a chemotherapeutic agent, e.g. doxorubicin and cisplatin, complemented each other. miRNA-200c expression led to elevated apoptotic rates and therefore to the sensitization of cancer cells to chemotherapeutics. Moreover, it was demonstrated that the expression of miRNA-200c impaired GSTM3 expression even when treated with chemotherapeutics and thus explains the observed reduced detoxification rate.
The superior effect of combined miRNA-200c expression with chemotherapeutic drug treatment was also shown in xenograft mouse models. Breast cancer tumors were resensitized to doxorubicin treatment when miRNA-200c was expressed. Therefore, the hypothesized link between miRNA-200c expression and the diminished expression of GSTM3 as a part of the phase II detoxification was confirmed *in vivo*.
In this part of the thesis a novel regulatory pathway in combating drug resistance via miRNA-200c expression was uncovered. Impairing cellular phase II detoxification which is a crucial mechanism in drug resistance via inhibition of GSTs might be a promising strategy to overcome drug resistance formation in patients and might unravel a path for novel treatment strategies for breast cancer patients with miRNA-200c depleted tumors.

The second part of the thesis was focusing on metastasis formation in breast cancer and whether this process is hampered upon solely expressing miRNA-200c in primary tumors. The conducted *in vivo* studies presented a significant overall reduction of the metastatic burden in mice when the primary tumors expressed the 23 nucleotides of miRNA-200c. Especially the most prevalent organ for metastases i.e., the lung, was less affected when miRNA-200c was expressed in the tumor. Noteworthy, combinatorial treatment with the chemotherapeutic drug doxorubicin prevented metastasis formation in any of the examined organs.

To elucidate a cause for the reduced formation of metastases, migration as a prerequisite was investigated in detail. miRNA-200c was shown to affect collective-cell migration of cells in classical monolayers and spheroids as well as single-cell migration in structured confining microenvironments. Additionally, anoikis rates were enhanced in miRNA-200c-expressing cells.

Sole miRNA-200c expression in breast cancer can reduce the metastatic burden *in vitro* and *in vivo* and therefore miR-200c can be termed a metastasis suppressor.

Herein, miRNA-200c was found to play crucial roles in reconstituting sensitivity of tumors to chemotherapeutic drugs like doxorubicin and in hampering breast cancer to metastasize to different distant organs. Therefore, an administration of the tumor- and metastasis suppressor miRNA-200c as a therapeutic agent might be highly relevant. Moreover, strategies for a delivery of miRNA-200c, combined with chemotherapeutic drugs might be of great benefit for patients with miRNA-200c low or non-expressing tumors as overall survival is significantly reduced in TNBC patients as shown in the first part of this thesis.

The present work contributes to understand the role of miRNA-200c in chemoresistance and metastasis formation *in vitro* and *in vivo*. This scientific progress makes miRNAs attractive as new therapeutic options and biomarkers in future breast cancer treatment regimens.

7. Supplementary Materials

7.1 Supplementary Data Chapter I: MicroRNA-200c Prevents Drug Resistance by Downregulating Glutathione S-transferases

This chapter was directly adapted from the original publication, which was published as Köhler *et al.*, Cancers (Basel). 2022 Nov; 14(22): 5554 (see chapter 10.1 Articles), if not stated otherwise.

The following supporting information can be downloaded at: https://www.mdpi.com/article/10.3390/cancers14225554/s1.

A

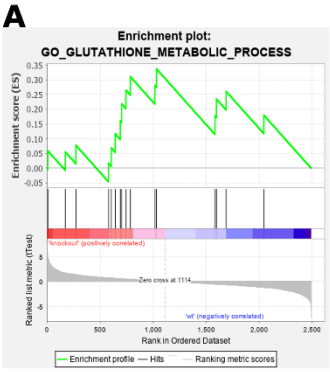

Gene	Rank in gene list	Rank metric score	Running ES	Core enrichment	P-value	Adj. p-value	Fold change
GSTM3	9	4.81225	0.0588622	Yes	0.0007	0.0058	3.2
G6PD	174	1.65421	0.0550728	Yes	0.0001	0.0013	1.2
GSTK1	274	1.29608	0.0775566	Yes	0.1477	0.3940	1.2
PARK7	581	0.647684	0.0163703	Yes	0.0544	0.2903	1.1
ALDH5A1	607	0.614908	0.0687652	Yes	0.1996	0.4144	1.1
GSTZ1	644	0.557833	0.116714	Yes	0.3008	0.4144	1.1
SOD1	692	0.491151	0.160216	Yes	0.6070	0.6937	1.1
GGCT	705	0.478132	0.217866	Yes	0.3367	0.4144	1.1
CNDP2	745	0.433922	0.264602	Yes	0.2601	0.4144	1.1
GSR	787	0.37562	0.31053	Yes	0.3117	0.4144	1.1
GLO1	1018	0.108919	0.280063	Yes	0.7180	0.7180	1.0
GSS	1033	0.0955065	0.336904	Yes	0.7036	0.7180	1.1
GCLC	1584	-0.558671	0.177092	No	0.2598	0.4144	0.9
IDH1	1598	-0.577975	0.234337	No	0.1296	0.3940	0.9
HAGH	1689	-0.692166	0.260459	No	0.2727	0.4144	0.9
MGST1	2044	-1.23087	0.179871	No	0.0889	0.3556	0.7

B

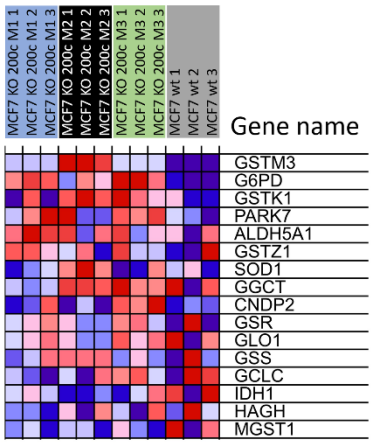

C

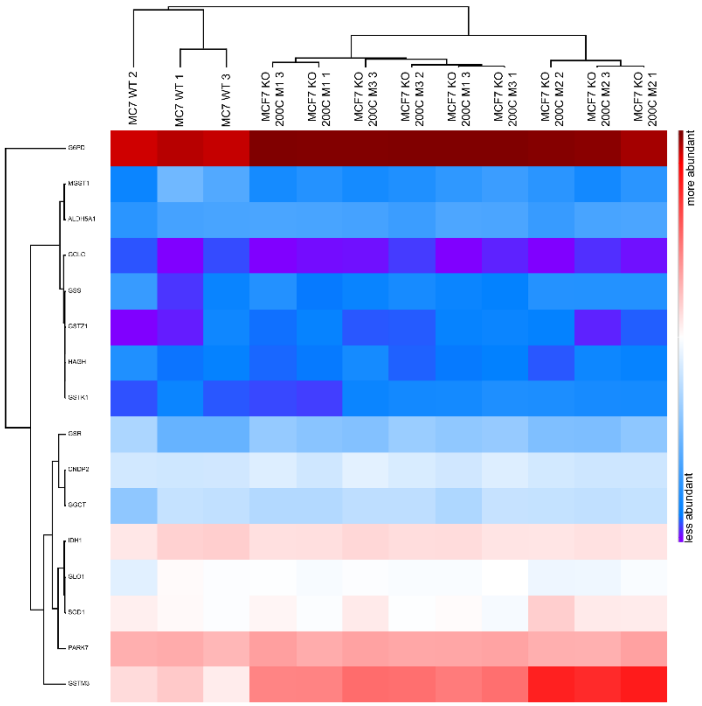

Figure S1: Proteomic analysis of MCF7 KO 200c (M1, M2, M3) vs. MCF7 wt upon doxorubicin (DXR) treatment. Differential protein expression depending on the

hsa-miR-200c expression. **(A)** Gene set enrichment plot of the glutathione metabolic process pathway (left) and table of altered protein expression ranked upon metric score (right). **(B)** Corresponding heatmap of the glutathione metabolic process pathway (n = 3). **(C)** An unsupervised hierarchical clustering of the proteins of the GO term "Glutathione Metabolic Process".
Data collection and figure layout was performed by Dr. Jan Bernd Stöckl and Dr. Thomas Fröhlich from Laboratory of Functional Genome Analysis (LAFUGA), Gene Center, Ludwig-Maximilians-Universität München, Germany.

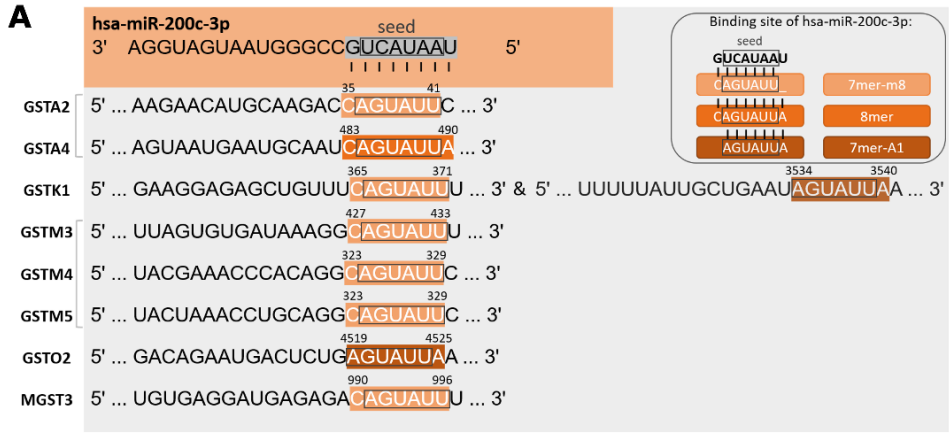

B

Gene Name	MCF7 KO 200c	MCF7 Tripz 200c sponge	MDA-MB 231 Tripz 200c	Binding Site	Results
GSTM1	n.d.	n.d.	↓	-	∞ (regulated even if no predicted binding site)
GSTM2	n.d.	n.d.	ns	-	✓
GSTM3	↑	↑	↓	+	✓
GSTM4	↑	↑	ns	+	∞ (not significant in MDA-MB 231 Tripz 200c)
GSTM5	n.d.	n.d.	n.d.	+	✓
GSTA1	n.d.	n.d.	n.d.	-	✓
GSTA2	n.d.	n.d.	n.d.	+	✓
GSTA3	n.d.	n.d.	n.d.	-	✓
GSTA4	n.d.	n.d.	n.d.	+	✓
GSTA5	n.d.	n.d.	n.d.	-	✓
GSTK1	↑	↑	↑	+	∞ (differently regulated in MDA-MB 231 Tripz 200c)
MGST1	↑	↑	n.d.	-	∞ (regulated even if no predicted binding site)
MGST2	ns	n.d.	n.d.	-	✓
MGST3	↑	↑	n.d.	+	✓
LTC4S	n.d.	n.d.	n.d.	-	✓
FLAP	n.d.	n.d.	ns	-	✓
GSTO1	↑	↓	↓	-	∞ (differently regulated in MCF7 Tripz 200c sponge and regulated even if no predicted binding site)
GSTO2	↑	ns	↑	+	∞ (differently regulated in MDA-MB 231 Tripz 200c and not significant in MCF7 Tripz 200c sponge)
GSTP1	n.d.	n.d.	↓	-	∞ (regulated even if no predicted binding site)
GSTT1	ns	ns	n.d.	-	✓
GSTT2	↑	↑	n.d.	-	∞ (regulated even if no predicted binding site)
GSTZ1	ns	ns	↓	-	∞ (regulated even if no predicted binding site)

D

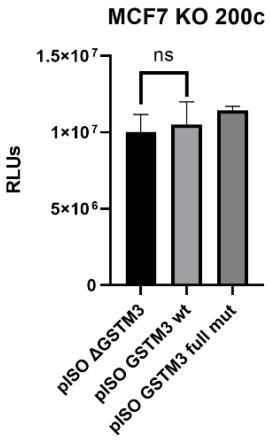

C

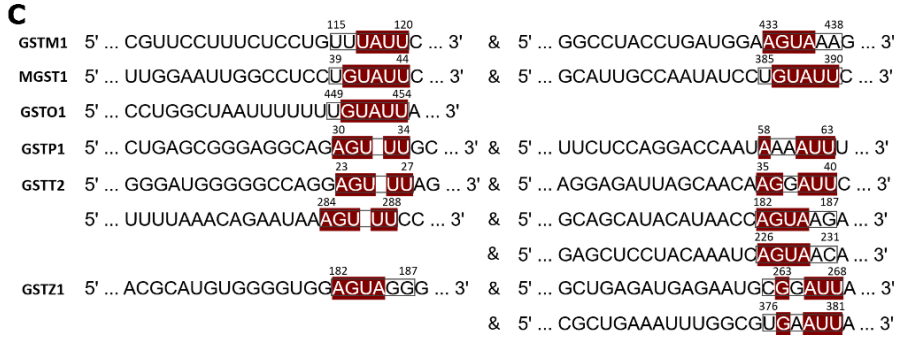

Figure S2: *In silico* miRNA-mRNA seed-site interaction. **(A)** 3`UTR sequences of GSTs with a predicted target site for hsa-miR-200c-3p. The seed region and complementary region are framed. Numbers indicate position within the 3`UTR sequence. Illustration of the 7mer-m8, 8mer and 7mer-A1 is shown on the right. Adapted from TargetScan. **(B)** Comparison of the regulation of all GSTs in the three hsa-miR-200c expression systems. Results, indicated with a check mark, verify the predicted miRNA-mRNA seed-site interaction. Further evaluation of the interaction is needed if the infinity symbol is displayed. n.d. = not detected, ns = not significant **(C)** Possible target sites for hsa-miR-200c-3p seed region. Framed sequences display possible complementary regions. Dark red highlighted nucleotides show a complementary match with the hsa-miR-200c-3p seed region. Sequences are adapted from TargetScan. **(D)** Luciferase assay of different GSTM3 3`UTR reporter plasmids co-transfected with a scrambled siRNA in MCF7 KO 200c cells. One representative

diagram is shown. A two-tailed Student's t-test for pISO ΔGSTM3 and pISO GSTM3 wt was performed. Values are displayed as mean with SD.
The generation of the plasmids was generously performed by Sviatlana Dubovik (Pharmaceutical Biotechnology, Department of Pharmacy, Ludwig-Maximilians-Universität München, Germany).

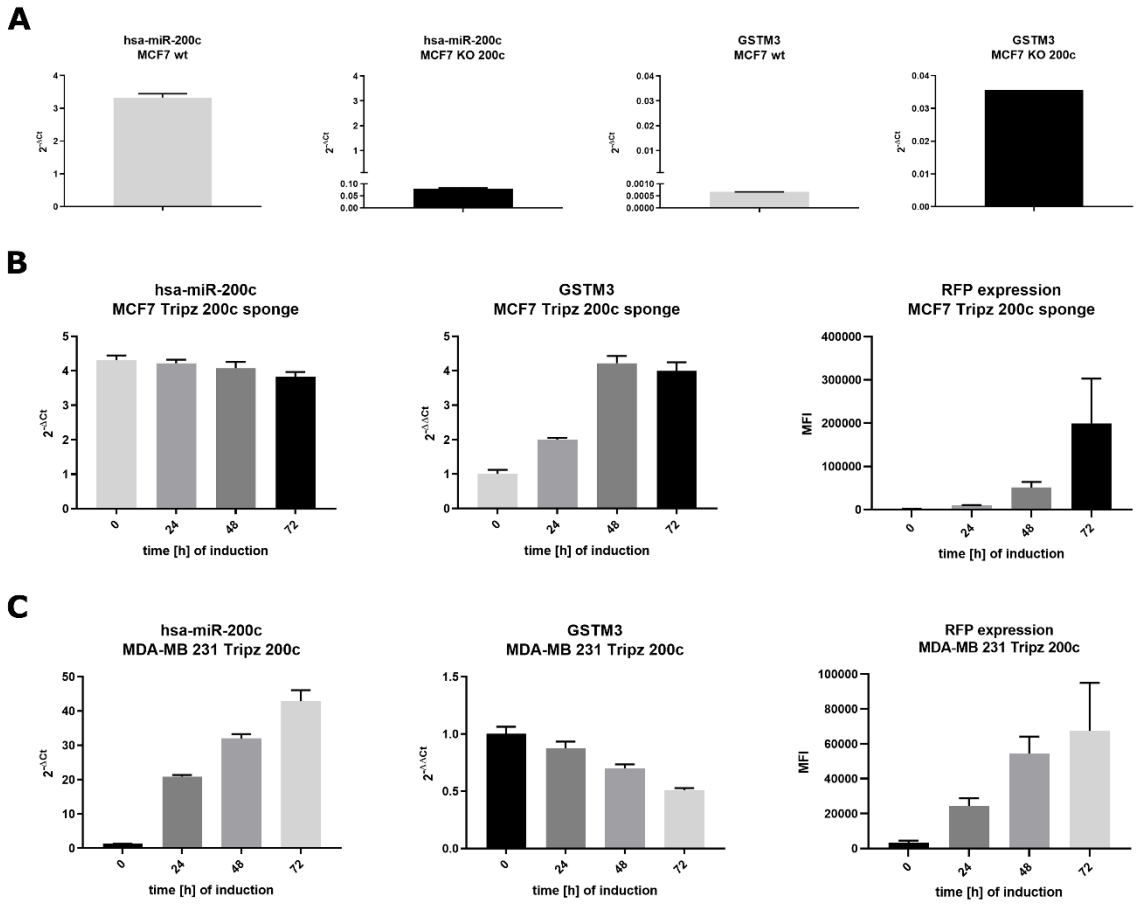

Figure S3: Characterization of hsa-miR-200c expression systems. **(A)** qRT-PCR analysis of hsa-miR-200c and GSTM3 expression in MCF7 wt and KO 200c cells. Quantitative RT-PCR analysis of hsa-miR-200c and GSTM3 expression in **(B)** MCF7 Tripz 200c sponge cells and **(C)** in MDA-MB 231 Tripz 200c cells, each induced with 5 µg/mL doxycycline and FACS analysis of RFP expression of the same cells displayed as MFI. One representative replicate out of three is displayed. Values are displayed as mean with SD.

For figure 6B:

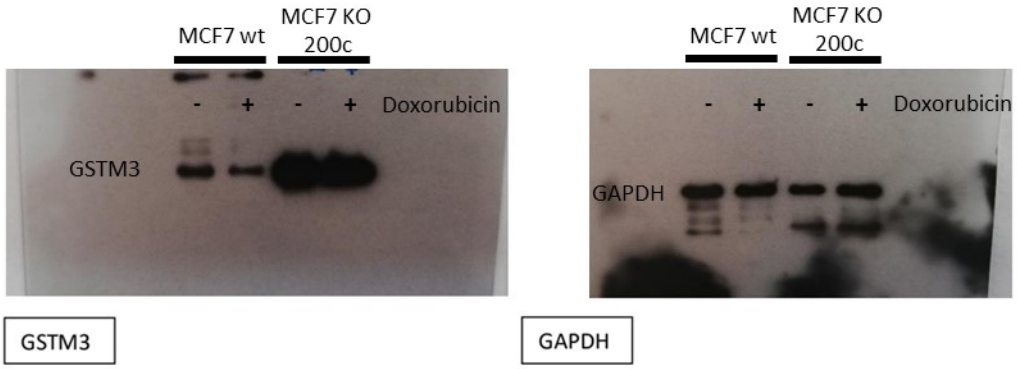

For figure 6D:

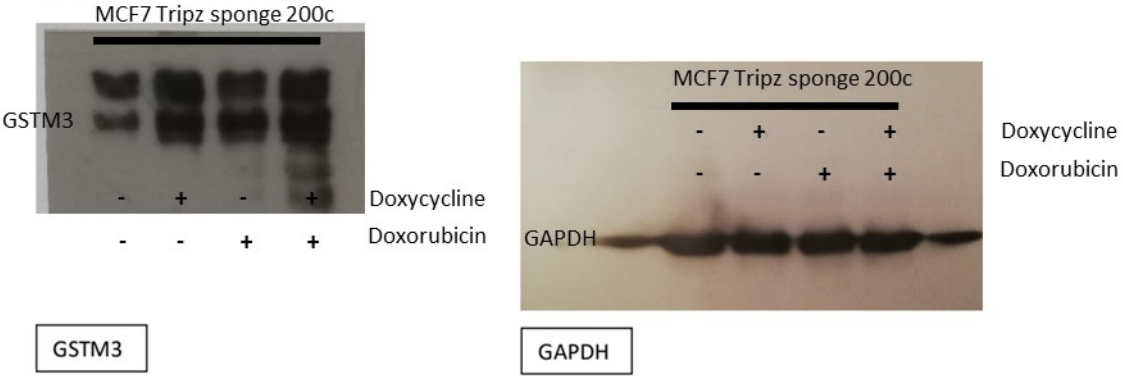

For figure 6F:

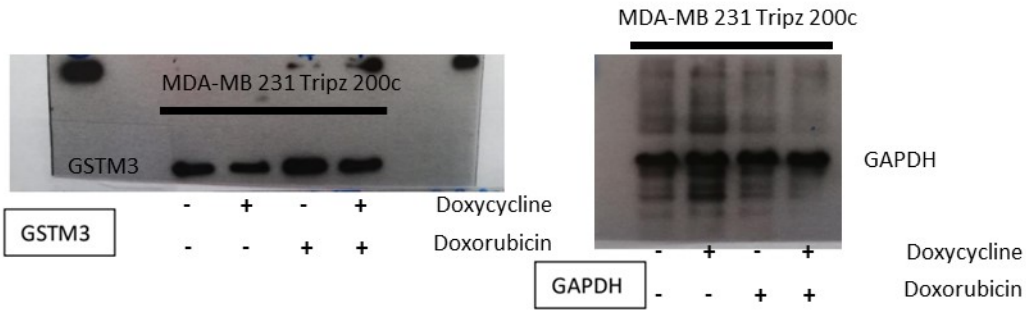

Figure S4: Uncropped blots of western blots presented in Figure 6B,D,F. This Figure was adapted from the original publication (113).

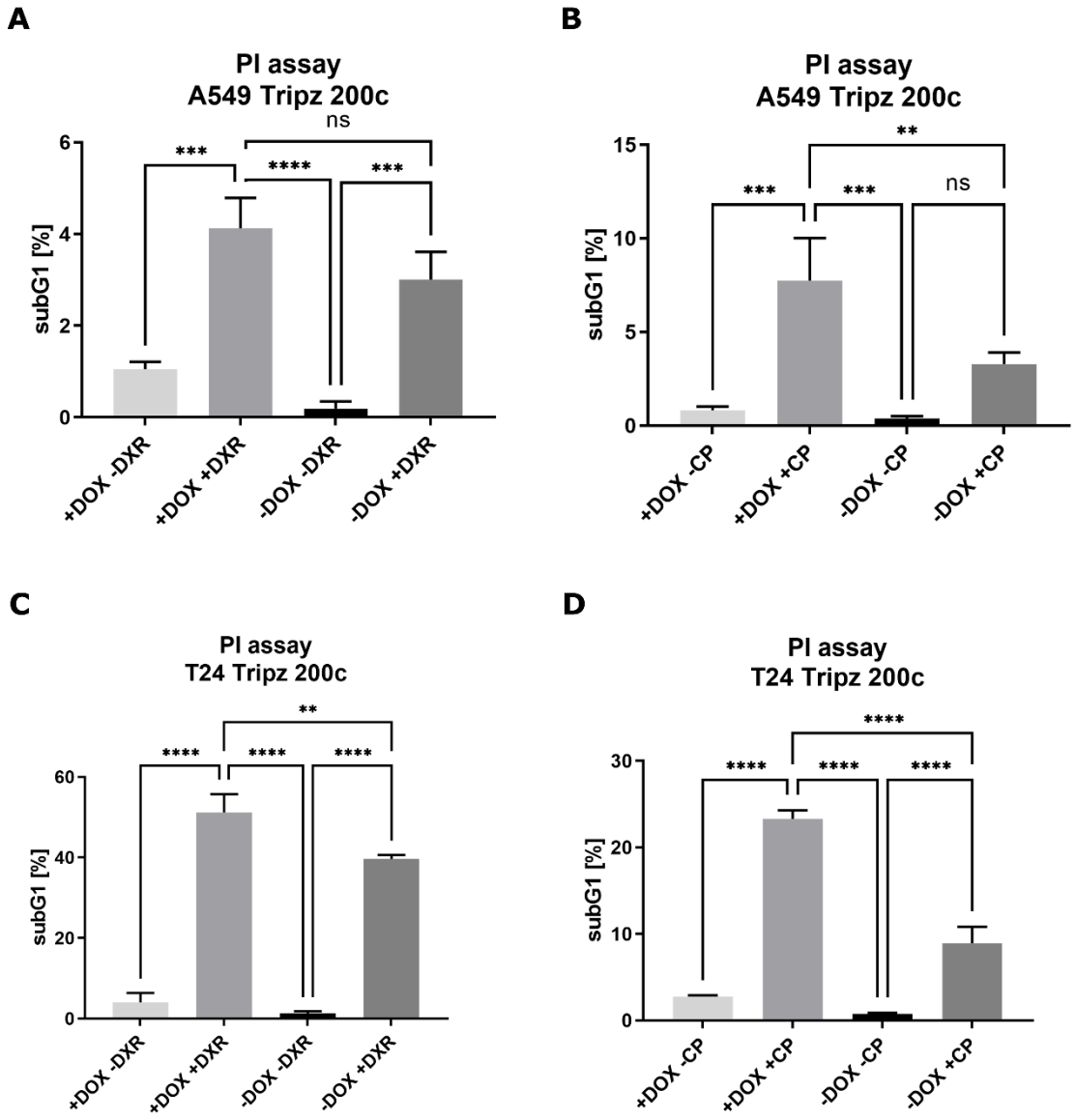

Figure S5: Effect of hsa-miR-200c on cell death in two additional cancer types in combination with chemotherapeutic treatment. Analysis of subG1 population in **(A, B)** A549 lung cancer cells in combination with doxorubicin (DXR) or cisplatin (CP) treatment and **(C, D)** T24 bladder cancer cells in combination with DXR or CP treatment using propidium iodide assay. Both cell lines were 72 hours pre-induced with DOX or not (-DOX). An ordinary one-way ANOVA with Tukey's multiple comparison test was performed for statistics. ns = not significant, ** $p < 0.01$, *** $p < 0.001$, ****$p < 0.0001$. One representative diagram out of three is displayed. Values are displayed as mean with SD.

A

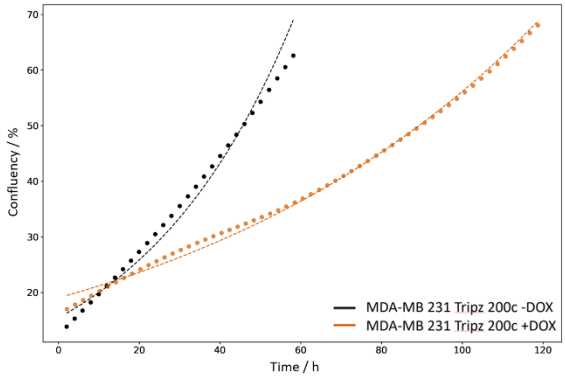

Period of time for confluency change from 30% to 60%	
MDA-MB 231 Tripz 200c -DOX	32.2 h
MDA-MB 231 Tripz 200c +DOX	68.38 h

Figure S6: Proliferation curves of hsa-miR-200c positive or negative MDA-MB 231 cells. Proliferation of **(A)** MDA-MB 231 Tripz 200c with doxycycline induction every 48 to 72 hours. Comparison of proliferation slopes and doubling times in hsa-miR-200c expressing (+DOX, orange curve) and hsa-miR-200c depleted (-DOX, black curve) cells. One representative diagram out of three is presented.
Data analysis and the figure were prepared by Dr. Philipp Paulitschke and his team from PHIO (PHIO Scientific GmbH, Esswurmstr. 16, Munich).

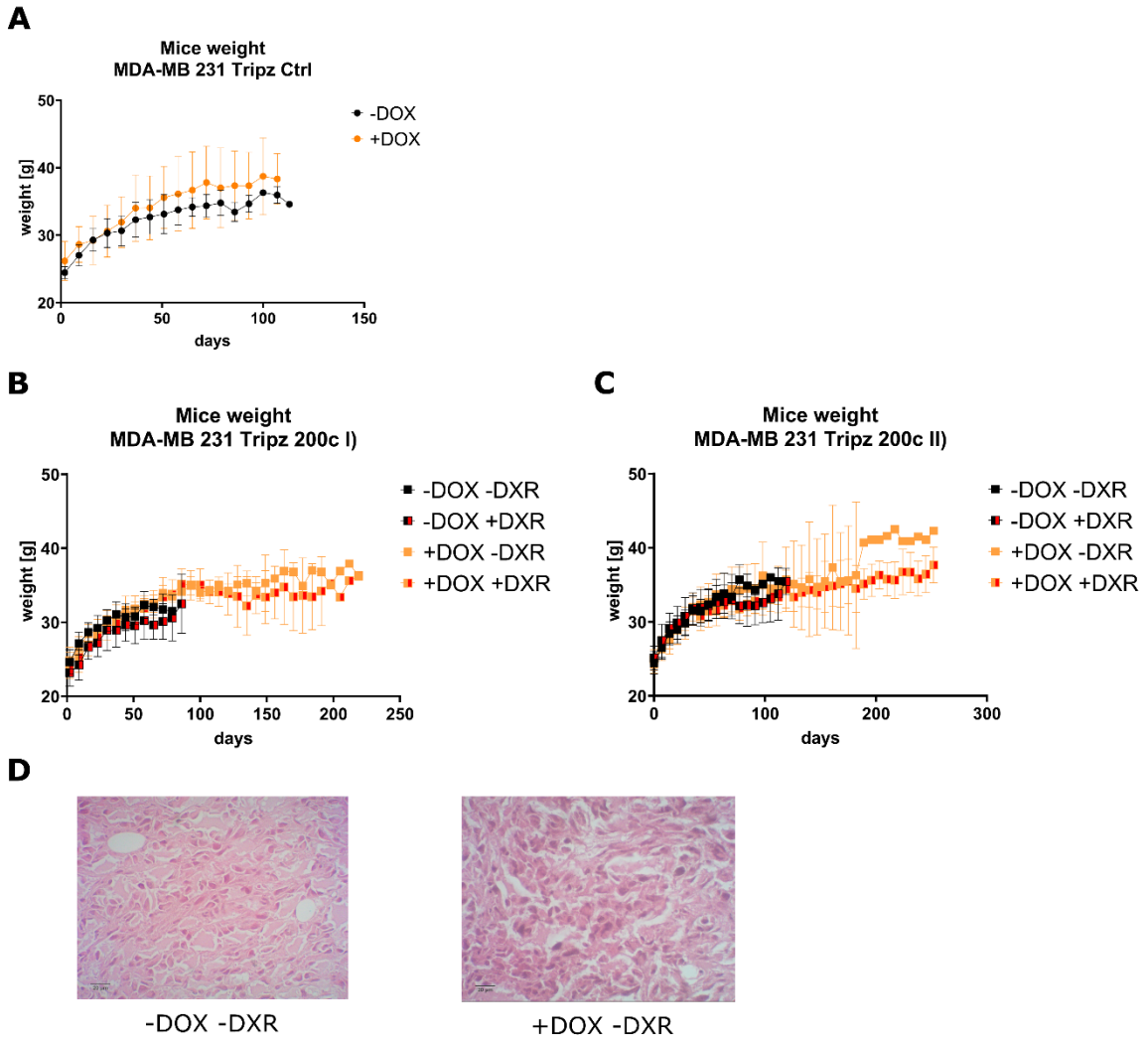

Figure S7: Animal welfare monitoring of the different xenograft mouse models and histological analysis of hsa-miR-200c-positive and negative tumors. **(A)** Weekly body weight mean of mice bearing control tumors (MDA-MB 231 Tripz Ctrl) and fed with regular (black curves) or doxycycline (DOX, orange curves) diet (n = 5). **(B)** Body weight mean displayed once a week of mice with hsa-miR-200c positive (MDA-MB 231 Tripz 200 +DOX, orange curves) or negative (-DOX, black curves) tumors and additional chemotherapeutic treatment (n = 5, red filled squares) related to animal experiment I) Treatment of hsa-miR-200c positive and negative tumors. **(C)** Mean body weight (displayed once a week) of mice with initial hsa-miR-200c negative tumors and their subsequent treatment with either doxorubicin (DXR, black curve and red filled squares) or miRNA-200c (orange curve) or their combination (orange curve and red filled squares) related to animal experiment II) Single or double treatment of hsa-miR-200c negative tumors, (n = 10 per group). Body weight graphs do not terminate when mice were euthanized. **(D)** H&E staining of hsa-miR-200c negative (-DOX) or positive (+DOX) tumors without DXR treatment. Values are displayed as mean with SD.
Weight data was collected by the veterinarians Dr. Elisa Hörterer and Dr. Ulrich Wilk (Pharmaceutical Biotechnology, Department of Pharmacy, Ludwig-Maximilians-Universität München, Germany). Pictures of the H&E staining were taken by Dr. Ulrich Wilk.

Kaplan-Meier plot for hsa-miR-200c	
miRNA: miRpower for breast cancer	
miRNA ID	hsa-miR-200c
Survival	Overall survival
Split patients by	auto select best cutoff
Follow up threshold	60 months, censore at threshold
Dataset	TCGA
ER status	IHC and gene chip: all
PGR status	IHC: all
HER2 status	IHC and gene chip: all
Molecular subtype	TNBC
Grade	all
Lymph node status	all
Restrict analysis to selected cohorts	do not use cohorts

Kaplan-Meier plot for GSTM3	
mRNA gene chip for breast cancer	
Affy ID	202554_s_at
Survival	Relapse free survival (RFS)
Split patients by	median
Follow up threshold	60 months, censore at threshold
Probe set option	only JetSet best probe set
ER status	IHC and array: all
PR status	IHC: all
HER2 status	array: all
Subtype - StGallen	basal
Subtype - PAM50	all
Lymph node status	all
Grade	all
TP53 status	all
Pietenpol subtype	all
Use earlier release of the database	all
Use following dataset for the analysis	all
Quality control - remove redundant samples	checked
Quality control - array quality control	exclude biased arrays
Quality control - proportional hazards assumption	checked
Cohorts	patients with following systemic treatment
Endocrine therapy	any
Chemotherapy	neoadjuvant only

Figure S8: Overview of the parameters entered into the Kaplan-Meier Plotter for the analysis of hsa-miR-200c and GSTM3 in breast cancer patients.

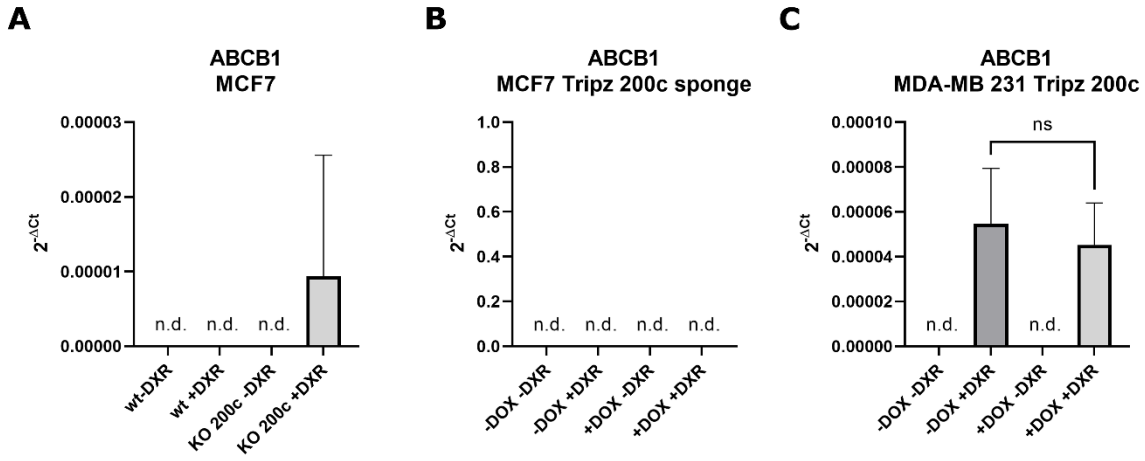

Figure S9: hsa-miR-200c expression and the abundance of ABCB1. Expression of ABCB1 analyzed with qRT-PCR in the **(A)** MCF7 wt and KO 200c (treatment with 5 µM of DXR for 6 hours), **(B)** the MCF7 Tripz 200c sponge (72 hours DOX pre-induced and treated with 0.1 µM DXR for 24 hours) and **(C)** the MDA-MB 231 Tripz 200c cell system (72 hours DOX pre-induced and subsequently treated with 0.6 µM DXR for 24 hours). Ct values of 35 and more are uncertain values and therefore were excluded from the analysis and termed as not detected (n.d.). ns = not significant. Values are displayed as mean with SD.
Data collection was performed by Altea Oliva (Pharmaceutical Biotechnology, Department of Pharmacy, Ludwig-Maximilians-Universität München, Germany).

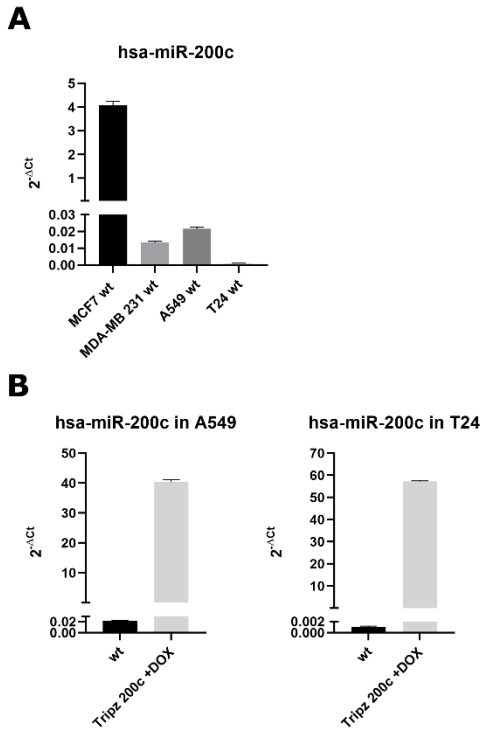

Figure S10: hsa-miR-200c expression profile. **(A)** qRT-PCR analysis of hsa-miR-200c expression in the wt cell lines. **(B)** Induction of hsa-miR-200c in A549 Tripz 200c (left) and T24 Tripz 200c (right) upon doxycycline application (5 µg/mL) compared to the corresponding wt cell line. Values are displayed as mean with SD.

	MCF7 wt			MCF7 KO		
gene	Ct value 1	Ct value 2	Ct value 3	gene	Ct value 1	Ct value 2	Ct value 3
mu family				mu family			
GSTM1	38.19	37.92		GSTM1			
GSTM2	36.84	36.64	37.84	GSTM2	35.08	35.05	35.72
GSTM3	28.2	28.18	28.18	GSTM3	22.68	22.68	22.68
GSTM4	26.85	26.88	26.91	GSTM4	24.46	24.44	24.43
GSTM5	36.83	35.62	36.15	GSTM5	35.9	35.1	35.25
GAPDH	17.63	17.62	17.6	GAPDH	17.91	17.86	17.84
alpha and kappa family				alpha and kappa family			
GSTA1	36.84		38.74	GSTA1	35.08	36.44	34.81
GSTA2	37.27	36.94	35.99	GSTA2	34.45	34.43	34.92
GSTA3	40	36	36.37	GSTA3	32.77	32.54	32.8
GSTA4	39.64	39.55	39.36	GSTA4	38.31	39.04	39.28
GSTA5	37.97	38.19	36.64	GSTA5	33.24	33.44	33.49
GSTK1	24.83	24.94	24.87	GSTK1	24.27	24.27	24.26
GAPDH	17.72	17.54	17.54	GAPDH	17.89	17.88	17.85
MAPEG family part 1				MAPEG family part 1			
MGST1	25.17	24.96	25.04	MGST1	23.26	23.42	23.41
MGST3	25.18	25.55	25.21	MGST3	23.79	23.65	23.74
GAPDH	17.72	17.54	17.54	GAPDH	17.89	17.88	17.85
MAPEG family part 2				MAPEG family part 2	38.46		
LTC4S	37.73	39.12	40	LTC4S	38.35	40	
FLAP	40			FLAP	17.97	18.04	18.1
GAPDH	18.03	18.05	18.14	GAPDH			
MAPEG family part 3				MAPEG family part 3	32.92	34.35	34.08
MGST2	33.16	32.93	31.93	MGST2	17.91	17.86	17.84
GAPDH	17.63	17.62	17.6	GAPDH			
omega, pi, theta and zeta family				omega, pi, theta and zeta family	32.12	31.99	32.18
GSTO1	32.11	32.36	32.16	GSTO1	25.32	25.35	25.42
GSTO2	25.17	25.26	25.24	GSTO2	37.86	40	40
GSTP1	36.15	36.56	35.53	GSTP1	26.65	26.66	26.8
GSTT1	26.52	26.52	26.37	GSTT1	31.88	31.59	31.26
GSTT2	32.6	32.87	32.2	GSTT2	24.14	24.16	24.13
GSTZ1	23.71	23.81	23.58	GSTZ1	17.89	17.88	17.85
GAPDH	17.72	17.54	17.54	GAPDH			

	MCF7 Tripz 200c sponge -DOX			MCF7 Tripz 200c sponge +DOX		
gene	Ct value 1	Ct value 2	Ct value 3	gene	Ct value 1	Ct value 2	Ct value 3
mu family				mu family			
GSTM1				GSTM1			
GSTM2	36.16	36.62	36.16	GSTM2	33.96	34	33.73
GSTM3	29.36	29.33	29.34	GSTM3	28.03	28	28
GSTM4	27.21	27.17	27.25	GSTM4	26.76	26.76	26.66
GSTM5				GSTM5			
GAPDH	19.13	19.25	19.24	GAPDH	19.27	19.22	19.11
alpha and kappa family				alpha and kappa family			
GSTA1	40	40	40	GSTA1	40	40	40
GSTA2	35.8	36.58	36.84	GSTA2	35.2	36.19	35.49
GSTA3				GSTA3		40	
GSTA4			40	GSTA4			
GSTA5	36.36	37	37.62	GSTA5	36.84	35.96	36.09
GSTK1	24.9	24.94	25	GSTK1	24.26	24.25	24.3
GAPDH	19.13	19.25	19.24	GAPDH	19.27	19.22	19.11
MAPEG family part 1				MAPEG family part 1			
MGST1	27.05	26.87	27.03	MGST1	26.54	26.67	26.35
MGST2	37.27	37.09	37.17	MGST2	36.79	37.04	36.72
MGST3	25.32	25.4	25.56	MGST3	24.95	24.87	24.79
LTC4S		39.11	38.43	LTC4S	40	38.03	40
GAPDH	19.13	19.25	19.24	GAPDH	19.27	19.22	19.11
MAPEG family part 2				MAPEG family part 2			
FLAP		40		FLAP	19.15	19.14	19.13
GAPDH	18.99	19.11	19.13	GAPDH			
omega, pi, theta and zeta family				omega, pi, theta and zeta family			
GSTO1	33.67	33.52	33.44	GSTO1	33.94	34.05	34.37
GSTO2	25.75	25.8	25.9	GSTO2	25.9	25.84	25.87
GSTP1	35.46	35.98	37.31	GSTP1	36.74	36.3	35.94
GSTT1	25.6	25.79	25.73	GSTT1	25.13	25.9	25.49
GSTT2	35.43	35.51	35.66	GSTT2	34.95	34.66	34.93
GSTZ1	23.78	23.53	23.67	GSTZ1	23.64	23.68	23.73
GAPDH	18.99	19.11	19.13	GAPDH	19.15	19.14	19.13

	MDA-MB 231 Tripz 200c -DOX			MDA-MB 231 Tripz 200c +DOX		
gene	Ct value 1	Ct value 2	Ct value 3	gene	Ct value 1	Ct value 2	Ct value 3
mu family				mu family			
GSTM1	26.85	26.87	26.92	GSTM1	27.51	27.53	27.62
GSTM2	28.25	28.29	28.91	GSTM2	29.05	28.86	29.12
GSTM3	27.84	27.78	27.82	GSTM3	28.37	28.28	28.25
GSTM4	25.86	26	26.03	GSTM4	26.23	26.16	26.23
GSTM5	37.65	37.11	40	GSTM5	37.61	38.18	
GAPDH	19.6	19.47	19.46	GAPDH	19.74	19.68	19.66
alpha and kappa family				alpha and kappa family			
GSTA1				GSTA1			
GSTA2				GSTA2			
GSTA3	37.42	40	40	GSTA3	38.53	40	37.25
GSTA4	37.42	36.76	37.28	GSTA4	40	40	37.63
GSTA5	38.38	40		GSTA5	40	40	
GSTK1	24.88	24.87	24.86	GSTK1	24.67	24.66	24.67
GAPDH	19.42	19.24	19.01	GAPDH	19.26	19.34	19.16
MAPEG family part 1				MAPEG family part 1			
MGST1				MGST1			
MGST2				MGST2			
MGST3				MGST3			
GAPDH	19.42	19.24	19.01	GAPDH	19.26	19.34	19.16
MAPEG family part 2				MAPEG family part 2			
LTC4S		40	40	LTC4S			
FLAP	31.89	31.98	31.9	FLAP	32.21	32.43	32.34
GAPDH	19.34	19.46	19.46	GAPDH	19.63	19.66	19.68
omega, pi, theta and zeta family				omega, pi, theta and zeta family			
GSTO1	29.73	29.67	29.54	GSTO1	30	30.09	30.06
GSTO2	30.8	30.79	30.76	GSTO2	29.98	30.11	30.08
GSTP1	23.23	23.2	23.25	GSTP1	23.62	23.62	23.82
GSTT1				GSTT1			
GSTT2				GSTT2			
GSTZ1	24.13	24.06	23.87	GSTZ1	24.67	24.6	24.65
GAPDH	19.42	19.24	19.01	GAPDH	19.26	19.34	19.16

Table S1: Raw Ct values of qRT-PCR analysis of all glutathione S-transferases in different hsa-miR-200c expression systems. Table shows raw Ct values in triplicates for each sample gene. Every GST family is displayed with its corresponding housekeeper (GAPDH) values. Undetectable Ct values (Ct> 40) are not displayed. For the analysis the 2-ΔCt method was used. Ct values between 35 and 40 are uncertain values and therefore termed as not detected (n.d.) in Figure 5B-D.

7.2 Supplementary Data Chapter II: Unraveling the Metastasis-Preventing Effect of miR-200c *In Vitro* and *In Vivo*

This chapter was directly adapted from the original publication which was published as Köhler *et al.*, Mol Oncol. 2024 Oct 15 (see chapter 10.1 Articles). Additional sections were included.

The following supporting information can be downloaded at: https://febs.onlinelibrary.wiley.com/action/downloadSupplement?doi=10.1002%2F1878-0261.13712&file=mol213712-sup-0001-Figures.pdf

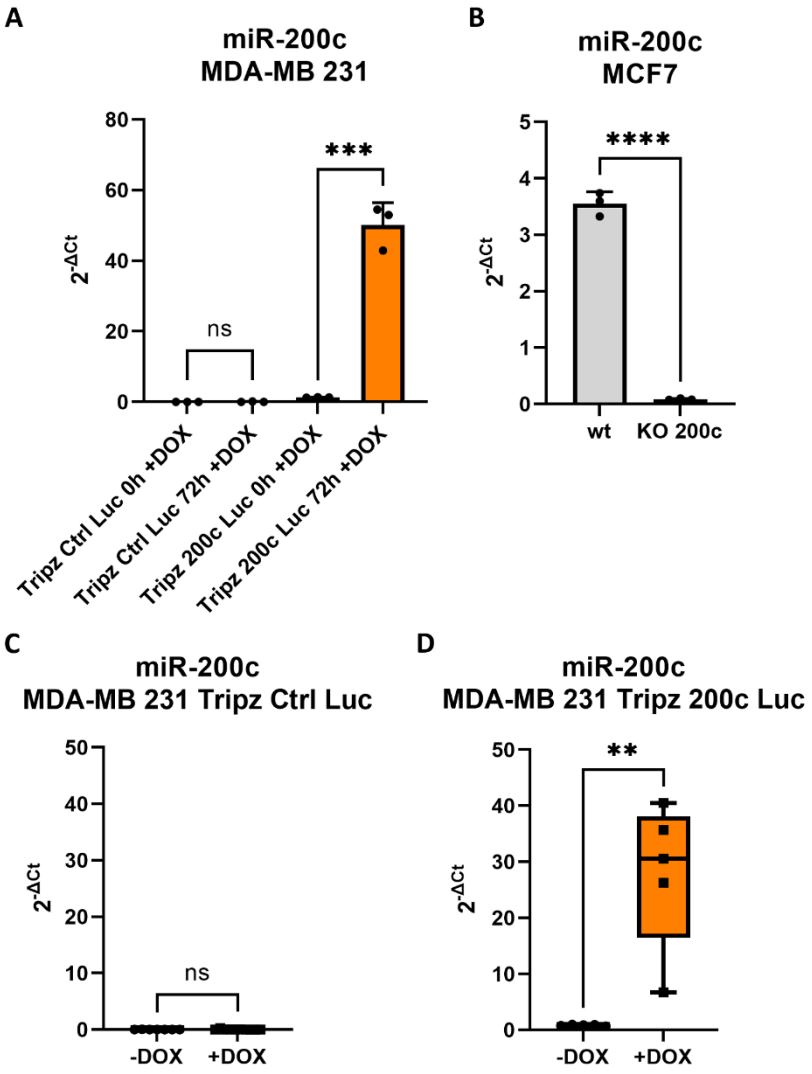

Figure S11: Expression of miR-200c is enhanced in MCF7 wildtype (wt) and MDA-MB 231 Tripz 200c Luc induced with doxycycline (+DOX) cells and tumors, respectively. Validation of miR-200c expression in vitro and in vivo. **(A)** Expression level in MDA-MB 231 Tripz cell systems, at 0 and 72 hours after doxycycline induction

(n = 3) and in **(B)** MCF7 wildtype and knockout (KO) miR-200c (n = 3). Values in (A) and (B) are displayed as mean with SD. For statistical evaluation an unpaired, two tailed student's t-test was performed. ns = not significant, *** $p < 0.001$, **** $p < 0.0001$. miR-200c expression levels in **(C)** MDA-MB 231 Tripz Ctrl Luc (n = 7 -DOX and n = 10 +DOX) and **(D)** MDA-MB 231 Tripz 200c Luc tumors (n = 5). Data in (C) and (D) are presented as box and whiskers plots with minimal to maximal values including all data points. The median is plotted with a line. For statistical evaluation an unpaired, two tailed student's t-test was performed. ns = not significant, ** $p < 0.01$.

The grinding of the tumors for subsequent RNA isolation was generously performed by the veterinarians Dr. Elisa Hörterer and Dr. Ulrich Wilk (Pharmaceutical Biotechnology, Department of Pharmacy, Ludwig-Maximilians-Universität München, Germany).

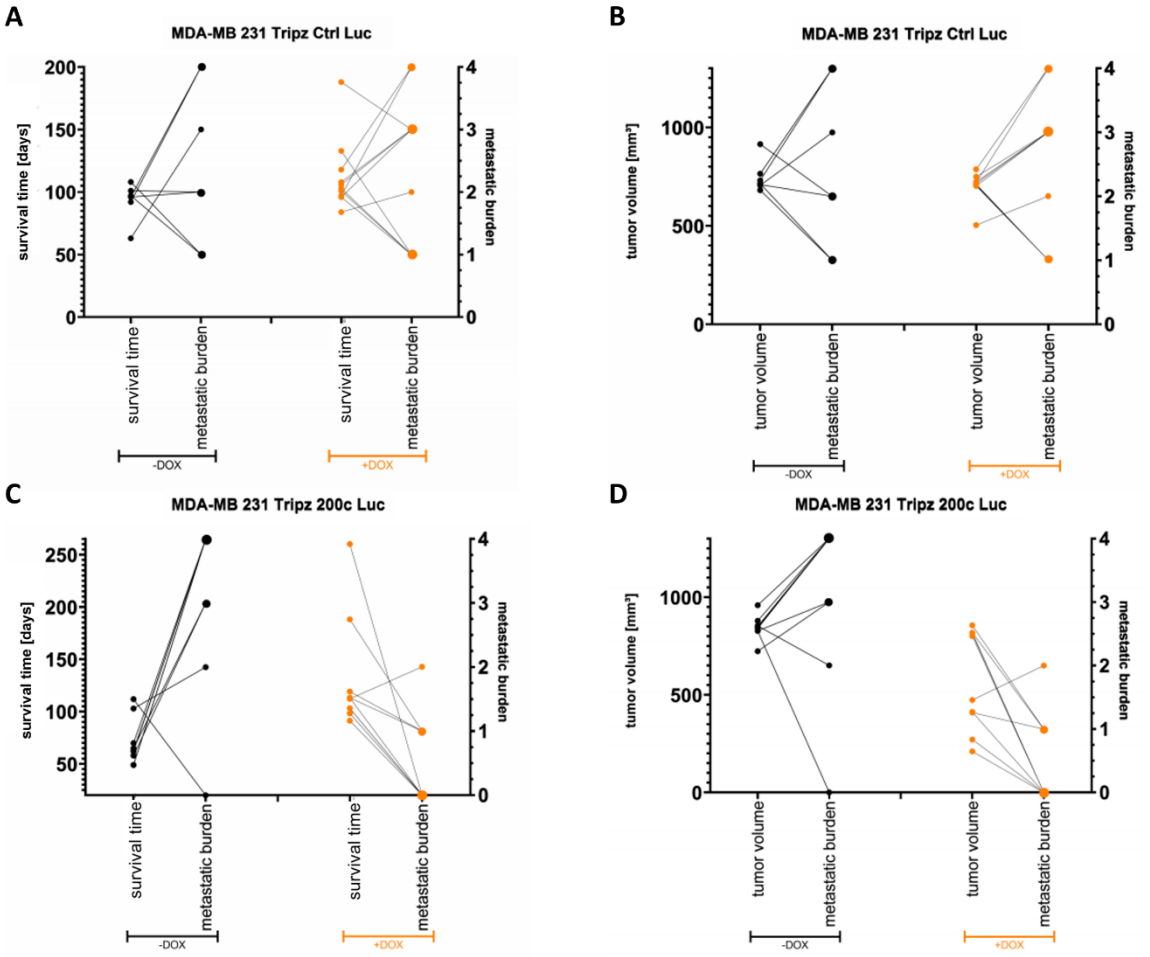

Figure S12: Reduced metastatic burden in mice with miR-200c-expressing tumor. Presentation of **(A)** survival time compared to the metastatic burden and **(B)** tumor volume compared to the metastatic burden of every individual control mouse. Results are separated into normal (black dots, n = 7) or doxycycline containing feed (orange dots, n = 11) group. Evaluation of **(C)** survival time compared to the metastatic burden and **(D)** tumor volume compared to the metastatic burden of every individual mouse with (orange) or without (gray) miR-200c expression of the primary tumor. Results are separated into normal (black dots, n = 10) or doxycycline containing feed (orange dots, n = 10) group. The bigger the dots the more frequently the same value of the metastatic burden was achieved.
Data collection of the survival time and tumor growth of the mice was generously performed by the veterinarians Dr. Elisa Hörterer, Dr. Ulrich Wilk, and Dr. Jana Pöhmerer (Pharmaceutical Biotechnology, Department of Pharmacy, Ludwig-Maximilians-Universität München, Germany).

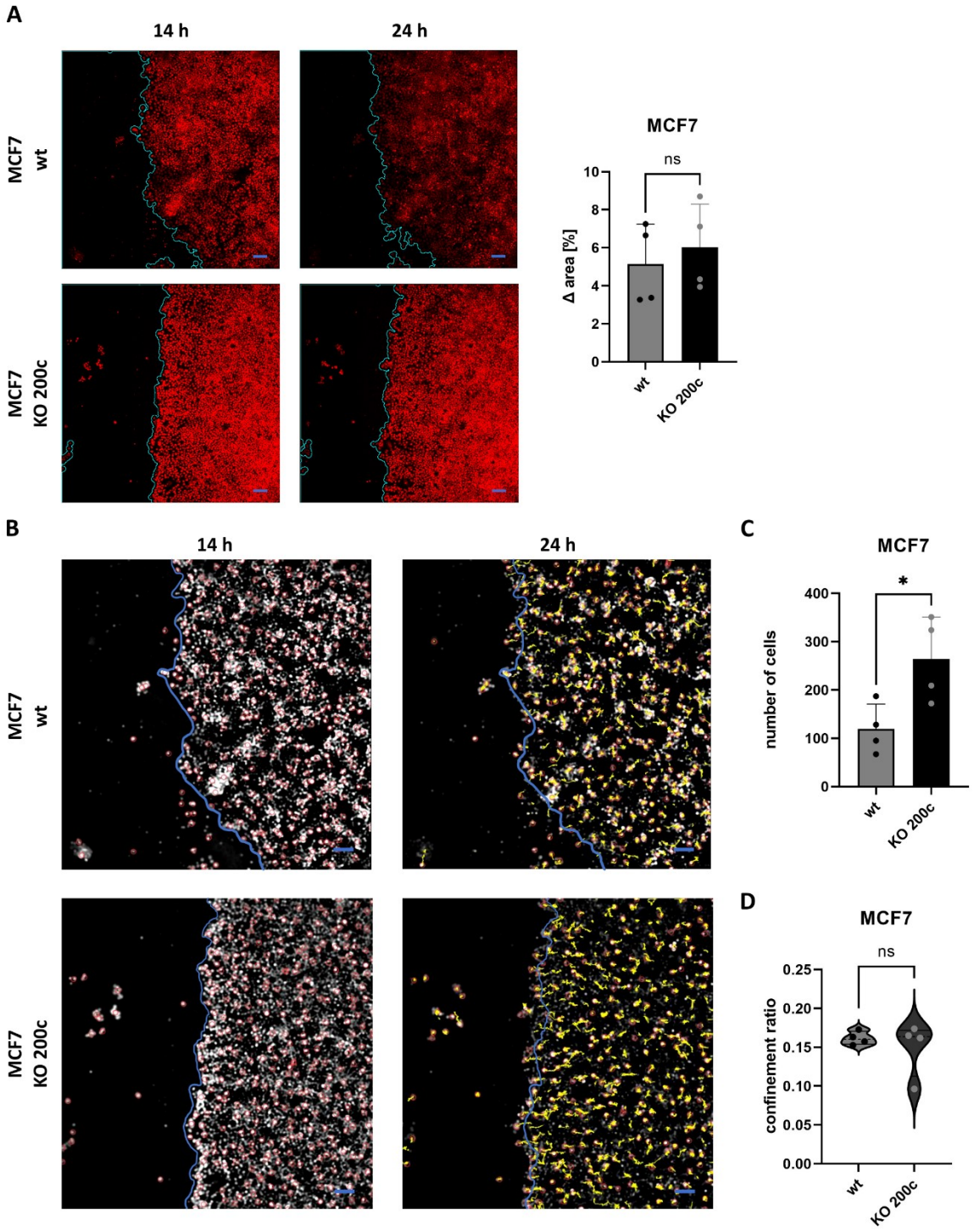

Figure S13: MCF7 breast cancer cells lacking miR-200c expression tend to leave cell clusters more frequently. **(A)** Wound closure of MCF7 cells with (wildtype, wt) or without (knockout, KO 200c) miR-200c expression. Blue lines in the microscopic pictures (left) indicate the borders of the wound. MCF7 cells tended to get stacked on top of each other when performing the scratch and later on were rolling out slowly. Therefore, the wound closure was monitored for 10 hours but starting 14 hours post scratching. The difference in the area in [%] (right) is used to quantify the scratch closure (n = 4). Cells are stained with siR-DNA. Values are displayed as mean with SD. For statistical evaluation an unpaired, two-tailed student's t-test was performed. ns = not significant. **(B)** Microscopic pictures of MCF7 cells with different miR-200c

expression for the analysis of **(C)** the number of cells closing the scratch and **(D)** the confinement ratio (n = 4). Scale bar equals 50 µm and applies to both (A) and (B). Blue lines represent the border of the scratch at 14 hours. Yellow lines in the microscopic pictures represent the trajectories of the cells at 24 hours after scratch. Values in (C) are displayed as mean with SD. The dashed line shows the median and the full lines the quartiles of the violin plot in (D). For statistical evaluation an unpaired, two-tailed student's t-test was performed in (C) and (D). ns = not significant, * $p < 0.05$.
The data collection of the scratch assay was performed by Dr. Andreas Roidl (Pharmaceutical Biotechnology, Department of Pharmacy, Ludwig-Maximilians-Universität München, Germany) and Prof. Dr. Stefan Zahler (microscopy, Pharmaceutical Biology, Department of Pharmacy, Ludwig-Maximilians-Universität, Germany). The raw analysis with TrackMate was performed by Dr. Andreas Roidl.

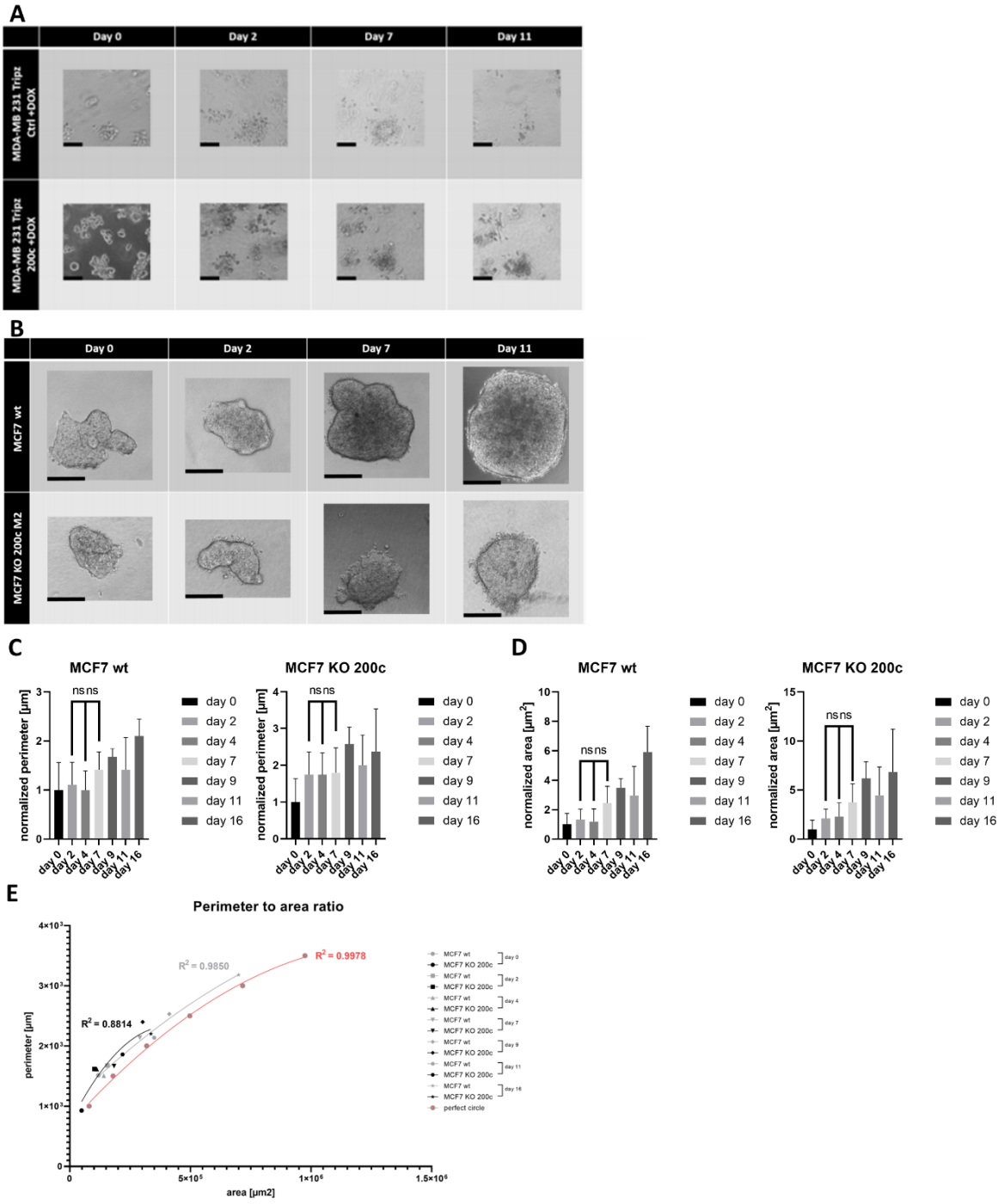

Figure S14: Characterization of 3D cell aggregates embedded in collagen revealed aggregate formation over time in MCF7 cells but not in MDA-MB 231 cells. **(A)** MDA-MB 231 Tripz Ctrl or Tripz 200c cell line induced with DOX show only loose aggregates which do not change over time. Aggregates are exemplarily presented for each day. Scale bar is 100 µm. **(B)** MCF7 wt and KO 200c cell aggregates and their development over time. Aggregates are exemplarily presented for each day. Scale bar is 200 µm. Over time comparison of **(C)** perimeter or **(D)** area normalized to day 0 in MCF7 wt and KO 200c aggregates. Day 4 was chosen for further evaluation since at this time no significant difference in the perimeter and size (given as area) of the aggregates could be measured. For statistical evaluation a 2 way ANOVA with Tukey's multiple comparison test was performed. At least n = 4 cell aggregates were analyzed per timepoint. ns = not significant. **(E)** Perimeter to area ratio of MCF7 wt and KO 200c

aggregates. Red curve indicates the growth of a perfect circle (coefficient of determination: 0.9978). The gray curve indicates the trend line of the growth of MCF7 wt aggregates over time (coefficient of determination: 0.9850) and the black trend line shows the growth of MCF7 KO 200c aggregates over time (coefficient of determination: 0.8814). For each time point at least n = 4 aggregates per cell line were measured. The trend line of all 3 conditions was created using the second-grade polynomic function.

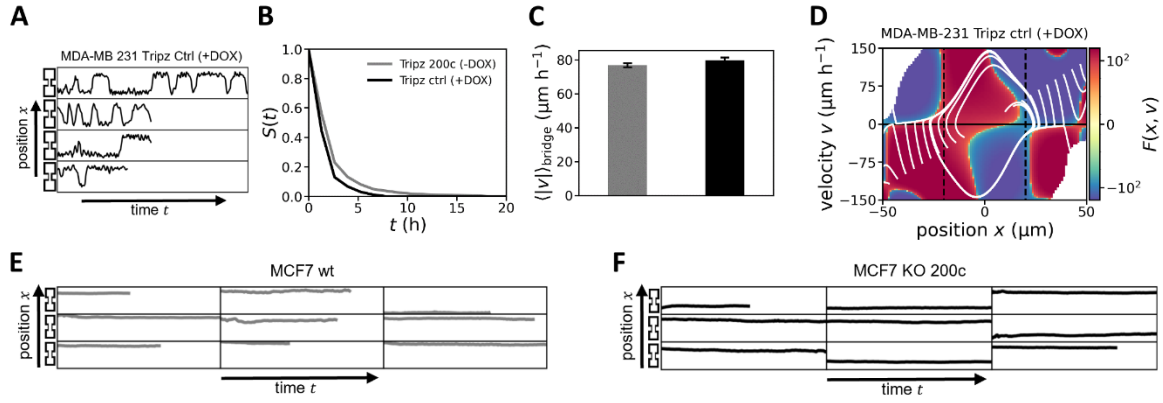

Figure S15: Doxycycline (DOX) induction is not affecting confined cell migration of mesenchymal cells. No measurable hopping dynamics in epithelial MCF7 cells. Selection of nucleus trajectories for **(A)** MDA-MB 231 Tripz Ctrl (control) +DOX cells (n = 89). **(B)** Stay probability of the miR-200c-non-expressing cell lines. Comparison of miR-200c-negative cell lines (MDA-MB 231 Tripz Ctrl +DOX, black and MDA-MB 231 Tripz 200c -DOX, gray). Both in (B) and (C) MDA-MB 231 Tripz 200c (-DOX) (n = 85) and MDA-MB 231 Tripz Ctrl (+DOX) cells (n = 89) are evaluated. **(C)** Average speed of the MDA-MB 231 Tripz Ctrl (+DOX) and MDA-MB 231 Tripz 200c (-DOX) cells while making a transition on the bridge. Values are displayed as mean with SEM. **(D)** Inferred deterministic part of the hopping dynamics. White lines show the deterministic behavior in the two-dimensional phase space of the cells for MDA-MB 231 Tripz Ctrl +DOX. Selection of nucleus trajectories for **(E)** MCF7 wildtype (wt) (n = 62) and (F) MCF7 knockout (KO) 200c cells (n = 44). Small dumbbell symbols next to the trajectories in (A), (E) and (F) indicate the location of the cell.
The data collection and analysis of the 1D dumbbell assay as well as the figure layout was performed by Emily Brieger (under the supervision of Prof. Dr. Joachim Rädler, Faculty of Physics and Center for NanoScience, Ludwig-Maximilians-Universität München, Germany) and Tom Brandstätter (under the supervision of Prof. Dr. Chase Broedersz, Department of Physics and Astronomy, Vrije Universiteit Amsterdam, Netherlands; Arnold-Sommerfeld-Center for Theoretical Physics, Ludwig-Maximilians-Universität, Germany).

8. References

1. Sung H, Ferlay J, Siegel RL, Laversanne M, Soerjomataram I, Jemal A, et al. Global Cancer Statistics 2020: GLOBOCAN Estimates of Incidence and Mortality Worldwide for 36 Cancers in 185 Countries. CA Cancer J Clin. 2021;71(3):209-49.

2. World Health Organization. Global health estimates 2020: deaths by cause, age, sex, by country and by region, 2000–2019. WHO Geneva, Switzerland; 2020.

3. Wang X, Zhang H, Chen X. Drug resistance and combating drug resistance in cancer. Cancer Drug Resist. 2019;2(2):141-60.

4. Barzaman K, Karami J, Zarei Z, Hosseinzadeh A, Kazemi MH, Moradi-Kalbolandi S, et al. Breast cancer: Biology, biomarkers, and treatments. Int Immunopharmacol. 2020;84:106535.

5. Polyak K. Breast cancer: origins and evolution. J Clin Invest. 2007;117(11):3155-63.

6. Grandér D. How do mutated oncogenes and tumor suppressor genes cause cancer? Med Oncol. 1998;15(1):20-6.

7. Lee EY, Muller WJ. Oncogenes and tumor suppressor genes. Cold Spring Harb Perspect Biol. 2010;2(10):a003236.

8. Osborne C, Wilson P, Tripathy D. Oncogenes and tumor suppressor genes in breast cancer: potential diagnostic and therapeutic applications. Oncologist. 2004;9(4):361-77.

9. Rahman MA, Saha SK, Rahman MS, Uddin MJ, Uddin MS, Pang MG, et al. Molecular Insights Into Therapeutic Potential of Autophagy Modulation by Natural Products for Cancer Stem Cells. Front Cell Dev Biol. 2020;8:283.

10. Bradshaw A, Wickremsekera A, Tan ST, Peng L, Davis PF, Itinteang T. Cancer Stem Cell Hierarchy in Glioblastoma Multiforme. Front Surg. 2016;3:21.

11. Shackleton M, Quintana E, Fearon ER, Morrison SJ. Heterogeneity in cancer: cancer stem cells versus clonal evolution. Cell. 2009;138(5):822-9.

12. Anastasiadi Z, Lianos GD, Ignatiadou E, Harissis HV, Mitsis M. Breast cancer in young women: an overview. Updates Surg. 2017;69(3):313-7.

13. Orrantia-Borunda E, Anchondo-Nuñez P, Acuña-Aguilar LE, Gómez-Valles FO, Ramírez-Valdespino CA. Subtypes of Breast Cancer. In: Mayrovitz HN, editor. Breast Cancer [Internet]. Brisbane (AU): Exon Publications; 2022.

14. American Cancer Society. Breast Cancer Facts & Figures 2022-2024. Inc. 2022. Atlanta: American Cancer Society.

15. Roulot A, Héquet D, Guinebretière JM, Vincent-Salomon A, Lerebours F, Dubot C, et al. Tumoral heterogeneity of breast cancer. Ann Biol Clin (Paris). 2016;74(6):653-60.

16. Tran B, Bedard PL. Luminal-B breast cancer and novel therapeutic targets. Breast Cancer Res. 2011;13(6):221.

17. Yersal O, Barutca S. Biological subtypes of breast cancer: Prognostic and therapeutic implications. World J Clin Oncol. 2014;5(3):412-24.

18. Dai X, Li T, Bai Z, Yang Y, Liu X, Zhan J, et al. Breast cancer intrinsic subtype classification, clinical use and future trends. Am J Cancer Res. 2015;5(10):2929-43.

19. Burguin A, Diorio C, Durocher F. Breast Cancer Treatments: Updates and New Challenges. J Pers Med. 2021;11(8).

20. Shaath H, Elango R, Alajez NM. Molecular Classification of Breast Cancer Utilizing Long Non-Coding RNA (lncRNA) Transcriptomes Identifies Novel Diagnostic lncRNA Panel for Triple-Negative Breast Cancer. Cancers (Basel). 2021;13(21).

21. Łukasiewicz S, Czeczelewski M, Forma A, Baj J, Sitarz R, Stanisławek A. Breast Cancer-Epidemiology, Risk Factors, Classification, Prognostic Markers, and Current Treatment Strategies-An Updated Review. Cancers (Basel). 2021;13(17).

22. Inic Z, Zegarac M, Inic M, Markovic I, Kozomara Z, Djurisic I, et al. Difference between Luminal A and Luminal B Subtypes According to Ki-67, Tumor Size, and Progesterone Receptor Negativity Providing Prognostic Information. Clin Med Insights Oncol. 2014;8:107-11.

23. Ades F, Zardavas D, Bozovic-Spasojevic I, Pugliano L, Fumagalli D, de Azambuja E, et al. Luminal B breast cancer: molecular characterization, clinical management, and future perspectives. J Clin Oncol. 2014;32(25):2794-803.

24. Kashyap D, Pal D, Sharma R, Garg VK, Goel N, Koundal D, et al. Global Increase in Breast Cancer Incidence: Risk Factors and Preventive Measures. Biomed Res Int. 2022;2022:9605439.

25. Wang J, Xu B. Targeted therapeutic options and future perspectives for HER2-positive breast cancer. Signal Transduct Target Ther. 2019;4:34.

26. Sharma P. Biology and Management of Patients With Triple-Negative Breast Cancer. Oncologist. 2016;21(9):1050-62.

27. Howard FM, Olopade OI. Epidemiology of Triple-Negative Breast Cancer: A Review. Cancer J. 2021;27(1):8-16.

28. Emborgo TS, Saporito D, Muse KI, Barrera AMG, Litton JK, Lu KH, et al. Prospective Evaluation of Universal BRCA Testing for Women With Triple-Negative Breast Cancer. JNCI Cancer Spectr. 2020;4(2):pkaa002.

29. Prat A, Adamo B, Cheang MC, Anders CK, Carey LA, Perou CM. Molecular characterization of basal-like and non-basal-like triple-negative breast cancer. Oncologist. 2013;18(2):123-33.

30. Yin L, Duan JJ, Bian XW, Yu SC. Triple-negative breast cancer molecular subtyping and treatment progress. Breast Cancer Res. 2020;22(1):61.

31. Mollaei M, Hassan ZM, Khorshidi F, Langroudi L. Chemotherapeutic drugs: Cell death- and resistance-related signaling pathways. Are they really as smart as the tumor cells? Transl Oncol. 2021;14(5):101056.

32. Yang TJ, Ho AY. Radiation therapy in the management of breast cancer. Surg Clin North Am. 2013;93(2):455-71.

33. Lumachi F, Luisetto G, Basso SM, Basso U, Brunello A, Camozzi V. Endocrine therapy of breast cancer. Curr Med Chem. 2011;18(4):513-22.

34. Tremont A, Lu J, Cole JT. Endocrine Therapy for Early Breast Cancer: Updated Review. Ochsner J. 2017;17(4):405-11.

35. Figueroa-Magalhães MC, Jelovac D, Connolly R, Wolff AC. Treatment of HER2-positive breast cancer. Breast. 2014;23(2):128-36.

36. Maximiano S, Magalhães P, Guerreiro MP, Morgado M. Trastuzumab in the Treatment of Breast Cancer. BioDrugs. 2016;30(2):75-86.

37. Ishii K, Morii N, Yamashiro H. Pertuzumab in the treatment of HER2-positive breast cancer: an evidence-based review of its safety, efficacy, and place in therapy. Core Evid. 2019;14:51-70.

38. Nguyen X, Hooper M, Borlagdan JP, Palumbo A. A Review of Fam-Trastuzumab Deruxtecan-nxki in HER2-Positive Breast Cancer. Ann Pharmacother. 2021;55(11):1410-8.

39. Moreira C, Kaklamani V. Lapatinib and breast cancer: current indications and outlook for the future. Expert Rev Anticancer Ther. 2010;10(8):1171-82.

40. Park JW, Liu MC, Yee D, Yau C, van 't Veer LJ, Symmans WF, et al. Adaptive Randomization of Neratinib in Early Breast Cancer. N Engl J Med. 2016;375(1):11-22.

41. Swain SM, Shastry M, Hamilton E. Targeting HER2-positive breast cancer: advances and future directions. Nat Rev Drug Discov. 2023;22(2):101-26.

42. Pegram MD, Reese DM. Combined biological therapy of breast cancer using monoclonal antibodies directed against HER2/neu protein and vascular endothelial growth factor. Semin Oncol. 2002;29(3 Suppl 11):29-37.

43. Higgins MJ, Baselga J. Targeted therapies for breast cancer. J Clin Invest. 2011;121(10):3797-803.

44. Riccardi F, Colantuoni G, Diana A, Mocerino C, Cartenì G, Lauria R, et al. Exemestane and Everolimus combination treatment of hormone receptor positive, HER2 negative metastatic breast cancer: A retrospective study of 9 cancer centers in the Campania Region (Southern Italy) focused on activity, efficacy and safety. Mol Clin Oncol. 2018;9(3):255-63.

45. Steger GG, Gnant M, Bartsch R. Palbociclib for the treatment of postmenopausal breast cancer - an update. Expert Opin Pharmacother. 2016;17(2):255-63.

46. Shah A, Bloomquist E, Tang S, Fu W, Bi Y, Liu Q, et al. FDA Approval: Ribociclib for the Treatment of Postmenopausal Women with Hormone Receptor-Positive, HER2-Negative Advanced or Metastatic Breast Cancer. Clin Cancer Res. 2018;24(13):2999-3004.

47. Bardia A, Hurvitz SA, Tolaney SM, Loirat D, Punie K, Oliveira M, et al. Sacituzumab Govitecan in Metastatic Triple-Negative Breast Cancer. N Engl J Med. 2021;384(16):1529-41.

48. Heimes AS, Schmidt M. Atezolizumab for the treatment of triple-negative breast cancer. Expert Opin Investig Drugs. 2019;28(1):1-5.

49. Hanahan D, Weinberg RA. The hallmarks of cancer. Cell. 2000;100(1):57-70.

50. Hanahan D, Weinberg RA. Hallmarks of cancer: the next generation. Cell. 2011;144(5):646-74.

51. Hanahan D. Hallmarks of Cancer: New Dimensions. Cancer Discov. 2022;12(1):31-46.

52. Ma J, Dong C, Ji C. MicroRNA and drug resistance. Cancer Gene Ther. 2010;17(8):523-31.

53. Lønning PE, Knappskog S. Mapping genetic alterations causing chemoresistance in cancer: identifying the roads by tracking the drivers. Oncogene. 2013;32(46):5315-30.

54. Si W, Shen J, Zheng H, Fan W. The role and mechanisms of action of microRNAs in cancer drug resistance. Clin Epigenetics. 2019;11(1):25.

55. Santos P, Almeida F. Role of Exosomal miRNAs and the Tumor Microenvironment in Drug Resistance. Cells. 2020;9(6).

56. Singh S, Gomez HJ, Thakkar S, Singh SP, Parihar AS. Overcoming Acquired Drug Resistance to Cancer Therapies through Targeted STAT3 Inhibition. Int J Mol Sci. 2023;24(5).

57. Konieczkowski DJ, Johannessen CM, Garraway LA. A Convergence-Based Framework for Cancer Drug Resistance. Cancer Cell. 2018;33(5):801-15.

58. Guo C, Liu J, Zhou Q, Song J, Zhang Z, Li Z, et al. Exosomal Noncoding RNAs and Tumor Drug Resistance. Cancer Res. 2020;80(20):4307-13.

59. Szakács G, Paterson JK, Ludwig JA, Booth-Genthe C, Gottesman MM. Targeting multidrug resistance in cancer. Nat Rev Drug Discov. 2006;5(3):219-34.

60. Fodale V, Pierobon M, Liotta L, Petricoin E. Mechanism of cell adaptation: when and how do cancer cells develop chemoresistance? Cancer J. 2011;17(2):89-95.

61. Zheng HC. The molecular mechanisms of chemoresistance in cancers. Oncotarget. 2017;8(35):59950-64.

62. Xue X, Liang XJ. Overcoming drug efflux-based multidrug resistance in cancer with nanotechnology. Chin J Cancer. 2012;31(2):100-9.

63. Townsend DM, Tew KD. The role of glutathione-S-transferase in anti-cancer drug resistance. Oncogene. 2003;22(47):7369-75.

64. Luo W, Kinsey M, Schiffman JD, Lessnick SL. Glutathione s-transferases in pediatric cancer. Front Oncol. 2011;1:39.

65. Oakley A. Glutathione transferases: a structural perspective. Drug Metab Rev. 2011;43(2):138-51.

66. Phang-Lyn S LV. Biochemistry, Biotransformation. : StatPearls [Internet]. Treasure Island (FL): StatPearls Publishing;; 2024. Available from: https://www.ncbi.nlm.nih.gov/books/NBK544353/.

67. Allocati N, Masulli M, Di Ilio C, Federici L. Glutathione transferases: substrates, inihibitors and pro-drugs in cancer and neurodegenerative diseases. Oncogenesis. 2018;7(1):8.

68. Tew KD, Townsend DM. Glutathione-s-transferases as determinants of cell survival and death. Antioxid Redox Signal. 2012;17(12):1728-37.

69. Mazari AMA, Zhang L, Ye ZW, Zhang J, Tew KD, Townsend DM. The Multifaceted Role of Glutathione S-Transferases in Health and Disease. Biomolecules. 2023;13(4).

70. Chatterjee A, Gupta S. The multifaceted role of glutathione S-transferases in cancer. Cancer Lett. 2018;433:33-42.

71. Hayes JD, Flanagan JU, Jowsey IR. Glutathione transferases. Annu Rev Pharmacol Toxicol. 2005;45:51-88.

72. Sau A, Pellizzari Tregno F, Valentino F, Federici G, Caccuri AM. Glutathione transferases and development of new principles to overcome drug resistance. Arch Biochem Biophys. 2010;500(2):116-22.

73. Wang S, Yang J, You L, Dai M, Zhao Y. GSTM3 Function and Polymorphism in Cancer: Emerging but Promising. Cancer Manag Res. 2020;12:10377-88.

74. Bièche I, Girault I, Urbain E, Tozlu S, Lidereau R. Relationship between intratumoral expression of genes coding for xenobiotic-metabolizing enzymes and benefit from adjuvant tamoxifen in estrogen receptor alpha-positive postmenopausal breast carcinoma. Breast Cancer Res. 2004;6(3):R252-63.

75. Lin JH, Tu SH, Chen LC, Huang CC, Chang HL, Cheng TC, et al. Oestrogen receptor-regulated glutathione S-transferase mu 3 expression attenuates hydrogen peroxide-induced cytotoxicity, which confers tamoxifen resistance on breast cancer cells. Breast Cancer Res Treat. 2018;172(1):45-59.

76. Humphries B, Yang C. The microRNA-200 family: small molecules with novel roles in cancer development, progression and therapy. Oncotarget. 2015;6(9):6472-98.

77. Chaffer CL, Weinberg RA. A perspective on cancer cell metastasis. Science. 2011;331(6024):1559-64.

78. Park M, Kim D, Ko S, Kim A, Mo K, Yoon H. Breast Cancer Metastasis: Mechanisms and Therapeutic Implications. Int J Mol Sci. 2022;23(12).

79. Waks AG, Winer EP. Breast Cancer Treatment: A Review. Jama. 2019;321(3):288-300.

80. Sporn MB. The war on cancer. Lancet. 1996;347(9012):1377-81.

81. Mehlen P, Puisieux A. Metastasis: a question of life or death. Nature Reviews Cancer. 2006;6(6):449-58.

82. Hunter KW, Crawford NP, Alsarraj J. Mechanisms of metastasis. Breast Cancer Res. 2008;10 Suppl 1(Suppl 1):S2.

83. Chiang AC, Massagué J. Molecular basis of metastasis. N Engl J Med. 2008;359(26):2814-23.

84. Yokota J. Tumor progression and metastasis. Carcinogenesis. 2000;21(3):497-503.

85. Welch DR, Hurst DR. Defining the Hallmarks of Metastasis. Cancer Res. 2019;79(12):3011-27.

86. Fares J, Fares MY, Khachfe HH, Salhab HA, Fares Y. Molecular principles of metastasis: a hallmark of cancer revisited. Signal Transduct Target Ther. 2020;5(1):28.

87. Seyfried TN, Huysentruyt LC. On the origin of cancer metastasis. Crit Rev Oncog. 2013;18(1-2):43-73.

88. Eccles SA, Welch DR. Metastasis: recent discoveries and novel treatment strategies. Lancet. 2007;369(9574):1742-57.

89. Lambert AW, Pattabiraman DR, Weinberg RA. Emerging Biological Principles of Metastasis. Cell. 2017;168(4):670-91.

90. Valastyan S, Weinberg RA. Tumor metastasis: molecular insights and evolving paradigms. Cell. 2011;147(2):275-92.

91. Scully OJ, Bay B-H, Yip G, Yu Y. Breast Cancer Metastasis. Cancer Genomics - Proteomics. 2012;9(5):311.

92. Roussos ET, Condeelis JS, Patsialou A. Chemotaxis in cancer. Nat Rev Cancer. 2011;11(8):573-87.

93. Paul CD, Mistriotis P, Konstantopoulos K. Cancer cell motility: lessons from migration in confined spaces. Nat Rev Cancer. 2017;17(2):131-40.

94. Bravo-Cordero JJ, Hodgson L, Condeelis J. Directed cell invasion and migration during metastasis. Curr Opin Cell Biol. 2012;24(2):277-83.

95. Wirtz D, Konstantopoulos K, Searson PC. The physics of cancer: the role of physical interactions and mechanical forces in metastasis. Nat Rev Cancer. 2011;11(7):512-22.

96. van Zijl F, Krupitza G, Mikulits W. Initial steps of metastasis: cell invasion and endothelial transmigration. Mutat Res. 2011;728(1-2):23-34.

97. Friedl P, Wolf K. Tumour-cell invasion and migration: diversity and escape mechanisms. Nat Rev Cancer. 2003;3(5):362-74.

98. Wang L, Wang J. MicroRNA-mediated breast cancer metastasis: from primary site to distant organs. Oncogene. 2012;31(20):2499-511.

99. Tang J, Ahmad A, Sarkar FH. The role of microRNAs in breast cancer migration, invasion and metastasis. International journal of molecular sciences. 2012;13(10):13414-37.

100. Ratti M, Lampis A, Ghidini M, Salati M, Mirchev MB, Valeri N, et al. MicroRNAs (miRNAs) and Long Non-Coding RNAs (lncRNAs) as New Tools for Cancer Therapy: First Steps from Bench to Bedside. Target Oncol. 2020;15(3):261-78.

101. Peter ME. Targeting of mRNAs by multiple miRNAs: the next step. Oncogene. 2010;29(15):2161-4.

102. Shimono Y, Zabala M, Cho RW, Lobo N, Dalerba P, Qian D, et al. Downregulation of miRNA-200c links breast cancer stem cells with normal stem cells. Cell. 2009;138(3):592-603.

103. Mutlu M, Raza U, Saatci Ö, Eyüpoğlu E, Yurdusev E, Şahin Ö. miR-200c: a versatile watchdog in cancer progression, EMT, and drug resistance. Journal of Molecular Medicine. 2016;94(6):629-44.

104. Friedman RC, Farh KK, Burge CB, Bartel DP. Most mammalian mRNAs are conserved targets of microRNAs. Genome Res. 2009;19(1):92-105.

105. Ha M, Kim VN. Regulation of microRNA biogenesis. Nature Reviews Molecular Cell Biology. 2014;15(8):509-24.

106. Dai X, Chen A, Bai Z. Integrative investigation on breast cancer in ER, PR and HER2-defined subgroups using mRNA and miRNA expression profiling. Sci Rep. 2014;4:6566.

107. Macfarlane LA, Murphy PR. MicroRNA: Biogenesis, Function and Role in Cancer. Curr Genomics. 2010;11(7):537-61.

108. O'Brien J, Hayder H, Zayed Y, Peng C. Overview of MicroRNA Biogenesis, Mechanisms of Actions, and Circulation. Front Endocrinol (Lausanne). 2018;9:402.

109. Winter J, Jung S, Keller S, Gregory RI, Diederichs S. Many roads to maturity: microRNA biogenesis pathways and their regulation. Nat Cell Biol. 2009;11(3):228-34.

110. Perron MP, Provost P. Protein interactions and complexes in human microRNA biogenesis and function. Front Biosci. 2008;13:2537-47.

111. Nallamshetty S, Chan SY, Loscalzo J. Hypoxia: a master regulator of microRNA biogenesis and activity. Free Radic Biol Med. 2013;64:20-30.

112. Inui M, Martello G, Piccolo S. MicroRNA control of signal transduction. Nat Rev Mol Cell Biol. 2010;11(4):252-63.

113. Köhler B, Dubovik S, Hörterer E, Wilk U, Stöckl JB, Tekarslan-Sahin H, et al. Combating Drug Resistance by Exploiting miRNA− 200c-Controlled Phase II Detoxification. Cancers. 2022;14(22):5554.

114. Ljepoja B, Schreiber C, Gegenfurtner FA, García-Roman J, Köhler B, Zahler S, et al. Inducible microRNA-200c decreases motility of breast cancer cells and reduces filamin A. PLoS One. 2019;14(11):e0224314.

115. Ljepoja B, García-Roman J, Sommer AK, Fröhlich T, Arnold GJ, Wagner E, et al. A proteomic analysis of an in vitro knock-out of miR-200c. Sci Rep. 2018;8(1):6927.

116. Müller K, Klein PM, Heissig P, Roidl A, Wagner E. EGF receptor targeted lipo-oligocation polyplexes for antitumoral siRNA and miRNA delivery. Nanotechnology. 2016;27(46):464001.

117. Kopp F, Wagner E, Roidl A. The proto-oncogene KRAS is targeted by miR-200c. Oncotarget. 2014;5(1):185-95.

118. Kopp F, Oak PS, Wagner E, Roidl A. miR-200c sensitizes breast cancer cells to doxorubicin treatment by decreasing TrkB and Bmi1 expression. PLoS One. 2012;7(11):e50469.

119. Wen B, Zhu R, Jin H, Zhao K. Differential expression and role of miR-200 family in multiple tumors. Anal Biochem. 2021;626:114243.

120. Neves R, Scheel C, Weinhold S, Honisch E, Iwaniuk KM, Trompeter HI, et al. Role of DNA methylation in miR-200c/141 cluster silencing in invasive breast cancer cells. BMC Res Notes. 2010;3:219.

121. Castilla M, Díaz-Martín J, Sarrió D, Romero-Pérez L, López-García M, Vieites B, et al. MicroRNA-200 family modulation in distinct breast cancer phenotypes. PLoS One. 2012;7(10):e47709.

122. Kolesnikoff N, Attema JL, Roslan S, Bert AG, Schwarz QP, Gregory PA, et al. Specificity protein 1 (Sp1) maintains basal epithelial expression of the miR-200 family: implications for epithelial-mesenchymal transition. J Biol Chem. 2014;289(16):11194-205.

123. Kim T, Veronese A, Pichiorri F, Lee TJ, Jeon YJ, Volinia S, et al. p53 regulates epithelial-mesenchymal transition through microRNAs targeting ZEB1 and ZEB2. J Exp Med. 2011;208(5):875-83.

124. Chang CJ, Chao CH, Xia W, Yang JY, Xiong Y, Li CW, et al. p53 regulates epithelial-mesenchymal transition and stem cell properties through modulating miRNAs. Nat Cell Biol. 2011;13(3):317-23.

125. Kumar S, Nag A, Mandal CC. A Comprehensive Review on miR-200c, A Promising Cancer Biomarker with Therapeutic Potential. Curr Drug Targets. 2015;16(12):1381-403.

126. Kawaguchi T, Yan L, Qi Q, Peng X, Gabriel EM, Young J, et al. Overexpression of suppressive microRNAs, miR-30a and miR-200c are associated with improved survival of breast cancer patients. Sci Rep. 2017;7(1):15945.

127. Xu F, He H, Huang W, Lin Y, Luo S, Du Q, et al. Decreased expression of MicroRNA-200 family in human breast cancer is associated with lymph node metastasis. Clin Transl Oncol. 2016;18(3):283-8.

128. Mansoori B, Silvestris N, Mohammadi A, Khaze V, Baghbani E, Mokhtarzadeh A, et al. miR-34a and miR-200c Have an Additive Tumor-Suppressive Effect on Breast Cancer Cells and Patient Prognosis. Genes. 2021;12(2):267.

129. Saleeb R, Kim SS, Ding Q, Scorilas A, Lin S, Khella HW, et al. The miR-200 family as prognostic markers in clear cell renal cell carcinoma. Urol Oncol. 2019;37(12):955-63.

130. Jo H, Shim K, Jeoung D. Potential of the miR-200 Family as a Target for Developing Anti-Cancer Therapeutics. Int J Mol Sci. 2022;23(11).

131. Santasusagna S, Moreno I, Navarro A, Martinez Rodenas F, Hernández R, Castellano JJ, et al. Prognostic Impact of miR-200 Family Members in Plasma and Exosomes from Tumor-Draining versus Peripheral Veins of Colon Cancer Patients. Oncology. 2018;95(5):309-18.

132. Xie L, Jing R, Qi J, Lin Z, Ju S. Drug resistance-related microRNAs in hematological malignancies: translating basic evidence into therapeutic strategies. Blood Rev. 2015;29(1):33-44.

133. Mulrane L, McGee SF, Gallagher WM, O'Connor DP. miRNA dysregulation in breast cancer. Cancer Res. 2013;73(22):6554-62.

134. Liu S, Tetzlaff MT, Cui R, Xu X. miR-200c inhibits melanoma progression and drug resistance through down-regulation of BMI-1. Am J Pathol. 2012;181(5):1823-35.

135. Choi CH. ABC transporters as multidrug resistance mechanisms and the development of chemosensitizers for their reversal. Cancer Cell Int. 2005;5:30.

136. Haenisch S, Werk AN, Cascorbi I. MicroRNAs and their relevance to ABC transporters. Br J Clin Pharmacol. 2014;77(4):587-96.

137. Chen J, Tian W, Cai H, He H, Deng Y. Down-regulation of microRNA-200c is associated with drug resistance in human breast cancer. Med Oncol. 2012;29(4):2527-34.

138. Puhr M, Hoefer J, Schäfer G, Erb HH, Oh SJ, Klocker H, et al. Epithelial-to-mesenchymal transition leads to docetaxel resistance in prostate cancer and is mediated by reduced expression of miR-200c and miR-205. Am J Pathol. 2012;181(6):2188-201.

139. Liu J, Zhang X, Huang Y, Zhang Q, Zhou J, Zhang X, et al. miR-200b and miR-200c co-contribute to the cisplatin sensitivity of ovarian cancer cells by targeting DNA methyltransferases. Oncol Lett. 2019;17(2):1453-60.

140. Christowitz C, Davis T, Isaacs A, van Niekerk G, Hattingh S, Engelbrecht AM. Mechanisms of doxorubicin-induced drug resistance and drug resistant tumour growth in a murine breast tumour model. BMC Cancer. 2019;19(1):757.

141. Senfter D, Madlener S, Krupitza G, Mader RM. The microRNA-200 family: still much to discover. Biomol Concepts. 2016;7(5-6):311-9.

142. Klicka K, Grzywa TM, Mielniczuk A, Klinke A, Włodarski PK. The role of miR-200 family in the regulation of hallmarks of cancer. Front Oncol. 2022;12:965231.

143. Perdigão-Henriques R, Petrocca F, Altschuler G, Thomas MP, Le MT, Tan SM, et al. miR-200 promotes the mesenchymal to epithelial transition by suppressing multiple members of the Zeb2 and Snail1 transcriptional repressor complexes. Oncogene. 2016;35(2):158-72.

144. van Staalduinen J, Baker D, Ten Dijke P, van Dam H. Epithelial-mesenchymal-transition-inducing transcription factors: new targets for tackling chemoresistance in cancer? Oncogene. 2018;37(48):6195-211.

145. Cavallari I, Ciccarese F, Sharova E, Urso L, Raimondi V, Silic-Benussi M, et al. The miR-200 Family of microRNAs: Fine Tuners of Epithelial-Mesenchymal Transition and Circulating Cancer Biomarkers. Cancers (Basel). 2021;13(23).

146. Wu Y, Ginther C, Kim J, Mosher N, Chung S, Slamon D, et al. Expression of Wnt3 activates Wnt/β-catenin pathway and promotes EMT-like phenotype in trastuzumab-resistant HER2-overexpressing breast cancer cells. Mol Cancer Res. 2012;10(12):1597-606.

147. Della Corte CM, Bellevicine C, Vicidomini G, Vitagliano D, Malapelle U, Accardo M, et al. SMO Gene Amplification and Activation of the Hedgehog Pathway as Novel Mechanisms of Resistance to Anti-Epidermal Growth Factor Receptor Drugs in Human Lung Cancer. Clin Cancer Res. 2015;21(20):4686-97.

148. Ferrari P, Scatena C, Ghilli M, Bargagna I, Lorenzini G, Nicolini A. Molecular Mechanisms, Biomarkers and Emerging Therapies for Chemotherapy Resistant TNBC. Int J Mol Sci. 2022;23(3).

149. Bracken CP, Khew-Goodall Y, Goodall GJ. Network-Based Approaches to Understand the Roles of miR-200 and Other microRNAs in Cancer. Cancer Res. 2015;75(13):2594-9.

150. Sommerova L, Ondrouskova E, Martisova A, Zoumpourlis V, Galtsidis S, Hrstka R. ZEB1/miR-200c/AGR2: A New Regulatory Loop Modulating the Epithelial-Mesenchymal Transition in Lung Adenocarcinomas. Cancers (Basel). 2020;12(6).

151. Jones R, Watson K, Bruce A, Nersesian S, Kitz J, Moorehead R. Re-expression of miR-200c suppresses proliferation, colony formation and in vivo tumor growth of murine claudin-low mammary tumor cells. Oncotarget. 2017;8(14):23727-49.

152. Simpson KE, Watson KL, Moorehead RA. Elevated Expression of miR-200c/141 in MDA-MB-231 Cells Suppresses MXRA8 Levels and Impairs Breast Cancer Growth and Metastasis In Vivo. Genes (Basel). 2022;13(4).

153. Shi L, Zhang S, Wu H, Zhang L, Dai X, Hu J, et al. MiR-200c increases the radiosensitivity of non-small-cell lung cancer cell line A549 by targeting VEGF-VEGFR2 pathway. PLoS One. 2013;8(10):e78344.

154. Dong L, Zhang L, Liu H, Xie M, Gao J, Zhou X, et al. Circ_0007331 knock-down suppresses the progression of endometriosis via miR-200c-3p/HiF-1α axis. J Cell Mol Med. 2020;24(21):12656-66.

155. Jurmeister S, Baumann M, Balwierz A, Keklikoglou I, Ward A, Uhlmann S, et al. MicroRNA-200c represses migration and invasion of breast cancer cells by targeting actin-regulatory proteins FHOD1 and PPM1F. Mol Cell Biol. 2012;32(3):633-51.

156. Yuan X, Liu J, Ye X. Effect of miR-200c on the proliferation, migration and invasion of breast cancer cells and relevant mechanisms. J buon. 2019;24(1):61-7.

157. Hurteau GJ, Carlson JA, Spivack SD, Brock GJ. Overexpression of the microRNA hsa-miR-200c leads to reduced expression of transcription factor 8 and increased expression of E-cadherin. Cancer Res. 2007;67(17):7972-6.

158. Chen H, Li Z, Zhang L, Zhang L, Zhang Y, Wang Y, et al. MicroRNA-200c Inhibits the Metastasis of Triple-Negative Breast Cancer by Targeting ZEB2, an Epithelial-Mesenchymal Transition Regulator. Ann Clin Lab Sci. 2020;50(4):519-27.

159. Korpal M, Lee ES, Hu G, Kang Y. The miR-200 family inhibits epithelial-mesenchymal transition and cancer cell migration by direct targeting of E-cadherin transcriptional repressors ZEB1 and ZEB2. J Biol Chem. 2008;283(22):14910-4.

160. Li J, Tan Q, Yan M, Liu L, Lin H, Zhao F, et al. miRNA-200c inhibits invasion and metastasis of human non-small cell lung cancer by directly targeting ubiquitin specific peptidase 25. Mol Cancer. 2014;13:166.

161. Howe EN, Cochrane DR, Richer JK. Targets of miR-200c mediate suppression of cell motility and anoikis resistance. Breast Cancer Res. 2011;13(2):R45.

162. Bai WD, Ye XM, Zhang MY, Zhu HY, Xi WJ, Huang X, et al. MiR-200c suppresses TGF-β signaling and counteracts trastuzumab resistance and metastasis by targeting ZNF217 and ZEB1 in breast cancer. Int J Cancer. 2014;135(6):1356-68.

163. Luo D, Wilson JM, Harvel N, Liu J, Pei L, Huang S, et al. A systematic evaluation of miRNA:mRNA interactions involved in the migration and invasion of breast cancer cells. J Transl Med. 2013;11:57.

164. Sigloch FC, Burk UC, Biniossek ML, Brabletz T, Schilling O. miR-200c dampens cancer cell migration via regulation of protein kinase A subunits. Oncotarget. 2015;6(27):23874-89.

165. Korpal M, Ell BJ, Buffa FM, Ibrahim T, Blanco MA, Celià-Terrassa T, et al. Direct targeting of Sec23a by miR-200s influences cancer cell secretome and promotes metastatic colonization. Nat Med. 2011;17(9):1101-8.

166. Uhlmann S, Zhang JD, Schwäger A, Mannsperger H, Riazalhosseini Y, Burmester S, et al. miR-200bc/429 cluster targets PLCgamma1 and differentially regulates proliferation and EGF-driven invasion than miR-200a/141 in breast cancer. Oncogene. 2010;29(30):4297-306.

167. Schickel R, Park SM, Murmann AE, Peter ME. miR-200c regulates induction of apoptosis through CD95 by targeting FAP-1. Mol Cell. 2010;38(6):908-15.

168. Lerner M, Haneklaus M, Harada M, Grandér D. MiR-200c regulates Noxa expression and sensitivity to proteasomal inhibitors. PLoS One. 2012;7(5):e36490.

169. Howe EN, Cochrane DR, Cittelly DM, Richer JK. miR-200c targets a NF-κB up-regulated TrkB/NTF3 autocrine signaling loop to enhance anoikis sensitivity in triple negative breast cancer. PLoS One. 2012;7(11):e49987.

170. Drake JM, Strohbehn G, Bair TB, Moreland JG, Henry MD. ZEB1 enhances transendothelial migration and represses the epithelial phenotype of prostate cancer cells. Mol Biol Cell. 2009;20(8):2207-17.

171. Dull T, Zufferey R, Kelly M, Mandel RJ, Nguyen M, Trono D, et al. A third-generation lentivirus vector with a conditional packaging system. J Virol. 1998;72(11):8463-71.

172. Stewart SA, Dykxhoorn DM, Palliser D, Mizuno H, Yu EY, An DS, et al. Lentivirus-delivered stable gene silencing by RNAi in primary cells. Rna. 2003;9(4):493-501.

173. Campeau E, Ruhl VE, Rodier F, Smith CL, Rahmberg BL, Fuss JO, et al. A versatile viral system for expression and depletion of proteins in mammalian cells. PLoS One. 2009;4(8):e6529.

174. Tyanova S, Temu T, Sinitcyn P, Carlson A, Hein MY, Geiger T, et al. The Perseus computational platform for comprehensive analysis of (prote)omics data. Nat Methods. 2016;13(9):731-40.

175. Perez-Riverol Y, Csordas A, Bai J, Bernal-Llinares M, Hewapathirana S, Kundu DJ, et al. The PRIDE database and related tools and resources in 2019: improving support for quantification data. Nucleic Acids Res. 2019;47(D1):D442-d50.

176. Lewis BP, Burge CB, Bartel DP. Conserved seed pairing, often flanked by adenosines, indicates that thousands of human genes are microRNA targets. Cell. 2005;120(1):15-20.

177. Grimson A, Farh KK, Johnston WK, Garrett-Engele P, Lim LP, Bartel DP. MicroRNA targeting specificity in mammals: determinants beyond seed pairing. Mol Cell. 2007;27(1):91-105.

178. Berger S, Krhač Levačić A, Hörterer E, Wilk U, Benli-Hoppe T, Wang Y, et al. Optimizing pDNA Lipo-polyplexes: A Balancing Act between Stability and Cargo Release. Biomacromolecules. 2021;22(3):1282-96.

179. Sommer AK, Falcenberg M, Ljepoja B, Fröhlich T, Arnold GJ, Wagner E, et al. Downregulation of GRK5 hampers the migration of breast cancer cells. Sci Rep. 2019;9(1):15548.

180. Lánczky A, Nagy Á, Bottai G, Munkácsy G, Szabó A, Santarpia L, et al. miRpower: a web-tool to validate survival-associated miRNAs utilizing expression data from 2178 breast cancer patients. Breast Cancer Res Treat. 2016;160(3):439-46.

181. Győrffy B. Survival analysis across the entire transcriptome identifies biomarkers with the highest prognostic power in breast cancer. Comput Struct Biotechnol J. 2021;19:4101-9.

182. Lánczky A, Győrffy B. Web-Based Survival Analysis Tool Tailored for Medical Research (KMplot): Development and Implementation. J Med Internet Res. 2021;23(7):e27633.

183. Brückner DB, Fink A, Schreiber C, Röttgermann PJF, Rädler JO, Broedersz CP. Stochastic nonlinear dynamics of confined cell migration in two-state systems. Nature Physics. 2019;15(6):595-601.

184. Brückner DB, Ronceray P, Broedersz CP. Inferring the Dynamics of Underdamped Stochastic Systems. Phys Rev Lett. 2020;125(5):058103.

185. Suarez-Arnedo A, Torres Figueroa F, Clavijo C, Arbeláez P, Cruz JC, Muñoz-Camargo C. An image J plugin for the high throughput image analysis of in vitro scratch wound healing assays. PLoS One. 2020;15(7):e0232565.

186. Tinevez JY, Perry N, Schindelin J, Hoopes GM, Reynolds GD, Laplantine E, et al. TrackMate: An open and extensible platform for single-particle tracking. Methods. 2017;115:80-90.

187. Takashimizu Y, Iiyoshi M. New parameter of roundness R: circularity corrected by aspect ratio. Progress in Earth and Planetary Science. 2016;3(1):2.

188. Barth M, Nikol, Wörle. Mathematische Formeln und Definitionen. 8 ed: Lindauer Verlag; 2004. p. 118.

189. Xu XM, Chen Y, Chen J, Yang S, Gao F, Underhill CB, et al. A peptide with three hyaluronan binding motifs inhibits tumor growth and induces apoptosis. Cancer Res. 2003;63(18):5685-90.

190. Marfels C, Hoehn M, Wagner E, Günther M. Characterization of in vivo chemoresistant human hepatocellular carcinoma cells with transendothelial differentiation capacities. BMC Cancer. 2013;13:176.

191. Janvier Labs. NMRI-nu Immundeficient Mouse 2019 [9 July 2024]. Available from: https://janvier-labs.com/en/fiche_produit/nmri-nu_mouse/.

192. Bundesministerium der Justiz. Tierschutzgesetz (TierSchG) 2024 [9 July 2024]. Available from: https://www.gesetze-im-internet.de/tierschg/__11.html.

193. Chen W, Hoffmann AD, Liu H, Liu X. Organotropism: new insights into molecular mechanisms of breast cancer metastasis. npj Precision Oncology. 2018;2(1):4.

194. Yates LR, Knappskog S, Wedge D, Farmery JHR, Gonzalez S, Martincorena I, et al. Genomic Evolution of Breast Cancer Metastasis and Relapse. Cancer Cell. 2017;32(2):169-84.e7.

195. Meijering E, Dzyubachyk O, Smal I. Methods for cell and particle tracking. Methods Enzymol. 2012;504:183-200.

196. Beltman JB, Marée AF, de Boer RJ. Analysing immune cell migration. Nat Rev Immunol. 2009;9(11):789-98.

197. Paoli P, Giannoni E, Chiarugi P. Anoikis molecular pathways and its role in cancer progression. Biochimica et Biophysica Acta (BBA) - Molecular Cell Research. 2013;1833(12):3481-98.

198. Kim Y-N, Koo KH, Sung JY, Yun U-J, Kim H. Anoikis Resistance: An Essential Prerequisite for Tumor Metastasis. International Journal of Cell Biology. 2012;2012:306879.

199. Brückner DB, Fink A, Rädler JO, Broedersz CP. Disentangling the behavioural variability of confined cell migration. Journal of The Royal Society Interface. 2020;17(163).

200. Chen L, Sun H, Wang C, Yang Y, Zhang M, Wong G. miRNA arm switching identifies novel tumour biomarkers. EBioMedicine. 2018;38:37-46.

201. Ruzza P, Calderan A. Glutathione Transferase (GST)-Activated Prodrugs. Pharmaceutics. 2013;5(2):220-31.

202. Xu Y, Bankhead A, 3rd, Tian X, Tang J, Ljungman M, Neamati N. Deletion of Glutathione S-Transferase Omega 1 Activates Type I Interferon Genes and Downregulates Tissue Factor. Cancer Res. 2020;80(17):3692-705.

203. Kalinina EV, Berozov TT, Shtil AA, Chernov NN, Glasunova VA, Novichkova MD, et al. Expression of genes of glutathione transferase isoforms GSTP1-1, GSTA4-4, and GSTK1-1 in tumor cells during the formation of drug resistance to cisplatin. Bull Exp Biol Med. 2012;154(1):64-7.

204. Checa-Rojas A, Delgadillo-Silva LF, Velasco-Herrera MDC, Andrade-Domínguez A, Gil J, Santillán O, et al. GSTM3 and GSTP1: novel players driving tumor progression in cervical cancer. Oncotarget. 2018;9(31):21696-714.

205. Louie SM, Grossman EA, Crawford LA, Ding L, Camarda R, Huffman TR, et al. GSTP1 Is a Driver of Triple-Negative Breast Cancer Cell Metabolism and Pathogenicity. Cell Chem Biol. 2016;23(5):567-78.

206. Singh RR, Reindl KM. Glutathione S-Transferases in Cancer. Antioxidants (Basel). 2021;10(5).

207. Abd El-Aziz YS, Spillane AJ, Jansson PJ, Sahni S. Role of ABCB1 in mediating chemoresistance of triple-negative breast cancers. Biosci Rep. 2021;41(2).

208. Li Y, VandenBoom TG, 2nd, Kong D, Wang Z, Ali S, Philip PA, et al. Up-regulation of miR-200 and let-7 by natural agents leads to the reversal of epithelial-to-

mesenchymal transition in gemcitabine-resistant pancreatic cancer cells. Cancer Res. 2009;69(16):6704-12.

209. Sanli F, Tatar A, Gundogdu B, Karatas OF. IP3R1 dysregulation via mir-200c-3p/SSFA2 axis contributes to taxol resistance in head and neck cancer. Eur J Pharmacol. 2024;973:176592.

210. Zhu W, Xu H, Zhu D, Zhi H, Wang T, Wang J, et al. miR-200bc/429 cluster modulates multidrug resistance of human cancer cell lines by targeting BCL2 and XIAP. Cancer Chemother Pharmacol. 2012;69(3):723-31.

211. Anastasiadou E, Messina E, Sanavia T, Mundo L, Farinella F, Lazzi S, et al. MiR-200c-3p Contrasts PD-L1 Induction by Combinatorial Therapies and Slows Proliferation of Epithelial Ovarian Cancer through Downregulation of β-Catenin and c-Myc. Cells. 2021;10(3).

212. Song C, Liu LZ, Pei XQ, Liu X, Yang L, Ye F, et al. miR-200c inhibits breast cancer proliferation by targeting KRAS. Oncotarget. 2015;6(33):34968-78.

213. Knezevic J, Pfefferle AD, Petrovic I, Greene SB, Perou CM, Rosen JM. Expression of miR-200c in claudin-low breast cancer alters stem cell functionality, enhances chemosensitivity and reduces metastatic potential. Oncogene. 2015;34(49):5997-6006.

214. Watson KL, Jones RA, Bruce A, Moorehead RA. The miR-200b/200a/429 cluster prevents metastasis and induces dormancy in a murine claudin-low mammary tumor cell line. Exp Cell Res. 2018;369(1):17-26.

215. Schilb AL, Ayat NR, Vaidya AM, Hertz LM, Hall RC, Scheidt JH, et al. Efficacy of Targeted ECO/miR-200c Nanoparticles for Modulating Tumor Microenvironment and Treating Triple Negative Breast Cancer as Non-invasively Monitored by MR Molecular Imaging. Pharm Res. 2021;38(8):1405-18.

216. Vallejo DM, Caparros E, Dominguez M. Targeting Notch signalling by the conserved miR-8/200 microRNA family in development and cancer cells. Embo j. 2011;30(4):756-69.

217. Carvalho C, Santos RX, Cardoso S, Correia S, Oliveira PJ, Santos MS, et al. Doxorubicin: the good, the bad and the ugly effect. Curr Med Chem. 2009;16(25):3267-85.

218. Ghasabi M, Majidi J, Mansoori B, Mohammadi A, Shomali N, Shirafkan N, et al. The effect of combined miR-200c replacement and cisplatin on apoptosis induction and inhibition of gastric cancer cell line migration. J Cell Physiol. 2019;234(12):22581-92.

219. Truebenbach I, Zhang W, Wang Y, Kern S, Höhn M, Reinhard S, et al. Co-delivery of pretubulysin and siEG5 to EGFR overexpressing carcinoma cells. Int J Pharm. 2019;569:118570.

220. Xu F, Liao JZ, Xiang GY, Zhao PX, Ye F, Zhao Q, et al. MiR-101 and doxorubicin codelivered by liposomes suppressing malignant properties of hepatocellular carcinoma. Cancer Medicine. 2017;6(3):651-61.

221. Reddy TL, Garikapati KR, Reddy SG, Reddy BS, Yadav J, Bhadra U, et al. Simultaneous delivery of Paclitaxel and Bcl-2 siRNA via pH-Sensitive liposomal nanocarrier for the synergistic treatment of melanoma. Scientific reports. 2016;6(1):35223.

222. Steinborn B, Truebenbach I, Morys S, Lächelt U, Wagner E, Zhang W. Epidermal growth factor receptor targeted methotrexate and small interfering RNA co-delivery. J Gene Med. 2018;20(7-8):e3041.

223. Dasgupta I, Chatterjee A. Recent Advances in miRNA Delivery Systems. Methods Protoc. 2021;4(1).

224. Suárez B, Solé C, Márquez M, Nanetti F, Lawrie CH. Circulating MicroRNAs as Cancer Biomarkers in Liquid Biopsies. Adv Exp Med Biol. 2022;1385:23-73.

225. Alam F, Mezhal F, El Hasasna H, Nair VA, Aravind SR, Saber Ayad M, et al. The role of p53-microRNA 200-Moesin axis in invasion and drug resistance of breast cancer cells. Tumour Biol. 2017;39(9):1010428317714634.

226. Vrba L, Jensen TJ, Garbe JC, Heimark RL, Cress AE, Dickinson S, et al. Role for DNA methylation in the regulation of miR-200c and miR-141 expression in normal and cancer cells. PLoS One. 2010;5(1):e8697.

227. Zhang L, Cai QY, Liu J, Peng J, Chen YQ, Sferra TJ, et al. Ursolic acid suppresses the invasive potential of colorectal cancer cells by regulating the TGF-β1/ZEB1/miR-200c signaling pathway. Oncol Lett. 2019;18(3):3274-82.

228. Batista L, Bourachot B, Mateescu B, Reyal F, Mechta-Grigoriou F. Regulation of miR-200c/141 expression by intergenic DNA-looping and transcriptional read-through. Nat Commun. 2016;7:8959.

229. Tian Y, Pan Q, Shang Y, Zhu R, Ye J, Liu Y, et al. MicroRNA-200 (miR-200) cluster regulation by achaete scute-like 2 (Ascl2): impact on the epithelial-mesenchymal transition in colon cancer cells. J Biol Chem. 2014;289(52):36101-15.

230. Wiklund ED, Bramsen JB, Hulf T, Dyrskjøt L, Ramanathan R, Hansen TB, et al. Coordinated epigenetic repression of the miR-200 family and miR-205 in invasive bladder cancer. Int J Cancer. 2011;128(6):1327-34.

231. Li H, Zhou Y, Cheng H, Tian J, Yang S. Roles of a TMPO-AS1/microRNA-200c/TMEFF2 ceRNA network in the malignant behaviors and 5-FU resistance of ovarian cancer cells. Exp Mol Pathol. 2020;115:104481.

232. Zhang M, Wang F, Xiang Z, Huang T, Zhou WB. LncRNA XIST promotes chemoresistance of breast cancer cells to doxorubicin by sponging miR-200c-3p to upregulate ANLN. Clin Exp Pharmacol Physiol. 2020;47(8):1464-72.

233. Chen H, Zhang J, Yang L, Li Y, Wang Z, Ye C. circ-ZEB1 regulates epithelial-mesenchymal transition and chemotherapy resistance of colorectal cancer through acting on miR-200c-5p. Transl Oncol. 2023;28:101604.

234. Nabih HK. Crosstalk between NRF2 and Dicer through metastasis regulating MicroRNAs; mir-34a, mir-200 family and mir-103/107 family. Arch Biochem Biophys. 2020;686:108326.

235. Pljesa-Ercegovac M, Savic-Radojevic A, Matic M, Coric V, Djukic T, Radic T, et al. Glutathione Transferases: Potential Targets to Overcome Chemoresistance in Solid Tumors. Int J Mol Sci. 2018;19(12).

236. Li G, Cai Y, Wang C, Huang M, Chen J. LncRNA GAS5 regulates the proliferation, migration, invasion and apoptosis of brain glioma cells through targeting GSTM3 expression. The effect of LncRNA GAS5 on glioma cells. J Neurooncol. 2019;143(3):525-36.

237. Liu J, Shen JX, He D, Zhang GJ. Bioluminescence Imaging for Monitoring miR-200c Expression in Breast Cancer Cells and its Effects on Epithelial-Mesenchymal Transition Progress in Living Animals. Mol Imaging Biol. 2018;20(5):761-70.

238. Garrido-Cano I, Adam-Artigues A, Lameirinhas A, Blandez JF, Candela-Noguera V, Lluch A, et al. Delivery of miR-200c-3p Using Tumor-Targeted Mesoporous Silica Nanoparticles for Breast Cancer Therapy. ACS Appl Mater Interfaces. 2023;15(32):38323-34.

239. Williams MM, Christenson JL, O'Neill KI, Hafeez SA, Ihle CL, Spoelstra NS, et al. MicroRNA-200c restoration reveals a cytokine profile to enhance M1 macrophage polarization in breast cancer. NPJ Breast Cancer. 2021;7(1):64.

240. Ren Y, Han X, Yu K, Sun S, Zhen L, Li Z, et al. microRNA-200c downregulates XIAP expression to suppress proliferation and promote apoptosis of triple-negative breast cancer cells. Mol Med Rep. 2014;10(1):315-21.

241. Chambers AF, Groom AC, MacDonald IC. Dissemination and growth of cancer cells in metastatic sites. Nat Rev Cancer. 2002;2(8):563-72.

242. André F, Zielinski CC. Optimal strategies for the treatment of metastatic triple-negative breast cancer with currently approved agents. Ann Oncol. 2012;23 Suppl 6:vi46-51.

243. Wu Q, Li J, Zhu S, Wu J, Chen C, Liu Q, et al. Breast cancer subtypes predict the preferential site of distant metastases: a SEER based study. Oncotarget. 2017;8(17).

244. Khanna C, Hunter K. Modeling metastasis in vivo. Carcinogenesis. 2005;26(3):513-23.

245. Li X, Roslan S, Johnstone CN, Wright JA, Bracken CP, Anderson M, et al. MiR-200 can repress breast cancer metastasis through ZEB1-independent but moesin-dependent pathways. Oncogene. 2014;33(31):4077-88.

246. Ahmad A, Aboukameel A, Kong D, Wang Z, Sethi S, Chen W, et al. Phosphoglucose isomerase/autocrine motility factor mediates epithelial-mesenchymal transition regulated by miR-200 in breast cancer cells. Cancer Res. 2011;71(9):3400-9.

247. Dykxhoorn DM, Wu Y, Xie H, Yu F, Lal A, Petrocca F, et al. miR-200 enhances mouse breast cancer cell colonization to form distant metastases. PLoS One. 2009;4(9):e7181.

248. Damiano V, Brisotto G, Borgna S, di Gennaro A, Armellin M, Perin T, et al. Epigenetic silencing of miR-200c in breast cancer is associated with aggressiveness and is modulated by ZEB1. Genes Chromosomes Cancer. 2017;56(2):147-58.

249. Berber U, Yilmaz I, Narli G, Haholu A, Kucukodaci Z, Demirel D. miR-205 and miR-200c: Predictive Micro RNAs for Lymph Node Metastasis in Triple Negative Breast Cancer. J Breast Cancer. 2014;17(2):143-8.

250. Zhang T, Wan JG, Liu JB, Deng M. MiR-200c inhibits metastasis of breast tumor via the downregulation of Foxf2. Genet Mol Res. 2017;16(3).

251. Chang BP, Wang DS, Xing JW, Yang SH, Chu Q, Yu SY. miR-200c inhibits metastasis of breast cancer cells by targeting HMGB1. J Huazhong Univ Sci Technolog Med Sci. 2014;34(2):201-6.

252. Zhang DD, Li Y, Xu Y, Kim J, Huang S. Phosphodiesterase 7B/microRNA-200c relationship regulates triple-negative breast cancer cell growth. Oncogene. 2019;38(7):1106-20.

253. Cochrane DR, Spoelstra NS, Howe EN, Nordeen SK, Richer JK. MicroRNA-200c mitigates invasiveness and restores sensitivity to microtubule-targeting chemotherapeutic agents. Mol Cancer Ther. 2009;8(5):1055-66.

254. Medeiros B, Allan AL. Molecular Mechanisms of Breast Cancer Metastasis to the Lung: Clinical and Experimental Perspectives. Int J Mol Sci. 2019;20(9).

255. Xiao W, Zheng S, Liu P, Zou Y, Xie X, Yu P, et al. Risk factors and survival outcomes in patients with breast cancer and lung metastasis: a population-based study. Cancer Med. 2018;7(3):922-30.

256. Jin T, Suk Kim H, Ki Choi S, Hye Hwang E, Woo J, Suk Ryu H, et al. microRNA-200c/141 upregulates SerpinB2 to promote breast cancer cell metastasis and reduce patient survival. Oncotarget. 2017;8(20).

257. Sánchez-Cid L, Pons M, Lozano JJ, Rubio N, Guerra-Rebollo M, Soriano A, et al. MicroRNA-200, associated with metastatic breast cancer, promotes traits of mammary luminal progenitor cells. Oncotarget. 2017;8(48).

258. Xue B, Chuang CH, Prosser HM, Fuziwara CS, Chan C, Sahasrabudhe N, et al. miR-200 deficiency promotes lung cancer metastasis by activating Notch signaling in cancer-associated fibroblasts. Genes Dev. 2021;35(15-16):1109-22.

259. Obeng G, Park EJ, Appiah MG, Kawamoto E, Gaowa A, Shimaoka M. miRNA-200c-3p targets talin-1 to regulate integrin-mediated cell adhesion. Sci Rep. 2021;11(1):21597.

260. Svensson CM, Medyukhina A, Belyaev I, Al-Zaben N, Figge MT. Untangling cell tracks: Quantifying cell migration by time lapse image data analysis. Cytometry A. 2018;93(3):357-70.

261. De Pascalis C, Pérez-González C, Seetharaman S, Boëda B, Vianay B, Burute M, et al. Intermediate filaments control collective migration by restricting traction forces and sustaining cell-cell contacts. J Cell Biol. 2018;217(9):3031-44.

262. Ershov D, Phan M-S, Pylvänäinen JW, Rigaud SU, Le Blanc L, Charles-Orszag A, et al. TrackMate 7: integrating state-of-the-art segmentation algorithms into tracking pipelines. Nature Methods. 2022;19(7):829-32.

263. Wong IY, Javaid S, Wong EA, Perk S, Haber DA, Toner M, et al. Collective and individual migration following the epithelial-mesenchymal transition. Nat Mater. 2014;13(11):1063-71.

264. Froehlich K, Haeger J-D, Heger J, Pastuschek J, Photini SM, Yan Y, et al. Generation of Multicellular Breast Cancer Tumor Spheroids: Comparison of Different Protocols. Journal of Mammary Gland Biology and Neoplasia. 2016;21(3):89-98.

265. Li G, Satyamoorthy K, Herlyn M. N-cadherin-mediated intercellular interactions promote survival and migration of melanoma cells. Cancer research. 2001;61(9):3819-25.

266. Tryndyak VP, Beland FA, Pogribny IP. E-cadherin transcriptional down-regulation by epigenetic and microRNA-200 family alterations is related to mesenchymal and drug-resistant phenotypes in human breast cancer cells. International journal of cancer. 2010;126(11):2575-83.

267. Park SM, Gaur AB, Lengyel E, Peter ME. The miR-200 family determines the epithelial phenotype of cancer cells by targeting the E-cadherin repressors ZEB1 and ZEB2. Genes Dev. 2008;22(7):894-907.

268. Flommersfeld J, Stöberl S, Shah O, Rädler JO, Broedersz CP. Geometry-sensitive protrusion growth directs confined cell migration. arXiv:230808372 [physicsbio-ph]. 2023.

269. Brückner DB, Schmitt M, Fink A, Ladurner G, Flommersfeld J, Arlt N, et al. Geometry adaptation of protrusion and polarity dynamics in confined cell migration. Physical Review X. 2022.

270. Soares e Silva M, Alvarado J, Nguyen J, Georgoulia N, Mulder BM, Koenderink GH. Self-organized patterns of actin filaments in cell-sized confinement. Soft Matter. 2011;7(22).

271. Callan-Jones AC, Voituriez R. Actin flows in cell migration: from locomotion and polarity to trajectories. Curr Opin Cell Biol. 2016;38:12-7.

272. Battaglia RA, Delic S, Herrmann H, Snider NT. Vimentin on the move: new developments in cell migration. F1000Res. 2018;7.

273. Thompson EW, Torri J, Sabol M, Sommers CL, Byers S, Valverius EM, et al. Oncogene-induced basement membrane invasiveness in human mammary epithelial cells. Clin Exp Metastasis. 1994;12(3):181-94.

274. Arunkumar G, Deva Magendhra Rao AK, Manikandan M, Prasanna Srinivasa Rao H, Subbiah S, Ilangovan R, et al. Dysregulation of miR-200 family microRNAs and epithelial-mesenchymal transition markers in oral squamous cell carcinoma. Oncol Lett. 2018;15(1):649-57.

275. Mathieu E, Paul CD, Stahl R, Vanmeerbeeck G, Reumers V, Liu C, et al. Time-lapse lens-free imaging of cell migration in diverse physical microenvironments. Lab Chip. 2016;16(17):3304-16.

276. Sell MC, Ramlogan-Steel CA, Steel JC, Dhungel BP. MicroRNAs in cancer metastasis: biological and therapeutic implications. Expert Rev Mol Med. 2023;25:e14.

9. Indices

9.1 Index of Figures

Figure 1: Worldwide cancer incidence and mortality distribution in both sexes according to cancer site. 8
Figure 2: MicroRNA biogenesis. Major steps in the processing of miRs. 18
Figure 3: A proteomic analysis revealed novel hsa-miR-200c targets and altered signaling pathways in the field of detoxification from chemotherapy. 49
Figure 4: Validation of hsa-miR-200c-3p target site in the 3′UTR of glutathione S-transferases. 51
Figure 5: Expression of glutathione S-transferases (GSTs) in different hsa-miR-200c expression systems. 53
Figure 6: qRT-PCR and Western blot analysis of GSTM3 upon chemotherapeutic treatment. 55
Figure 7: Effect of hsa-miR-200c expression on the glutathione (GSH) pathway and cell death. In vitro long-term effect of hsa-miR-200c expression. 57
Figure 8: Long-term effect of hsa-miR-200c expression in vivo on tumor growth and resistance. 62
Figure 9: Analysis of clinical relevance. 64
Figure 10: Metastasis formation in mice is reduced when microRNA 200c (miR-200c) is expressed in the primary tumor. 68
Figure 11: MicroRNA 200c (miR-200c) positively alters survival time of mice whereas it negatively influences tumor volume and metastatic burden. 69
Figure 12: The combination of a chemotherapeutic treatment using doxorubicin with additional miRNA-200c expression hampered the metastasis formation. 71
Figure 13: Mean motility is modulated by microRNA 200c (miR-200c) expression dependent on the cellular phenotype. 73
Figure 14: MDA-MB 231 breast cancer cells without microRNA 200c (miR-200c) expression leave cell clusters more frequently. 75
Figure 15: Enhanced directionality and accumulated distance of the microRNA 200c (miR-200c) non-expressing MDA-MB 231 cells in the front region. 77
Figure 16: miR-200c-negative MCF7 cells tend to leave 3D aggregates more frequently compared to MCF7 wildtype cells. Quantification of cluster cell migration and outgrowth in 3D cell aggregates with different miR-200c expression. 79
Figure 17: An increased rate of anoikis in miR-200c-expressing cell systems. 80
Figure 18: MicroRNA 200c (miR-200c) expression negatively modulates relative migration in a transwell assay. 81
Figure 19: MicroRNA 200c (miR-200c) negatively affects the efficiency of confined cell migration. 84

9.2 Index of Supplementary Figures

Figure S1: Proteomic analysis of MCF7 KO 200c (M1, M2, M3) vs. MCF7 wt upon doxorubicin (DXR) treatment. 99
Figure S2: In silico miRNA-mRNA seed-site interaction. 101
Figure S3: Characterization of hsa-miR-200c expression systems. 103
Figure S4: Uncropped blots of western blots presented in Figure 6B,D,F. 104
Figure S5: Effect of hsa-miR-200c on cell death in two additional cancer types in combination with chemotherapeutic treatment. 105
Figure S6: Proliferation curves of hsa-miR-200c positive or negative MDA-MB 231 cells. 106
Figure S7: Animal welfare monitoring of the different xenograft mouse models and histological analysis of hsa-miR-200c-positive and negative tumors. 107
Figure S8: Overview of the parameters entered into the Kaplan-Meier Plotter for the analysis of hsa-miR-200c and GSTM3 in breast cancer patients. 108
Figure S9: hsa-miR-200c expression and the abundance of ABCB1. 109
Figure S10: hsa-miR-200c expression profile. 110
Figure S11: Expression of miR-200c is enhanced in MCF7 wildtype (wt) and MDA-MB 231 Tripz 200c Luc induced with doxycycline (+DOX) cells and tumors, respectively. 112
Figure S12: Reduced metastatic burden in mice with miR-200c-expressing tumor. 114
Figure S13: MCF7 breast cancer cells lacking miR-200c expression tend to leave cell clusters more frequently. 115
Figure S14: Characterization of 3D cell aggregates embedded in collagen revealed aggregate formation over time in MCF7 cells but not in MDA-MB 231 cells. 117
Figure S15: Doxycycline (DOX) induction is not affecting confined cell migration of mesenchymal cells. 119

9.3 Index of Videos

The Video 1 to Video 10 can be downloaded at:

https://febs.onlinelibrary.wiley.com/doi/10.1002/1878-0261.13712

Video 1: Undirected migration of MCF7 wildtype (wt) cells. Live cell imaging was performed with the Cellwatcher M.
Video 2: Undirected migration of MCF7 knockout (KO) 200c cells. Live cell imaging was performed with the Cellwatcher M.
Video 3: Undirected migration of MDA-MB 231 Tripz 200c cells without doxycycline induction (-DOX). Live cell imaging was performed with the Cellwatcher M.
Video 4: Undirected migration of MDA-MB 231 Tripz 200c cells induced with doxycycline (+DOX). Live cell imaging was performed with the Cellwatcher M.
Video 5: Wound closure of MDA-MB 231 Tripz 200c cells without doxycycline induction (-DOX) stained with 1 µM siR-DNA. The timeframe from 0 to 10 hours was monitored.
Video 6: Trajectories of migrating MDA-MB 231 Tripz 200c cells without doxycycline induction (-DOX) cells. The timeframe from 0 to 10 hours was monitored.
Video 7: Wound closure of MDA-MB 231 Tripz 200c cells with doxycycline induction (+DOX) stained with 1 µM siR-DNA. The timeframe from 0 to 10 hours was monitored.
Video 8: Trajectories of migrating MDA-MB 231 Tripz 200c cells with doxycycline induction (+DOX). The timeframe from 0 to 10 hours was monitored.
Video 9: MDA-MB 231 Tripz 200c cell without doxycycline induction (-DOX) moving on the two-state dumbbell micropattern coated with fibronectin. Nucleus is stained in blue.
Video 10: MDA-MB 231 Tripz 200c cell with doxycycline induction (+DOX) moving on the two-state dumbbell micropattern coated with fibronectin. Nucleus is stained in blue. Induced miR-200c and RFP expression shown in red.

9.4 Index of Supplementary Videos

The supplementary Video S1 and Video S2 can be downloaded at:

https://www.mdpi.com/article/10.3390/cancers14225554/s1

The supplementary Video S3 to Video S9 can be downloaded at:

https://febs.onlinelibrary.wiley.com/doi/10.1002/1878-0261.13712

Video S1: Live cell imaging of MDA-MB 231 Tripz 200c uninduced (-DOX) with doxycycline and additional doxorubicin treatment.
Video S2: Live cell imaging of MDA-MB 231 Tripz 200c induced (+DOX) with doxycycline and additional doxorubicin treatment.
Video S3: Wound closure of MCF7 wildtype (wt)stained with 1 µM siR-DNA. The timeframe from 14 to 24 hours after scratch induction was monitored.
Video S4: Trajectories of migrating MCF7 wildtype (wt) cells. The timeframe from 14 to 24 hours was monitored.
Video S5: Wound closure of MCF7 knockout (KO) 200c stained with 1 µM siR-DNA. The timeframe from 14 to 24 hours after scratch induction was monitored.

Video S6: Trajectories of migrating MCF7 knockout (KO) 200c cells. The timeframe from 14 to 24 hours was monitored.
Video S7: MDA-MB 231 Tripz Ctrl cell (control cell with doxycycline treatment, +DOX) moving on the two-state dumbbell micropattern coated with fibronectin. Nucleus is stained in blue. Induced scrambled control sequence and RFP expression shown in red.
Video S8: MCF7 wildtype (wt) moving on the two-state dumbbell micropattern coated with fibronectin. Nucleus is stained in blue.
Video S9: MCF7 knockout (KO) 200c moving on the two-state dumbbell micropattern coated with fibronectin. Nucleus is stained in blue.

9.5 Index of Tables

Table 1: Breast cancer molecular subtypes with the corresponding receptor expression, prevalence, prognosis, and treatment opportunities 10
Table 2: Targeting approaches of the hallmarks of cancer 14
Table 3: An overview on the different steps of the invasion-metastasis cascade with possible miR-200c targets. 22
Table 4: Sequences of qRT-PCR primers and TaqMan qRT-PCR analysis. 33
Table 5: TaqMan assays for qRT-PCR analyses with the LightCycler 480. 33

9.6 Index of Supplementary Tables

Table S1: Raw Ct values of qRT-PCR analysis of all glutathione S-transferases in different hsa-miR-200c expression systems. 111

9.7 Index of Abbreviations

Abbreviation	Description
3'-UTR	Three prime untranslated region
ABC transporter	ATP Binding Cassette transporter
AI	Aromatase inhibitor
ATP	Adenosine triphosphate
BCA	Bicinchoninic acid
BCS	Breast-conserving surgery
CC adhesion	Cell-cell adhesion
cDNA	Complementary DNA
ceRNA	Competitive endogenous RNA
CM adhesion	Cell-matrix adhesion
CMV	Cytomegalovirus
COVID-19	Coronavirus Disease of 2019
CP	Cis-platinum(II)diamine dichloride
Ct	Cycle Threshold
Ctrl	Control

DMEM	Dulbecco's Modified Eagle Medium
DMF	Dimethylformamide
DMSO	Dimethyl sulfoxide
DNA	Deoxyribonucleic acid
DOX	Doxycycline
DSMZ	Deutsche Sammlung von Mikroorganismen und Zellkulturen GmbH
DTE	Dithioerythritol
DXR	Doxorubicin
e.g.	exempli gratia
ECL	Enhanced chemiluminescence
EDTA	Ethylenediaminetetraacetic acid
EMT	Epithelial-mesenchymal transition
ER	Estrogen receptor
et al.	et alii
FACS	Fluorescence-activated cell sorting
FCS	Fetal calf serum
GO	Gene Ontology
GSEA	Gene set enrichment analysis
GSH	Glutathione
GSSG	Glutathione disulfide
H&E	Hematoxylin and eosin
HEPES	4-(2-hydroxyethyl)-1-piperazineethanesulfonic acid
HER2	Human epidermal growth factor receptor 2
i.e.	id est
i.v.	Intravenous
KO	Knockout
LAFUGA	Laboratory of Functional Genome Analysis
LAR buffer	Luciferase Assay Reagent buffer
LC-MS/MS	Liquid chromatography-tandem mass spectrometry
LFQ	Label-free quantification
lncRNA	Long non-coding RNA
Luc	Luciferase
mAb	Monoclonal antibody
MFI	Mean fluorescence intensity
miR	microRNA
miRNA	microRNA
mPEG-SVA	Methoxypoly(ethylene glycol) succinimidyl valerate
mRNA	Messenger RNA
MS	Mass spectrometry
mTOR	Mammalian target of rapamycin
Mut	Mutation
n.d.	not detected
ns	not significant
PBS	Phosphate Buffered Saline

PCA	Principal component analysis
PCR	Polymerase chain reaction
pDNA	Plasmid DNA
PFA	Paraformaldehyde
pH	pondus Hydrogenii
PI	Propidium iodide
PLL	Poly-L-Lysine
PMT	Photomultiplier
PR	Progesterone receptor
pre-miRNA	precursor miRNA
pri-miRNA	primary miRNA
Puro	Puromycin
PVDF	Polyvinylidene fluoride
qRT-PCR	Quantitative real-time polymerase chain reaction
RFP	Red fluorescence protein
RGD	Arginine-glycine-aspartic acid
RISC	RNA-induced silencing complex
RLU	Relative Light Unit
RNA	Ribonucleic acid
rpm	revolutions per minute
RSV	Respiratory Syncytial Virus
S(t)	Stay probability
s.c.	subcutaneous
SARS-CoV-2	Severe acute respiratory syndrome coronavirus 2
SD	Standard deviation
SERD	Selective estrogen receptor degrader
SERM	Selective estrogen receptor modulator
siRNA	Small interfering RNA
TALENs	Transcription activator-like effector nucleases
T-DM1	Trastuzumab emtansine
TNBC	Triple negative breast cancer
ULI	Underdamped Langevin inference
UPL	Universal Probe Library
VLP	Virus like particle
wt	wildtype

9.8 Index of Genes and Proteins

Gene/Protein	Description
ABCB1	ATP-binding cassette sub-family B member 1
ABCG2	ATP Binding Cassette Subfamily G Member 2
ABCG5	ATP Binding Cassette Subfamily G Member 5
Ago2	Argonaute RISC Catalytic Component 2
AP-1	Activating protein-1

ARHGAP19	Rho GTPase activating protein 19
Ascl2	Achaete Scute-like 2
ASK1	Apoptosis signal-regulating kinase
ATP2A3	Sarcoplasmic/endoplasmic reticulum calcium ATPase 3
Bcl-2	BCL2 apoptosis regulator
Bmi1	B-cell specific Moloney murine virus integration site 1
BRCA1	Breast cancer gene 1
BRG1	Brahma-related gene-1
CDK	Cyclin-dependent kinase
CFL2	Cofilin-2
c-Met	Mesenchymal-epithelial transition factor
CtBPs	C-terminal binding proteins
CTLA4	Cytotoxic T-lymphocyte–associated antigen 4
DGCR8	DiGeorge syndrome critical region gene 8
DNMT1	DNA Methyltransferase 1
EGFR	Epidermal growth factor receptor
EP 300	E1A Binding Protein P300
ESPL1	Separin
FAP-1	Fibroblast activating protein 1
FGF	Fibroblast growth factor
FHOD1	Formin homology domain-containing protein 1
FLAP	5-lipoxygenase-activating protein
FLNA	Filamin A
Flt1	Fms Related Receptor Tyrosine Kinase 1
FN1	Fibronectin 1
FOXF2	Forkhead box F2
FSCN1	Fascin
FUT4	Fucosyltransferase 4
GAPDH	Glyceraldehyde-3-phosphate dehydrogenase
GAS5	Growth arrest-specific transcript 5
GST	Glutathione S-transferase
GSTA1	Glutathione S-transferase alpha 1
GSTA2	Glutathione S-transferase alpha 2
GSTA3	Glutathione S-transferase alpha 3
GSTA4	Glutathione S-transferase alpha 4
GSTA5	Glutathione S-transferase alpha 5
GSTK1	Glutathione S-transferase kappa 1
GSTM1	Glutathione S-transferase mu 1
GSTM2	Glutathione S-transferase mu 2
GSTM3	Glutathione S-transferase mu 3
GSTM4	Glutathione S-transferase mu 4
GSTM5	Glutathione S-transferase mu 5
GSTO1	Glutathione S-transferase omega 1
GSTO2	Glutathione S-transferase omega 2
GSTP1	Glutathione S-transferase pi 1

GSTT1	Glutathione S-transferase theta 1
GSTT2	Glutathione S-transferase theta 2
GSTZ1	Glutathione S-transferase zeta 1
HGF	Hepatocyte growth factor
HiF-1α	Hypoxia-inducible factor 1-alpha
HMGB1	High mobility group box 1 protein
IGF-1	Insulin-like growth factor 1
IP3R1	Inositol 1,4,5 trisphosphate receptor
JNK1	c-Jun N-terminal kinase 1
KDR	Kinase insert domain receptor
Kras	Kirsten rat sarcoma viral oncogene homologue
LCP1	Plastin-2
LEPR	Leptin receptor
LIMK1	Cofilin kinase LIM kinase 1
LRP1	Low-density lipoprotein receptor-related protein 1
LTC4 S	Leukotriene C4
MAP kinase (MAPK)	Mitogen activated protein kinases
MARCKS	Myristoylated alanine-rich C kinase substrate
MDR1	Multidrug resistance protein 1
MGST1	Microsomal glutathione S-transferase 1
MGST2	Microsomal glutathione S-transferase 2
MGST3	Microsomal glutathione S-transferase 3
MRP1	Multidrug resistance protein 1
MSN	Moesin
MXRA8	Matrix Remodeling Associated 8
Noxa	Phorbol-12-myristate-13-acetate-induced protein 1
NTRK2	Neurotrophic receptor tyrosine kinase 2
P53	tumor protein p53
PACT	PKR-activating protein
PARP	Poly(ADP-Ribose) polymerase
PD-1	Programmed Cell Death Protein 1
PDE7B	Phosphodiesterase 7B
PD-L1	Programmed cell death ligand 1
PI3K	Phosphoinositide 3-kinase
PLCγ1	Phospholipase C, gamma 1
PPM1F	Protein phosphatase 1F
PRKACB	cAMP-dependent protein kinase catalytic subunit beta
PRKAR1A	Protein Kinase cAMP-Dependent Regulatory Type I Alpha
RALB	Ras-related protein Ral-B
S100P	Protein S100-P
SCIN	Adseverin
Sec23a	SEC23 homolog A, COPII coat complex component
Snail	Snail Family Transcriptional Repressor 1
Sp1	Specificity protein 1

SSFA2	Sperm-specific antigen 2
STX4	Syntaxin-4
TIMP3	Metalloproteinase inhibitor 3
TLN-1	Talin-1
TMPO-AS1	TMPO antisense RNA 1
TRBP	TAR RNA binding protein
TrkB	Tropomyosin receptor kinase B
Trop-2	Trophoblast cell-surface antigen 2
Twist	Twist-related protein 1
TXNRD1	Thioredoxin Reductase 1, cytoplasmic
USP25	Ubiquitin Specific Peptidase 25
VEGF	Vascular endothelial growth factor
Vegfc	Vascular endothelial growth factor C
VEGFR1	Vascular endothelial growth factor receptor 1
Wnt	Wingless-related integration site
XIAP	X-linked inhibitor of apoptosis protein
XIST	X-inactive-specific transcript
ZEB1	Zinc finger e-box bind homeobox 1
ZEB2	Zinc finger e-box bind homeobox 2
ZNF217	Zinc-finger protein 217

10. Publications

10.1 Articles

10.1.1 First Author Publications

Köhler B, Dubovik S, Hörterer E, Wilk U, Stöckl JB, Tekarslan-Sahin H, Ljepoja B, Paulitschke P, Fröhlich T, Wagner E, Roidl A. Combating Drug Resistance by Exploiting miRNA-200c-Controlled Phase II Detoxification. Cancers (Basel). **2022** Nov 11;14(22):5554.

Köhler B, Brieger E, Brandstätter T, Hörterer E, Wilk U, Pöhmerer J, Jötten A, Paulitschke P, Broedersz CP, Zahler S, Rädler JO, Wagner E, Roidl A. Unraveling the metastasis-preventing effect of miR-200c in vitro and in vivo. Mol Oncol. **2024** Oct 15. doi: 10.1002/1878-0261.13712. Epub ahead of print.

10.1.2 Co-author Publication

Ljepoja B, Schreiber C, Gegenfurtner FA, García-Roman J, **Köhler B**, Zahler S, Rädler JO, Wagner E, Roidl A. Inducible microRNA-200c decreases motility of breast cancer cells and reduces filamin A. PLoS One. 2019 Nov 20;14(11):e0224314

10.2 Poster

Köhler B, Wagner E, Roidl A. Small molecule inhibitors of the BMP-signaling pathway act synergistically with doxorubicin. A Biochemical Society Scientific Meeting: BMPs Signalling in Cancer II, Oxford, United Kingdom

11. Copyright and licenses

12. Acknowledgements

An dieser Stelle möchte ich die Gelegenheit nutzen und mich bei all denjenigen bedanken, die mich während meiner Zeit als Doktorandin maßgeblich unterstützt und begleitet haben.

Mein großer Dank gilt zuallererst Prof. Dr. DI Ernst Wagner, meinem Doktorvater und Supervisor, für seine hervorragende Betreuung und enorme Unterstützung bei der Durchführung meiner Doktorarbeit. Seine mannigfaltigen Möglichkeiten haben mir den Eintritt in die Thematik der Krebsforschung erlaubt. Bereits als Bachelor- und Masterstudentin hat er mein wissenschaftliches Interesse an der Forschung gestärkt, gefordert und gefördert.

Ich danke Prof. Stefan Zahler für seine hilfsbereite und wissenschaftliche Betreuung als Zweitgutachter meiner Doktorarbeit und wichtiger Kooperationspartner. Seine konstruktive Kritik und fachliche Unterstützung haben maßgeblich zur Qualität meiner wissenschaftlichen Arbeit beigetragen.

Ein immenses Dankeschön geht an Dr. Andreas Roidl, Supervisor und Gruppenleiter, für all seine ansteckende Leidenschaft für die Forschung, die Begeisterung für neue Ideen, die aus langen und konstruktiven Gesprächen resultierten. Für seine hilfreiche Unterstützung und stete Ermunterung, mich kritisch mit den Themenkomplexen auseinander zu setzen, soll ihm gedankt werden.

Besonders möchte ich mich bei Prof. Dr. Joachim O. Rädler und seinem Sonderforschungsbereich (SFB1032) bedanken, dessen ein Teil ich während meiner Doktorandenzeit sein durfte. Beide in dieser Doktorarbeit präsentierten Studien wurden von der Deutschen Forschungsgemeinschaft (DFG) (project-ID 201269156 Collaborative Research Center SFB 1032, project B04) gefördert. Durch das Netzwerk innerhalb dieses Sonderforschungsbereichs war es möglich, eine Fusion aus Tumorbiologie und Physik zu schaffen, was eine immense wissenschaftliche Bereicherung für mich bedeutet. Ich bedanke mich bei meinen Kooperationspartnern aus dem Bereich der Physik: Prof. Dr. Joachim O. Rädler, Prof. Dr. Chase P. Broedersz, Emily Brieger und Tom Brandstätter.

Des Weiteren bedanke ich mich bei Dr. Philipp Paulitschke, CEO von PHIO GmbH, und seinem Team, insbesondere Dr. Anna Jötten und Konstantin Schaffert, für die

Einführung und Applikation des Cellwatchers, sowie deren wissenschaftliche Zusammenarbeit. Mein Dankeschön gilt auch Dr. Thomas Fröhlich und Dr. Jan B. Stöckl, vom Gene Center - Laboratory for Functional Genome Analysis, für die erfolgreiche Proteomics-Analyse für das miRNA-200c- und Chemoresistenz-Projekt.

Vielen Dank an Dr. Elisa Hörterer, Dr. Ulrich Wilk und Dr. Jana Pöhmerer, den Kollegen aus dem Bereich der Tiermedizin im AK Wagner, die unsere *in vivo*-Experimente durchgeführt haben.

Außerdem möchte ich mich bei meinen Kollegen für den konstruktiven wissenschaftlichen Austausch bedanken. Hervorzuheben sind Dr. Ann-Katrin Sommer-Joos und Dr. Bojan Ljepoja, die mich nach meinem Masterstudium in das Doktorandenleben eingeführt haben und mir einige Labormethoden erfolgreich vermittelt haben. Danke an Dr. Adam Hermawan, der mich mit seinem Enthusiasmus für die Arbeit in der Krebsforschung motiviert hat und mich als Bachelorstudentin in die Weiten des Laboralltags eingeführt hat. Für die kollegiale und internationale Zusammenarbeit bedanke ich mich bei meiner Kooperationspartnerin Dr. Hande Tekarslan-Sahin, sowie Dr. Martina Lichtenfels.

Eine große Bereicherung für mich war die Betreuung der Bachelorstudentinnen Rebecca Kiok, Savanna Süß und Anna Kübler sowie der Masterstudentin Elena Willig. Vielen Dank für die Zusammenarbeit an den BMP- und Spheroid-Projekten.

Zudem möchte ich mich bei den Technischen Assistenten Sviatlana Dubovik, Wolfgang Rödl, Enikö-Melinda Kiss, Lorina Bawej, Miriam Höhn, und Ursula Biebl bedanken, die die Infrastruktur im Labor und in der Zellkultur aufrecht gehalten haben. Danke an Markus Kovac für seine tierpflegerischen Arbeiten. Für die administrative Unterstützung bedanke ich mich bei Olga Brück.

Auch dem Arbeitskreis Wagner danke ich, denn durch die kameradschaftliche Atmosphäre waren die Laborarbeiten leichter durchführbar. Zu den unvergesslichen Highlights zählen die gemeinsamen Weihnachtsfeiern und Oktoberfestbesuche.

Mein besonderer und herzlicher Dank gebührt meiner Familie und Freunden. Durch ihre andauernde moralische Unterstützung und Motivation haben sie einen enormen Beitrag dazu geleistet, dass ich mein Doktorstudium erfolgreich abschließen konnte.